NASA/TP-20250002845

Moon to Mars (M2M)
M2M-30044
BASELINE

National Aeronautics and
Space Administration

RELEASE DATE: MARCH 18, 2025

Lora Dishongh
NASA, Johnson Space Center, Houston, TX

MOON TO MARS (M2M) LUNAR SURFACE DATA BOOK

.

REVISION AND HISTORY PAGE

Revision No.	Change No.	Description	Effective Date
ACD-50044 -	ACD-C0032	Initial Baseline Release (Reference Artemis Campaign Development (ACD) Control Board (ACB), dated 10/06/22)	10/06/22
ACD-50044 A	ACD-C0065	Editorial changes throughout; moved section 6.0 to new section 6.1; added content to sections 5.0 and 7.0; added new sections 3.1.1, 3.1.2, 3.2.2 through 3.2.8, 4.4 through 4.12, 5.3, 6.1, 6.2, 6.3, 6.4, 7.3.4, and 7.3.5; expanded section 3.2 beyond LRO; expanded section 4.3; broadened the scope of the traverse sections in 7.3; added content to Appendices A and B; added Appendices D and E; added links to all references; revised and expanded the reference documents list; assigned tracking numbers to baselined TBXs and added several more; reorganized Appendix C.	05/19/23
M2M-30044 Baseline	M2M-C0082	Changed document number to M2M-30044; editorial changes throughout; updated ACD references to M2M replacements throughout; 1.1 expanded purpose; 1.2 expanded scope; 2.1 added Lunar Sourcebook as Applicable Document; 2.2 removed specific vehicle documents from reference list and added NASA standards; 3 expanded to include more than LRO; 4.1 added paragraph on the AGDT; added section 4.2.5; 4.8 described how to use the DSNE thermal environment; 6.1 expanded discussion of regolith parameters; 6.2.1 expanded plume surface interaction discussion; 6.2.2 expanded trafficability discussion; 6.3 expanded illumination discussion; redesignated 7.1 for South Pole Exploration Sites; redesignated 7.2 for Terrain 101; 7.3 added a discussion of general traverse design methodology, renamed example traverses to be more descriptive and not reference earlier mission architectures, and added two very long traverses; swapped order of Appendices B and C (B is now open items, C is now references); added Table C1-3 and associated Short Names for links; and added Appendix F on Reference Frames	03/18/25

TABLE OF CONTENTS

SECTION **PAGE**

TABLE OF TABLES

TABLE OF FIGURES

1.0 INTRODUCTION

1.1 PURPOSE

Artemis missions will need to reference and work with a common set of lunar surface data, products, and analytical assumptions to accomplish Artemis mission science, exploration, and operational objectives. This Lunar Surface Data Book is intended to be used as a reference for candidate vendors and agency personnel who are addressing Artemis lunar surface challenges to ensure a common set of data sources and assumptions when interpreting remote sensing data specific to the needs of surface mission planning. Analogous to a road atlas or a hiker's guide, mission planners and hardware design requirement owners are encouraged to refer to the Lunar Surface Data Book piecemeal: use only the sections that make sense for the specific mission or hardware in question. This data book is intended to supplement requirements documents, providing additional supporting information to help designers understand the terrain and other characteristics of the lunar surface that may not be appropriate to detail in high-level requirements documents.

1.2 SCOPE

This document provides a common reference set of existing lunar surface data, products, analytical assumptions, and representative use cases to be incorporated into Artemis surface mission planning efforts. This document pertains solely to the surface of the Moon and the ecosystem of data and products to be used to describe the lunar surface. The focus of this document is the lunar south pole region, defined in the 2020 NASA Lunar Exploration Plan (more formally, NASA's Lunar Exploration Program Overview) as the region within six degrees latitude of the geographic lunar south pole. It is the region selected for long-term stays. Where the content presented does not apply directly in its details, users of this data book may either dig into the source data files and use this book as a guide for how to package and interpret that underlying data for themselves or seek assistance from the Artemis Geospatial Data Team (Appendix D). More specific data set interpretations will be added over time. While the book is not meant to be levied as a requirements document as a whole, users may find specific details such as individual traverses appropriate for reference by their requirements documents and for verification and validation. Additional scope includes use as background rationale for how requirements were derived.

1.3 CHANGE AUTHORITY/RESPONSIBILITY

NASA Office of Primary Responsibility (OPR) identified for this document is M2M Systems Engineering & Integration (SE&I). Proposed changes to this document shall be submitted via a Change Request (CR) to the appropriate Control Board for consideration and disposition. All such requests shall adhere to the M2M Configuration Management Process documented in M2M-30005, Moon to Mars (M2M) Program Configuration and Data Management Plan.

2.0 DOCUMENTS

2.1 APPLICABLE DOCUMENTS

Applicable documents are directly related to this document and cited within. The context and how to apply the applicable documents will be included as part of the document citation. The following documents include specifications, models, standards, guidelines, handbooks, and other special publications.

TABLE 2.1-1 APPLICABLE DOCUMENTS

Document Number	Document Revision	Document Title
SLS-SPEC-159 (M2M-30159)	Current Revision	Cross Program Design Specification for Natural Environments (DSNE)
ISBN 0-521-33444-6		Lunar Sourcebook, A User's Guide to the Moon

2.2 REFERENCE DOCUMENTS

A reference document is a document that provides additional information for the reader and may or may not be cited in this document. Additional references in this document can be found in Appendix C.

TABLE 2.2-1 REFERENCE DOCUMENTS

Document Number	Document Title
ESDMD-001	Moon-to-Mars Architecture Definition Document
ESDMD-410	Lunar Surface Exploration Planning: Terrain Characteristics
M2M-30080	Lunar Geospatial Data Process Plan
M2M-30007	Artemis Integrated Concept of Operations
M2M-30007-ANX01	Artemis Integrated Lunar Surface Concept of Operations
NASA-STD-1008	Classifications and Requirements for Testing Systems and Hardware to be Exposed to Dust in Planetary Environments
NASA-STD-3001 Volume 2	NASA Spaceflight Human-System Standard Volume 2: Human Factors, Habitability, and Environmental Health
NP-2020-05-2853-HQ	NASA's Lunar Exploration Program Overview

3.0 LUNAR SURFACE DATA SOURCES

SLS-SPEC-159 Cross-Program Design Specifications for Natural Environments (DSNE) is the baseline source for all natural lunar environments. The DSNE is a mandatory engineering technical authority document and is fully applicable to the Artemis Campaign. The DSNE contains lunar surface environment characteristics for surface hardware design and verification. The Lunar Surface Data Book complements the DSNE with additional site-specific characteristic data, products, analytical assumptions, and representative use cases.

Between 1963 and 1972, the Moon was a focus of an intense, integrated program of American exploration including robotic orbiters (Lunar Orbiter) and impactors (Ranger), soft landers (Surveyor) and crewed missions (Apollo). In the 21st century, an ambitious flotilla of international missions has developed a modern view of the Moon and its surface. These modern missions (e.g., the Japan Aerospace eXploration Agency (JAXA) Kaguya, European Space Agency (ESA) Smart 1, NASA/Department of Defense (DOD) Clementine, NASA Lunar Prospector, Indian Space Research Organisation (ISRO) Chandrayaan-1, NASA GRAIL (Gravity Recovery and Interior Laboratory), NASA LADEE (Lunar Atmosphere and Dust Environment Explorer), NASA LCROSS (Lunar Crater Observation and Sensing Satellite), and NASA Lunar Reconnaissance Orbiter (LRO), and Korea Pathfinder Lunar Orbiter (KPLO)) have all dramatically increased our understanding of the Moon's environment. Therefore, the Moon is the one planetary object besides Earth that has been systematically studied for over five decades from a variety of perspectives including remote observations, in situ measurements, human field work, and returned samples with appropriate geological context. With that full suite of data sources, lunar scientists and mission planners today have access to several data sources and products that characterize the lunar surface, making the Moon the most well-understood and well-characterized body in our solar system besides Earth. That relative wealth of knowledge compared to other solar system objects, especially when compared to the spartan state of our knowledge prior to the Apollo missions, enables 21st century lunar mission planners to optimize systems, do detailed mission planning, and enable transformative lunar science and exploration outcomes with future missions. This section describes the sources of data before reviewing the data themselves and only the most recent and relevant data is included.

This document presents a compilation of data readily available in NASA's Planetary Data System and other data repositories with source data and detailed explanations as well as data interpretation available in peer-reviewed literature. Future Science Mission Directorate (SMD) Lunar Discovery and Exploration Program missions to the lunar poles will improve our understanding of lunar surface characteristics, including the Commercial Lunar Payload Services (CLPS) Missions currently underway. The emphasis in this document is placed on the data from US missions, particularly that from the Lunar Reconnaissance Orbiter, because the provenance of those data is well-understand and fully characterized, and all Lunar Reconnaissance Orbiter source data is fully and publicly available per long-standing NASA Policy.

3.1 IN SITU LUNAR SURFACE DATA

A robust set of surface data exists for the multiple landing sites visited by NASA missions (Surveyor and Apollo). Data for surface (regolith) geotechnical and rock abundance properties is derived from both images/observations and physical measurements of the surface. The Lunar Sourcebook (Heiken et al., 1991) includes geotechnical data from the Lunokhod 1 and 2 uncrewed rovers that traversed 47 km of the lunar surface and collected on the order of 1000 cone vane penetrometer measurements of the upper 10 centimeters of the regolith. Much of the data from the 1960 and 1970s is not in modern formatting, only preserved as film negatives or tabular data formats. That said, the in-situ data presents our best understanding of the specific properties of the lunar surface which are directly applicable to Artemis mission planning. Given that, care must be used to not over-interpret landing site data that is NOT relevant to the lunar south pole. For example, much consternation could arise from assuming any site is similar to the rocky surface encountered by the Surveyor VII mission, which landed (autonomously) and without any active hazard avoidance in the rockiest region yet explored on the Moon. We have no reason to believe the south pole region will be in any way similar to that particular landing site. Instead, Artemis landing sites will be in the lunar highlands of the south pole region, resulting in operations much more comparable to the Apollo 14 and 16 landing sites. Data from these missions are available through NASA's Planetary Data System (PDS) (https://pds.nasa.gov/), hereafter referred to as the PDS Home Page, NASA's Space Science Data Coordinated Archive (NSSDC) (https://nssdc.gsfc.nasa.gov/), hereafter referred to as the NSSDC Home Page, and the Analyst's Notebook (https://an.rsl.wustl.edu/). Links to data sets are provided in each individual subsection that follows. Table C1-3 in Appendix C compiles the data sources' full names, short names used in this document, and web addresses.

3.1.1 Apollo Data

The Apollo program was the United States's human spaceflight program under NASA which resulted in landing the first humans on the Moon. Apollo ran from 1961 to 1972, with the first crewed flight in 1968 and set several major human spaceflight milestones.

It stands alone in sending crewed missions beyond low Earth orbit. Apollo 8 was the first crewed spacecraft to orbit another celestial body, and Apollo 11 was the first crewed spacecraft to land humans on the Moon.

The Apollo program returned 842 pounds (382 kg) of lunar rocks and soil to Earth, greatly contributing to the understanding of the Moon's composition and geological history. The program laid the foundation for NASA's subsequent human spaceflight capability. Apollo also advanced many areas of technology within rocketry and human spaceflight, including avionics, telecommunications, and computers.

Link to Apollo 11 Data: NASA - NSSDCA - Spacecraft – Details, NSSDCA/COSPAR ID: 1969-059C, https://nssdc.gsfc.nasa.gov/nmc/spacecraft/display.action?id=1969-059C

3.1.2 Lunokhod and Other Robotic Missions

3.1.2.1 Soviet Space Program Robotic Missions

The Luna/Lunokhod Missions are early examples of unmanned remote-controlled lunar vehicles.

Luna 16, NSSDCA/COSPAR ID 1970-072A, was the first robotic probe to land on the Moon and return a sample to Earth. It was the first lunar sample return mission by the Soviet Union. It followed the Apollo 11 and 12 missions, studying lunar gravity during its descent before landing as planned in the Sea of Fertility (Mare Fecunditatis) west of Webb crater. Luna 20, NSSDCA/COSPAR ID 1972-007A, followed in early 1972, also landing and returning with a sample taken from the Sea of Fertility. Luna 24, NSSDCA/COSPAR ID 1976-081E (descent craft only) and 1976-081A (overall), was the last Luna series spacecraft and the third Soviet Union mission to retrieve lunar ground samples. It performed its mission in August 1976, landing, retrieving a sample, and returning to Earth from the Sea of Crisis (Mare Crisium).

The Lunokhod missions were the rovers of the Luna series. NSSDC lists Lunokhod 1/Luna 17 as NSSDCA/COSPAR ID 1970-095A and provides a brief description; the Rand Corporation provides a downloadable PDF report of the Lunokhod-1 mission written by Simon Kassel in 1971, "Lunokhod-1 Soviet Lunar Surface Vehicle." https://www.rand.org/pubs/reports/R0802.html. Lunokhod 2/Luna 21 collected morphological data in the Sea of Rains (Mare Imbrium) and along the Fossa Recta; a downloadable PDF study of Lunokhod-2 data was published by Basilevsky (1977), "A possible lunar outcrop: a study of Lunokhod-2 data." https://doi.org/10.1007/BF00566850. The mission is also cataloged as NSSDCA/COSPAR ID 1973-001A by NASA NSSDC.

3.1.2.2 Chinese Lunar Exploration Program Robotic Missions

The Chang'e Missions are a current and on-going series of so-far robotic lunar vehicles.

Chang'e 1, NSSDCA/COSPAR ID 2007-051A, launched 24 October 2007, was China's first lunar orbiter. It validated the technology and engineering necessary to fly lunar missions and begin exploration of the lunar surface, providing experience for subsequent missions. Chang'e 1 was a success, orbiting the Moon for four months beyond its planned one-year life before exercising a planned impact north of the Sea of Fertility.

Chang'e 2, NSSDCA/COSPAR ID 2010-050A, followed in 2010. It expanded the high-resolution surface image collection started by Chang'e 1, then left lunar orbit to enter the L2 Sun-Earth Lagrange point orbit in August 2011 where it stayed until April 2012, waiting to execute an asteroid fly-by mission. It passed within a few kilometers of asteroid 4179 Toutatis on 13 December 2012, taking close-up images at a relative velocity of 10.7 km/s.

Chang'e 3, NSSDCA/COSPAR ID 2013-070A, launched in December 2013 and carried the Yutu "Jade Rabbit" rover (2013-070C) to the Sea of Rains, proving out that technological development. It was followed by Chang'e 4 (2018-103A), carrying rover Yutu-2 to the Von Karman crater in the South Pole-Aitkin Basin. Chang'e 4 landed 03 January 2019, making it the first spacecraft to make a controlled landing on the far side of the Moon. Landing coordinates were calculated from LRO images as 45.4561 S latitude, 177.5885 E longitude, to within a few meters. The Yutu-2 rover drove down ramps from the body of the Chang'e 4 craft and started its mission. On 6 January the rover went into a planned hibernation to protect itself from the heat of lunar noon and awoke on 10 January to continue travelling and making measurements. It shut down over the local lunar night that started January 13 or 14. The rover and lander each used a radioisotopic heat source to maintain survival temperatures, and successfully resumed daytime operations on 29 and 30 January 2019, respectively. As of the latest data available to NSSDC, Yutu-2 hibernated during the lunar night and operated during the lunar day, as planned, through at least October 2022.

Chang'e 5, NSSDCA/COSPAR ID 2020-087A, launched in November 2020 on a sample return mission, matured from test mission Chang'e 5-T1 (2014-065A). It consisted of an orbiter, lander, ascender, and return vehicle. The lander/ascender portion set down in the Mons Rümker region of Oceanus Procellarum (43.058 N, 51.916 W), collected samples, and launched the sample container in its small ascender module that rendezvoused with the orbiter/return vehicle and docked on December 5. The sample container was transferred to the return vehicle, then the ascender was jettisoned from the orbiter. The ascender impacted the Moon 7 December 2020 near 30 S, 0 E, and the orbiter/return vehicle continued to orbit the Moon for 5 days. The Chang'e 5 orbiter fired its rockets to enter an Earth-Moon transfer orbit. On the way back to Earth, the Chang'e 5 orbiter separated from the sample return vehicle, and fired its rockets to head for the Sun-Earth Lagrange point L1 for an extended mission to test technology and observe the Sun. The now-separate sample return craft performed an atmospheric "skip" reentry on December 16 and landed successfully with a reported 1.731 kg of lunar regolith.

Chang'e 6, NSSDCA/COSPAR ID CHANG-E-6, launched in May 2024 on a similar sample return mission to Chang'e 5, going to the far side of the Moon with a small rover like Chang'e 4. Chang'e 6 orbited for 20 days to find an appropriate landing site before the lander separated for descent and landing in the southern part of the Apollo crater, inside the South Pole Aitken Basin, at coordinates 41.6385 S, 153.9852 W. Solar panels, an antenna, and science experiments were deployed and communications were established via the Queqiao-2 relay satellite, enabling communications from the lunar far side after landing. The small rover deployed, drove a short distance away, and took pictures of the Chang'e 6 lander. Samples were collected, and the ascent vehicle launched and docked with the Chang'e 6 orbiter-return vehicle on June 6. The samples were transferred into the return vehicle and the ascender was again released to impact the lunar surface. The orbiter-return vehicle left orbit about June 21 with the sample return craft performing an atmospheric "skip" reentry on June 25 with over 1.9 kg of lunar material.

3.2 ORBITAL DATA RELEVANT TO THE SURFACE

To understand the lunar surface and its environment, NASA and other spacefaring nations have sent numerous missions to lunar orbit, leading to the largest volume of data for any planetary body outside of the Earth. This document focuses on lunar remote sensing data and the respective derived products.

3.2.1 Lunar Reconnaissance Orbiter (LRO)

The Lunar Reconnaissance Orbiter (NSSDCA/COSPAR ID 2009-031A) was launched on 18 June 2009 from what is now Cape Canaveral Space Force Station on an Atlas V 401 rocket. LRO remains in lunar orbit and is operational as of September 2024. LRO was designed to meet the requirements of the former Exploration Systems Mission Directorate (ESMD) to identify safe landing sites for crewed and robotic missions to the Moon, understand the lunar radiation environment, and characterize potential lunar resources. The LRO mission operations are funded until at least October 2025, spacecraft health non-withstanding. After arriving at the Moon in 2009, LRO spent several months in an elliptical, stable frozen 30 x 216 km orbit with apoapsis over the lunar south pole. Over the next two years the spacecraft transitioned into a 50 x 50 km circular polar mapping orbit. Following the completion of its baseline mapping mission in 2010, LRO transitioned into a quasi-stable 30 x 216 km polar orbit which has slowly evolved to a nearly circular 100 km orbit, where it remains today (2024). This polar orbit has allowed for the substantial collection of polar remote sensing data. These products are the best possible dataset that can be used to identify scientifically interesting and relatively safe exploration areas.

Despite the spacecraft's natural orbital procession away from direct south polar overflights, it is still possible that additional Lunar Reconnaissance Orbiter Camera images can be targeted for select areas in the polar regions; please contact the LRO Project Scientist for additional information using the formal data request process in Appendix D. The LRO mission instrument suite and scientific outcomes have been well-described in multiple publications, including Vondrak et al. 2010 and Keller et al. 2016. LRO carries seven instruments, each designed to investigate a specific aspect of the lunar environment relevant to future exploration. We briefly summarize the LRO instrument suite in this section.

3.2.1.1 The Cosmic Ray Telescope for the Effects of Radiation (CRaTER)

LRO's CRaTER instrument characterizes the lunar radiation environment and the associated biological impacts. It does this by collecting data from a variety of charged particles and their energies particularly above 10 MeV. This data allows scientists to better understand what hazards future human explorers will be subjected to.

Radiation in the lunar environment results from the Sun and beyond the solar system (galactic cosmic rays). CRaTER data has allowed scientists to determine the potential biological impacts of the radiation. Furthermore, CRaTER also tests models of radiation effects and shielding and measures radiation absorption by human tissue-like plastic, aiding in the development of protective technologies to help keep crews safe. CRaTER data is available through the NSSDC Master Catalog (https://nssdc.gsfc.nasa.gov/nmc/).

3.2.1.2 Diviner Lunar Radiometer Experiment (DLRE)

Understanding the lunar thermal environment at both the sub-surface and surface is critical for planning future crewed and robotic exploration missions. In contrast to the Apollo missions, which featured equatorial landing sites and whose surface activities were planned only during the lunar day, NASA's new lunar exploration program will have missions taking place at much higher latitudes. Furthermore, these missions will eventually consist of longer-term crewed stays of longer than two weeks.

LRO's DLRE (more commonly referred to as Diviner) is an instrument designed to measure lunar surface temperatures at scales that provide essential information for future surface operations and exploration. Diviner is the first instrument to capture day and night temperature observations. This data set has been used to identify potential polar ice deposits, derive subsurface temperatures and to map temporal surface variations. Since July 2009, Diviner has acquired about one trillion radiometric observations, making it the most highly detailed set of thermal measurements of any planetary body.

A key Diviner objective is to determine the temperatures within Permanently Shadowed Regions (PSRs), to understand the potential of these areas to harbor water ice. Orbital thermal mapping measurements also provide detailed information on surface parameters such as composition, hazards, rough terrain, and rocks. The Diviner instrument can determine surface temperatures to within 5 °C across areas as small as 300 m using 9 different wavelengths between 7 and 200 microns.

Diviner seasonal bolometric temperature data products are commonly used for preliminary evaluation of polar regions of interest. These include the maximum, average, minimum and amplitude maps at 240 meters per pixel (Williams et al., 2019).

The data product descriptions and links to seasonal and hourly temperature products are available from the project team's website:

Data | diviner (https://www.diviner.ucla.edu/data), will be referred to as the Diviner PDS Archive

Index of /~jpierre/diviner/level4_polar/additional_maps (https://luna1.diviner.ucla.edu/~jpierre/diviner/level4_polar/additional_maps/)

The seasonal temperature variations are described in detail and mapped by Williams et al (2019), available here: https://doi.org/10.1029/2019JE006028.

The Diviner data is available from the PDS archive at different levels of processing:

PDS Geosciences Node Data and Services: LRO Diviner Data Sets (https://pds-geosciences.wustl.edu/missions/lro/diviner.htm)

3.2.1.3 Lyman Alpha Mapping Project (LAMP)

LAMP is an imaging ultraviolet spectrometer, detecting UV light between 1200 and 1800 Å with an effective surface spatial resolution of up to 200 m per pixel near the poles (Gladstone et al. 2010). Developed and built by a team of scientists and engineers from the Southwest Research Institute (SwRI), LAMP maps the entire lunar surface in the far ultraviolet part of the spectrum, including areas in permanent shadow.

LAMP's primary mission objective is to search for surface ice and frost in the polar regions, providing images of permanently shadowed regions illuminated only by starlight and the glow of interplanetary hydrogen emission, known as the Lyman Alpha line. The valuable resources like water and ice that LAMP helps identify could play a role in determining suitable areas for the construction of crewed south pole infrastructure.

LAMP data is available through the NSSDC Master Catalog.

3.2.1.4 Lunar Exploration Neutron Detector (LEND)

LEND is a neutron spectrometer similar to the High Energy Neutron Detector (HEND) on the Mars Odyssey spacecraft. LEND was designed to search for water ice in permanently shadowed regions of the lunar south pole by mapping the distribution of hydrogen and hydrogen-bearing compounds. The dataset's spatial resolution at the polar regions is 10 km with a sensitivity not less than 0.01 mass fraction. Due to LRO's polar orbit configuration, LEND data is densest, and therefore of highest resolution, in areas around the south pole.

The LEND dataset has been used to identify areas of possibly enhanced hydrogen abundance, of interest for future in-situ resource utilization. Refer to LEND papers Mitrofanov et al (2010) and Sanin et al (2017).

LEND data is available through the NSSDC Master Catalog.

3.2.1.5 Miniature Radio Frequency (Mini-RF)

Mini-RF (Raney et al, 2011) is an advanced synthetic aperture radar (SAR) instrument. The first instrument was launched in October 2008 on board the Indian Space Research Organization's Chandrayaan-1 spacecraft. On this spacecraft, Mini-RF collected both north and south polar lunar data until August 2009. The second Mini-RF instrument is now flying onboard NASA's LRO and has been collecting observations for more than ten years.

Mini-RF is designed to search for subsurface water ice in the lunar polar regions and to map rock distributions. The instrument is capable of imaging terrain at two wavelengths, X-band (4.2 cm) and S-Band (12.6 cm), and two resolutions. The baseline resolution is 75 meters-per-pixel (mpp) and the zoom resolution is 15 mpp. The instrument also measures topography via interferometry at 15 mpp and sub-meter vertical resolution.

The instrument no longer has the capability to transmit radar signals, only to receive them. Therefore, it now operates in a receive-only mode measuring bistatic radar signals transmitted from ground-based radio telescopes and reflected off the lunar surface. Data from Mini-RF has been used to study crater geology and mineralogy, as well as material in PSRs of deep polar craters. Refer to Mandt et al, 2016.

Mini-RF data is available through the NSSDC Master Catalog.

3.2.1.6 Lunar Orbiter Laser Altimeter (LOLA)

The LOLA instrument (Smith et al, 2010) provides topographic measurements of the lunar surface to by pulsing a single laser at 1064 nm wavelength, splitting the output into five separate beams that illuminate the lunar surface 28 times per second. For each beam, LOLA measures the time of flight (range), pulse spreading (surface roughness), and transmit/return energy (surface reflectance). This allows the topography to be determined, along with an indication of whether the surface is rough or smooth at scales relevant for Exploration planning. LOLA is the "fundamental" dataset for all LRO instruments, providing the foundational global lunar topographic model and geodetic grid that will serve as the framework to enable precise positioning, safe landing, and surface mobility, as well as characterizing the polar illumination environment. LOLA data is available through the NSSDC Master Catalog.

3.2.1.7 Lunar Reconnaissance Orbiter Camera (LROC)

LROC consists of three cameras (Robinson et al., 2010). There are two Narrow Angle Cameras (NACs) that provide panchromatic images over a 5-km swath from the 50km nominal mapping orbit, with resolutions varying from 0.5 to 3 meters per pixel, depending on orbital altitude. There is also a Wide-Angle Camera (WAC), which provides multispectral images with a pixel scale of 100 meters per pixel over seven color bands with a 60 km swath. LROC is designed to address fundamental exploration objectives, including:

- Characterize potential landing sites at the meter scale.
- Map regions of permanent shadow or illumination.
- Create high-resolution maps of the surface, including polar massifs with near-permanent illumination.
- Observe regions from multiple angles to derive high-resolution meter-scale topography.
- Map the global distribution of the mineral ilmenite (a key lunar resource).
- Create a global morphology base map.
- Characterize lunar regolith.
- Establish impact rates for hazard analysis (impactor type requires instrument advancements).

LROC image data is available through the NSSDC Master Catalog.

3.2.2 Clementine

The objective of this joint project between the Ballistic Missile Defense Organization (BMDO) and NASA was to test sensors and spacecraft components exposed to the space environment, obtaining multi-spectral imaging of the entire lunar surface, assessing the surface mineralogy of the Moon, and obtaining altimetry from 60N to 60S latitude and gravity data for the near side. A significant result from the Bistatic Radar Experiment in 1998 was that the data obtained from Clementine indicated that there could be water in polar craters of the Moon. For more details go to the NSSDC Master Catalog, NSSDCA/COSPAR ID 1994-004A.

Data from the Clementine Mission can be found on the NSSDC Master Catalog, including the Bistatic Radar Experiment.

3.2.3 Lunar Prospector

The Lunar Prospector was designed by NASA and Lockheed Martin for a low polar orbit investigation of the Moon. Its mission was to map surface composition and polar ice deposits, take measurements of magnetic and gravity fields, and study lunar outgassing events. The

Lunar Prospector went into a near-circular 100 km altitude lunar polar orbit, then lowered to 40 km. The nominal mission ended after one year, and in the extended period the orbit was lowered to 30 km. On 31 July 1999 at 9:52:02 UT Lunar Prospector impacted the Moon near the south pole in a controlled crash to look for evidence of water ice – none was observed.

The Gamma Ray Spectrometer (GRS) and Neutron Spectrometer (NS) returned global data on elemental abundances, used to help understand the evolution of the lunar highland crust and the duration and extent of basaltic volcanism, and to assess lunar resources. The NS data will also locate any significant quantities of water ice which may exist in the permanently shadowed areas near the lunar poles.

The Magnetometer (MAG) and Electron Reflectometer (ER) returned data on the magnetic field of the lunar crust and the lunar induced magnetic dipole. These data will help provide an understanding of the origin of lunar paleomagnetism and the degree to which impacts can produce paleomagnetism and allow constraints on the size and composition of the lunar core (if there is one).

The Alpha Particle Spectrometer (APS) is being used to look for radon outgassing events on the lunar surface by detecting alpha particles from the radon gas itself and its decay product, polonium. Observations of the frequency and locations of the gas release events help characterize one possible source of the tenuous lunar atmosphere. Determination of the relationship of outgassing sites with crater age and tectonic features may be possible. This may in turn be used to characterize the current level of lunar tectonic activity.

The Doppler Gravity Experiment (DGE) uses Doppler tracking of S-Band radio signals to characterize the spacecraft orbit and determine the lunar gravity field. This data provides information on the lunar interior and, when combined with lunar topographic data, allow modelling of the global crustal asymmetry and structure, and any subsurface basin structure.

All the experiments can be found on the NSSDC Master Catalog, NSSDCA/COSPAR ID 1998-001A.

3.2.4 Kaguya

Kaguya (formerly SELENE, for SELenological and ENgineering Explorer), NSSDCA/COSPAR ID 2007-039A, was a Japanese Space Agency (JAXA) lunar orbiter mission. The primary objectives of the mission were a global survey of the Moon, obtaining data on elemental abundance, mineralogical composition, topography, geology, gravity, and the lunar and solar-terrestrial plasma environments, and to develop critical technologies for future lunar exploration by JAXA, such as lunar polar orbit injection, three-axis attitude stabilization, and thermal control. The mission consisted of three satellites: an orbiter containing most of the scientific equipment, a VLBI (Very Long Baseline Interferometry) Radio (VRAD) satellite, and a relay satellite designed to receive a doppler ranging signal from the orbiter when it was out of direct contact with Earth, to estimate the far-side gravitational field.

The mission module carried 13 instruments for use in science investigations: a multi-band imager, terrain camera, high-definition TV camera, spectral profiler, x-ray spectrometer, gamma-ray spectrometer, radar sounder, laser altimeter, magnetometer, plasma imager, charged particle spectrometer, plasma analyzer, and radio science equipment.

The VRAD (Very Long Baseline Interferometry Radio) subsatellite, Ouna (also designated Vstar), was an octagonal cylinder with a dipole antenna. It was spin-stabilized at 10 rpm with no propulsion units. It held one X-band and three S-band radio sources. The satellite in conjunction with the relay satellite enabled differential VLBI observations from the ground. Ouna was released from Kaguya October 12, 2007, in a 127 x 795 km polar orbit. Telemetry command was terminated on 29 June 2009. The orbit is assumed to have decayed and Ouna crashed into the lunar surface at an unknown time and location.

The relay subsatellite, Okina, was similar to the Ouna VRAD satellite, an octagonal cylinder with a dipole antenna. Okina also had four small S-band patch antennas mounted on it, two on top and two on bottom. The spacecraft was also spin-stabilized at 10 rpm with no propulsion units. The relay subsatellite contained one X-band and three S-band VLBI radio sources and a transponder; it relayed the 4-way Doppler ranging signal between a ground station and the orbiter for the far side gravity field investigation from a 100 x 2400 km orbit. Okina impacted the Moon on 12 February 2009.

Kaguya (SELENE) launched on 14 September 2007 from Tanegashima Space Center. It made its first lunar orbit injection at on 3 October 2007 and entered a 101 x 11741 km lunar orbit. The spacecraft made 6 orbit-transfer maneuvers to lower the orbit to an 80 x 128 km polar science orbit by 19 October. During the transition to lower orbit, the relay satellite Okina was released into a 100 km x 2400 km polar orbit on 9 October at 00:36 UT and the VRAD satellite Ouna was released into a 100 x 800 km orbit on 12 October 2007.

Normal operations from orbit for the Kaguya spacecraft started on 20 October 2007, the 12-meter magnetometer mast, two 15-meter Radar Sounder dipole antennas, and the telescope gimbal were deployed between 28 and 31 October. Checkout of the subsatellites was completed by 5 November, check out of other instruments continued until the beginning of December. The 10-month nominal science mission began on 21 December 2007. The main orbiter maintained the near circular orbit for 10 months of science operations, using correction burns roughly every two months to maintain the orbit within 30 km of the 100 km nominal orbit. The nominal mission was completed at the end of October 2008, with coverage of over 95% of the surface. The 100 km orbital observations were extended for 3 months. The altitude was then lowered to a 50 (±20) km orbit, operations from this orbit started on 1 February 2009. On 16 April the perilune altitude was reduced to 10-to-30 km.

Kaguya ended its mission as planned, impacting the Moon on 10 June 2009 at 18:25 UT (3:25 a.m. June 11 Japan Standard Time) near 80.4 degrees east longitude, 65.5 degrees south latitude on the Earth-facing side of the Moon. The area was in darkness at the time of the impact, allowing observation of the impact flash from Earth.

Kaguya is named for Kaguya-hime (Princess Kaguya), a visitor to Earth from the Moon in a tenth century Japanese folk tale “Taketori Monogatari” (The Tale of the Bamboo Cutter). The relay satellites, “Okina” and “Ouna” are named after the old man and woman who find and adopt Kaguya-hime.

All the experiments can be found on the NSSDC Master Catalog.

3.2.5 LCROSS

The Lunar Crater Observation and Sensing Satellite (LCROSS) was designed to search for water ice on the Moon's surface by using a Centaur upper stage to impact with the Moon while observing the collision. The objective was to observe the resulting plume and to look for water or hydrated materials that would indicate water ice is present at or near the surface at the lunar poles. Initial analyses of the spectral data generated by LCROSS impact found water is present, even if only about one percent by mass, and later analyses increased that estimate to on the order of five percent.

The mission consisted of a Shepherding Spacecraft (S-S/C) attached to the Centaur upper stage. The S-S/C took images and collected other data on the impact and cloud of ejecta for approximately four minutes as it flew through it before also striking the Moon. The S-S/C was equipped with two visible cameras, three infrared cameras, three spectrometers, and a photometer for observations.

Experiments and resulting data are available on the NSSDC Master Catalog, NSSDCA/COSPAR ID 2009-031B.

3.2.6 GRAIL

The Gravity Recovery And Interior Laboratory (GRAIL-A and GRAIL-B, NSSDCA/COSPAR IDs 2011-046A and 2011-046B) mission was a dual spacecraft project designed to study the lunar interior structure and the thermal evolution of the Moon. Several primary science objectives were to: map the structure of the crust and lithosphere; understand the Moon's asymmetric thermal evolution; determine the subsurface structure of impact basins and the origin of mascons (mass concentrations that affect the local gravitational pull), ascertain the temporal evolution of crustal brecciation and magmatism; constrain deep interior structure from tides; and place limits on the size of the possible inner core.

Refer to the NSSDC Master Catalog for all the experiments and resulting data.

3.2.7 Chandrayaan 1, 2, and 3

Chandrayaan 1, NSSDCA/COSPAR ID 2008-052A, was an Indian Space Research Organization (ISRO) mission designed to orbit the Moon over a two-year period with the objectives of upgrading and testing India's technological capabilities in space and returning scientific information on the lunar surface. Data was collected by star sensors, accelerometers, and an inertial reference unit. Telecommands were attained via S-band and science data transmission via X-band.

The scientific payload consisted of a Terrain Mapping Camera (TMC) used to produce a high-resolution map of the Moon, a Hyper Spectral Imager (HySI) to perform mineralogical mapping, a Lunar Laser Ranging Instrument (LLRI) to determine the surface topography, and an X-ray fluorescence spectrometer containing three components: an Imaging X-ray Spectrometer (CIXS), a High Energy X-ray/gamma ray spectrometer (HEX), and a Solar X-ray Monitor (SXM) to detect solar flux. CIXS was used to map Si, Al, Mg, Ca, Fe, and Ti at the surface, while the HEX measured U, Th, 210Pb, 222Rn degassing, and other radioactive elements, and the SXM monitored the solar flux to normalize the results of CIXS and HEX.

Additional instruments included the Sub-keV Atom Reflecting Analyzer (SARA), a Moon Mineralogy Mapper (M3) and a near-infrared spectrometer (SIR-2) to also map the mineral composition using an infrared grating spectrometer. A Miniature Synthetic Aperture Radar (Mini-SAR) performed radar scattering and imaging investigations at the poles in a search for water ice. The Radiation Dose Monitor (RADOM-7) characterized the local radiation environment.

Chandrayaan 1 carried a Moon Impact Probe (MIP) that was released from the spacecraft and hit the lunar surface in late 2008. The MIP carried a video camera, a radar altimeter, and a mass spectrometer.

Chandrayaan 1 Mini-RF (Part of the broader NASA LRO mission) and Mini-SAR experiment descriptions and resulting data are available on the NSSDC Master Catalog.

Chandrayaan 2 was comprised of an orbiting propulsion module and a soft lander carrying a rover. The primary objective was to demonstrate the ability to soft-land on the lunar surface and operate a robotic rover, a 6-wheeled vehicle based on the NASA Sojourner Rover. Scientific goals included studies of lunar topography, mineralogy, elemental abundance, the lunar exosphere, and signatures of hydroxyl and water ice. On September 6, 2019, the lander crashed on the surface in one piece, but communications and operations were not possible. The orbiter was designed for a mission life of one year and continues to operate as a relay satellite. No data from Chandrayaan 2 is publicly available at the time of this publication; see NSSDCA/COSPAR ID 2019-042A.

Chandrayaan 3 successfully completed the mission initially set for Chandrayaan 2. It put a lander and rover in the highlands near the south pole of the Moon on August 23, 2023, and demonstrated end-to-end landing and roving capabilities. It made a number of scientific measurements on the surface and from orbit.

Chandrayaan 3’s propulsion module was a box-like structure with one large solar panel mounted on one side and a large cylinder on top that acted as a mounting structure for the lander. Communication was via S-Band and attitude sensors included a star sensor, Sun sensor, and Inertial Reference unit and Accelerometer Package (IRAP). Like Chandrayaan 2, it carried a Vikram lander that was also generally box-shaped, with four landing legs and four landing thrusters. This second lander had an expanded sensor suite to ensure a safe touchdown, including an accelerometer, altimeters, Doppler velocimeter, star sensors, inclinometer, touchdown sensor, and cameras for hazard avoidance and positional knowledge. An X-band antenna was used for communication. The lander carried the rover in a compartment with a ramp for deployment onto the surface. The Pragyan rover had a rectangular chassis, mounted on a six-wheel rocker-bogie wheel drive assembly; it had navigation cameras and a solar panel that could generate 50 W for its own use, and it communicated directly with the lander via short-range antennas.

The Vikram lander carried an instrument called Chandra's Surface Thermophysical Experiment (ChaSTE) to measure surface thermal properties, the Instrument for Lunar Seismic Activity (ILSA) to measure seismicity around the landing site, the Radio Anatomy of Moon Bound Hypersensitive ionosphere and Atmosphere (RAMBHA) to study the gas and plasma environment, and a passive laser retroreflector array provided by NASA for lunar ranging studies. The Pragyan rover carried two instruments to study the local surface elemental composition, an Alpha Particle X-ray Spectrometer (APXS) and Laser Induced Breakdown Spectroscope (LIBS). The Propulsion Module / Orbiter had one experiment called the Spectropolarimetry of HAbitable Planet Earth (SHAPE) to study Earth from lunar orbit.

Chandrayaan 3 launched on July 14, 2023, on a heavy lift launch vehicle from Sriharikota, India, into an elliptic Earth parking orbit, followed by a number of maneuvers to send it to the Moon. On August 5, 2023, the spacecraft was placed into lunar orbit after which it maneuvered into a polar lunar orbit by August 17. The Vikram lander then separated and began powered descent, followed by a successful landing at 69.3741 S, 32.32 E. The Vikram rover was deployed on August 24, 2023, and the lander and rover conducted experiments on the surface as planned. The lander and rover were designed to operate for one lunar daylight period, about 14 Earth days, and they succeeded. On September 4, 2023, they entered sleep mode, from which they were not expected to recover. Efforts were still made to communicate with the rover and lander at the beginning of the next lunar sunlight period on September 22, 2023, and were unsuccessful.

Orbit-raising maneuvers brought Chandrayaan 3's propulsion module out of lunar orbit and into a high Earth orbit, demonstrating possible future sample return strategies for ISRO. The Propulsion module operated until August 22, 2024.

For the first time on the lunar surface, a laser beam from NASA's Lunar Reconnaissance Orbiter was broadcast on December 12, 2023, and reflected back by a tiny NASA-provided retroreflector on board the Vikram lander. The purpose of the experiment was to determine the retroreflector's surface location from the Moon's orbit. The Chandrayaan 3 lander's Laser Retroreflector Array (LRA) instrument now serves as a location marker close to the lunar south pole.

Chandrayaan 3 experiment descriptions are available on the NSSDC Master Catalog (2023-098A); no experimental data is publicly available at the time of this publication.

3.2.8 Danuri (KPLO)

Danuri, the Korea Pathfinder Lunar Orbiter (KPLO) listed as NSSDCA ID 2022-094A, is the first lunar mission of the Korea Aerospace Research Institute (KARI). It carries an array of South Korean experiments and one camera built by NASA. Its objectives are to develop South Korean lunar exploration technologies, demonstrate a "space internet", and conduct scientific investigations of the lunar environment, topography, and resources, as well as identify potential landing sites for future missions.

Danuri is equipped with five science instruments and a Disruption Tolerant Network experiment. The five experiments are a Lunar Terrain Imager (LUTI), a Wide-Angle Polarimetric Camera (PolCam), a Magnetometer (KMAG), a Gamma-Ray Spectrometer (KGRS), and a high-sensitivity camera developed by NASA (ShadowCam).

Danuri launched on 4 August 2022 and entered lunar orbit on 16 December 2022. After capture into an elliptical lunar orbit, it circularized to a 100 km nominal polar orbit (+/-30 km), from which it conducts science operations. After entering lunar orbit, the mission was extended by KARI for two more years based on the spacecraft's condition and remaining fuel. Danuri continues to take data.

Experiment descriptions are available via the NSSDC Master Catalog; no data collections are available as of this publication.

4.0 LUNAR SURFACE DATA PRODUCTS

4.1 FOUNDATIONAL PRODUCTS

Foundational lunar surface data products are essential descriptive elements built from the raw data collected by instruments described in Section 3. Foundational data products for lunar exploration have recently been described by Laura and Beyer (2021) and the joint Lunar Exploration Analysis Group (LEAG) and Mapping and Planetary Spatial Infrastructure Team (MAPSIT) Lunar Critical Data Products Specific Action Team (LEAG-MAPSIT, 2021). Some definitions of key foundational products are briefly summarized here based upon those sources. The intent of this section is to succinctly describe existing data products that are presently being used for mission planning purposes and provide information on relevant descriptive peer-reviewed publications and expedited ways of accessing relevant source data products.

When using raw data products independently to assess new proposed missions, users of this guide are advised to consult with the Artemis Geospatial Data Team (AGDT) to ensure the data is used appropriately. There are, for instance, some data sets that contain known artifacts of the process by which the data was gathered that the AGDT has developed ways to identify and account for by trial and error. Such artifacts limit the applicability of the data in ways that are not obvious. Refer to Appendix D for contact information for the AGDT.

4.2 VISIBLE IMAGERY & ALTIMETRY

While many subclassifications are possible, in general, visible wavelength imagery of the lunar surface (meaning observations produced by sensors designed to collect data in the visible spectrum wavelengths from 380 to 750 nanometers) can be broken down into three categories. The first two categories, Nadir Imagery (described in section 4.2.1) and Oblique Imagery (described in section 4.2.2), are defined based on the geometry of the camera relative to the surface from orbit. The third category, Image Mosaics (described in section 4.2.3), involves executing geodetic and cartographic processing to combine many smaller images into a larger mosaic useful for precision mapping and analyses. Figure 4.2-1 provides an idealized representation of sensor orientation relative to image geometries.

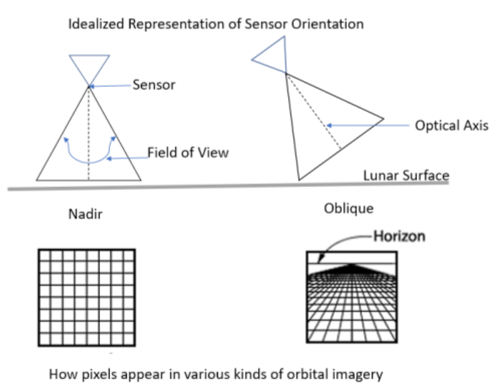

FIGURE 4.2-1 DEFINITIONS OF SENSOR ORIENTATION

4.2.1 Nadir Imagery

In aerial and satellite imagery, the nadir point is the ground directly beneath the center of the camera's lens or sensor detector. A nadir image is a satellite or aerial photo taken vertically of the nadir point and an unspecified extent around that point. Lunar nadir imagery is captured from orbit by the Narrow Angle Cameras (NAC) aboard LRO. Figure 4.2.1-1 is an example of nadir imagery produced by the LROC system.

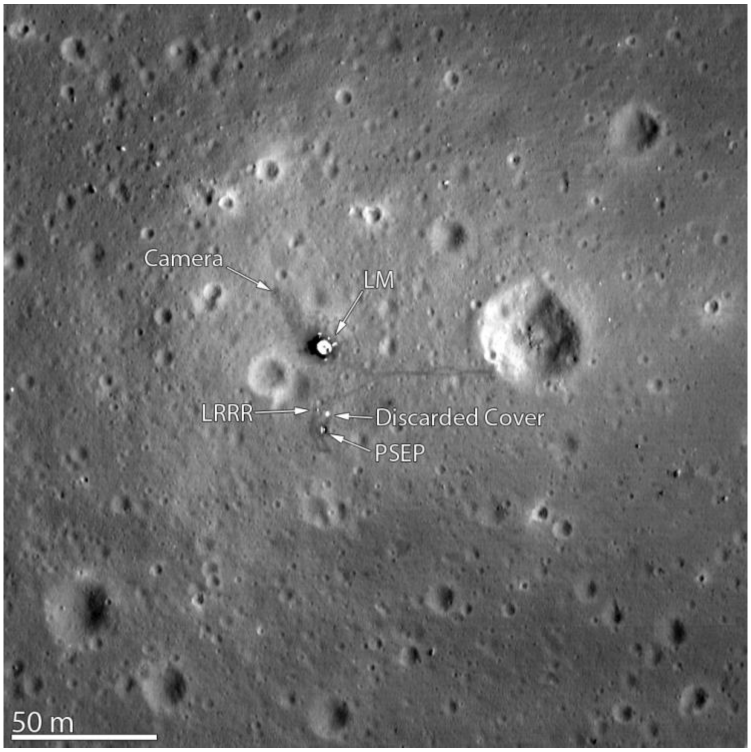

FIGURE 4.2.1-1 ANNOTATED EXAMPLE NADIR IMAGE OF THE APOLLO 11 LANDING SITE

Figure4.2.1-1 also shows human artifacts at Statio Tranquillitatis (Tranquility Base), imaged by LRO in 2011. The remnants of Armstrong and Aldrin's historic first steps onto the lunar surface are seen as dark paths.

4.2.2 Oblique Imagery

Oblique imagery is captured when the orbiting camera lens is canted off the surface normal, resulting in an oblique angle. A low oblique angle image shows only the surface, a high oblique angle image will also show the horizon. Although LROC is a body-fixed, nadir pointing instrument, with sufficient advance planning, LRO has the capability to roll the spacecraft to obtain oblique images with its Narrow Angle Camera system useful for context interpretation and validating lighting models. Figure 4.2.2-1 shows an example of an oblique NAC image.

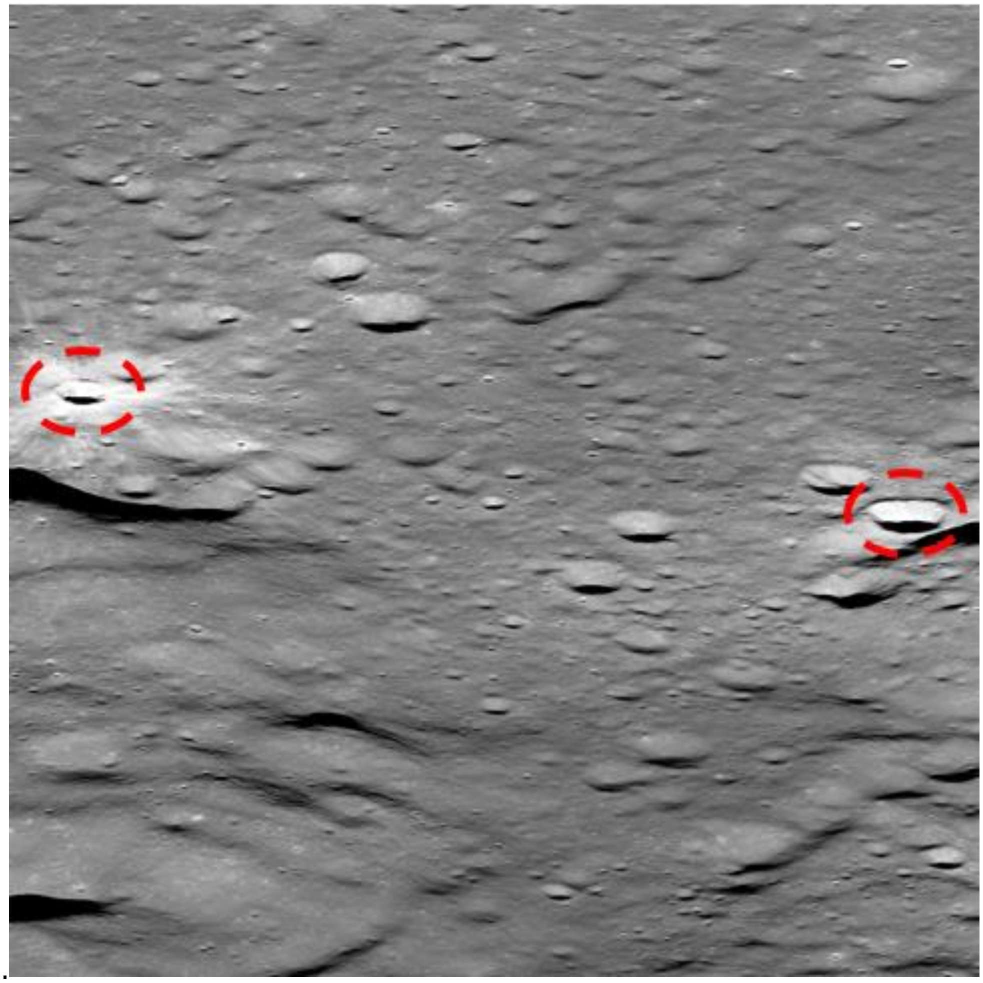

FIGURE 4.2.2-1 OBLIQUE LROC NAC IMAGE OF THE APOLLO 16 LANDING SITE

In Figure 4.2.2-1, the viewpoint is east to west. South Ray crater is center left and North Ray crater is center right. The distance between the two center craters is 10.5 km. This is a subset of LROC NAC M192817484LR [NASA/GSFC/Arizona], with dashed circles in red added to help identify the South Ray and North Ray craters.

4.2.3 Mosaics

A visible imagery mosaic is an assemblage of overlapping remotely sensed visible wavelength images whose edges have been matched cartographically to create a continuous photographic representation of a portion of the Moon's surface. There are three broad subcategories of image mosaics, uncontrolled, semi-controlled and controlled mosaics.

4.2.3.1 Uncontrolled Mosaics

An uncontrolled mosaic is comprised of images that have not been transformed to mitigate positional inaccuracies. For example, uncontrolled mosaics might feature visible seams, duplicated landforms and additional inaccuracies. Figure 4.2.3.1-1 is an example of an uncontrolled mosaic.

An uncontrolled mosaic of the south polar region has been assembled by the LRO Science Team using LRO NAC images and can be downloaded from the LROC subnode of the PDS Imaging and Cartographic Sciences Node (Viewing South Pole NAC Mosaic (https://wms.lroc.asu.edu/lroc/view_rdr/NAC_POLE_SOUTH))

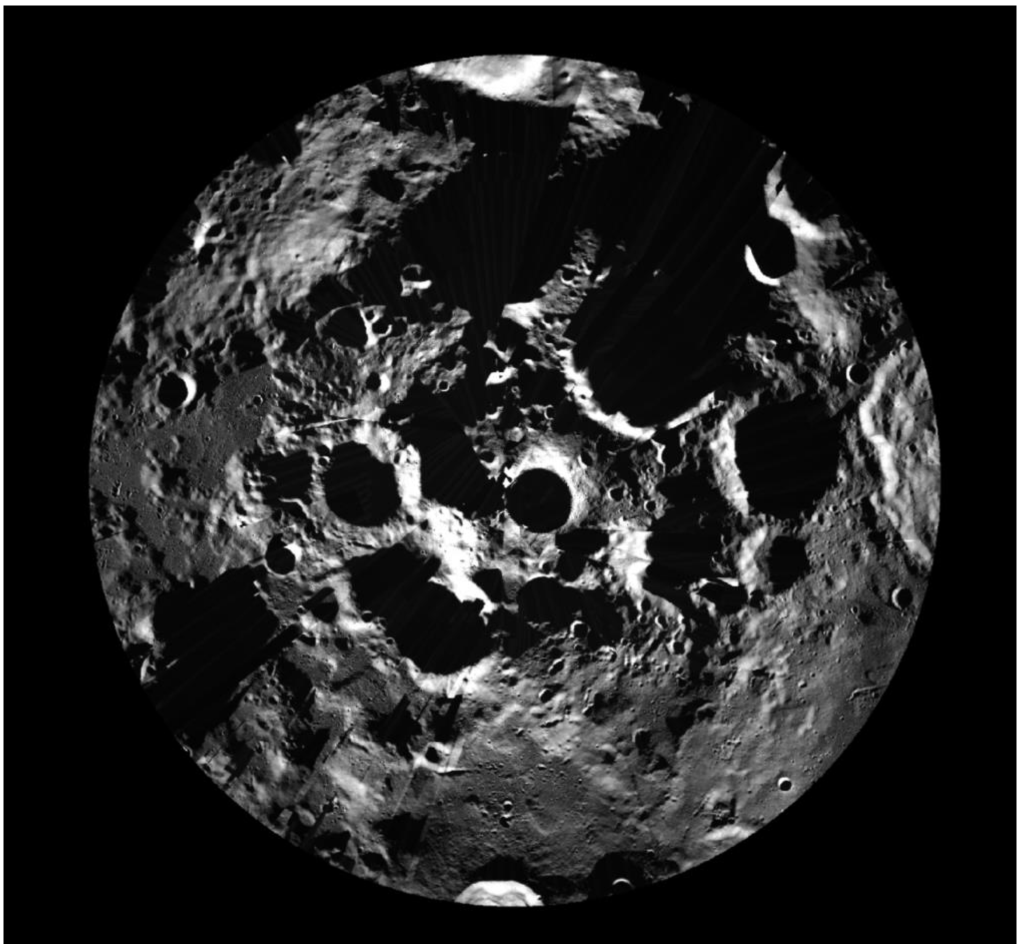

FIGURE 4.2.3.1-1 EXAMPLE UNCONTROLLED MOSAIC

Figure 4.2.3.1-1 is projected in polar stereographic, with a scale of 1 m/pixel from 85.5 - 90 degrees. It shows 1293 LROC NAC images of the south pole of the Moon.

4.2.3.2 Semi-Controlled Mosaics

A semi-controlled mosaic is comprised of images that have undergone a first-level transformation process to align the images to each other and the control source. Semi-controlled products are usually controlled via warping or “rubber-sheeting”, which does reduce positional errors, but is not as in-depth of a process as that seen in producing a controlled mosaic. A semi-controlled mosaic is an intermediate step in the process of getting to a controlled mosaic. As with many iterative processes, this is sometimes deemed “good enough” at semi- vs “perfect” at fully controlled due to resource utilization considerations. A fully controlled mosaic now exists for the entire lunar south pole after many years of work. **<FWD-30044-019>**

4.2.3.3 Controlled Mosaics

Controlled visible imagery mosaics are mosaics comprised of images that have been radiometrically, geometrically, and sometimes photometrically corrected to establish an accurate cartographic framework for regional areas of interest (e.g., Martin et al., 2019). Controlled mosaics produced by the LRO team are referred to as Feature Mosaics and are comprised of NAC images created on sequential orbits. The geodetic control process reduces locational uncertainty and ensures accurate distances can be measured from surface features found within the mosaic. An example of a controlled mosaic from a nonpolar region is provided as Figure 4.2.3.3-1. Controlled mosaics of LROC WAC frames for the south polar region have been produced by the LROC team (https://wms.lroc.asu.edu/lroc/view_rdr/WAC_ROI_SOUTH_SUMMER, South Pole WAC) and the US Geological Survey (available online at Moon Trek https://trek.nasa.gov/moon).

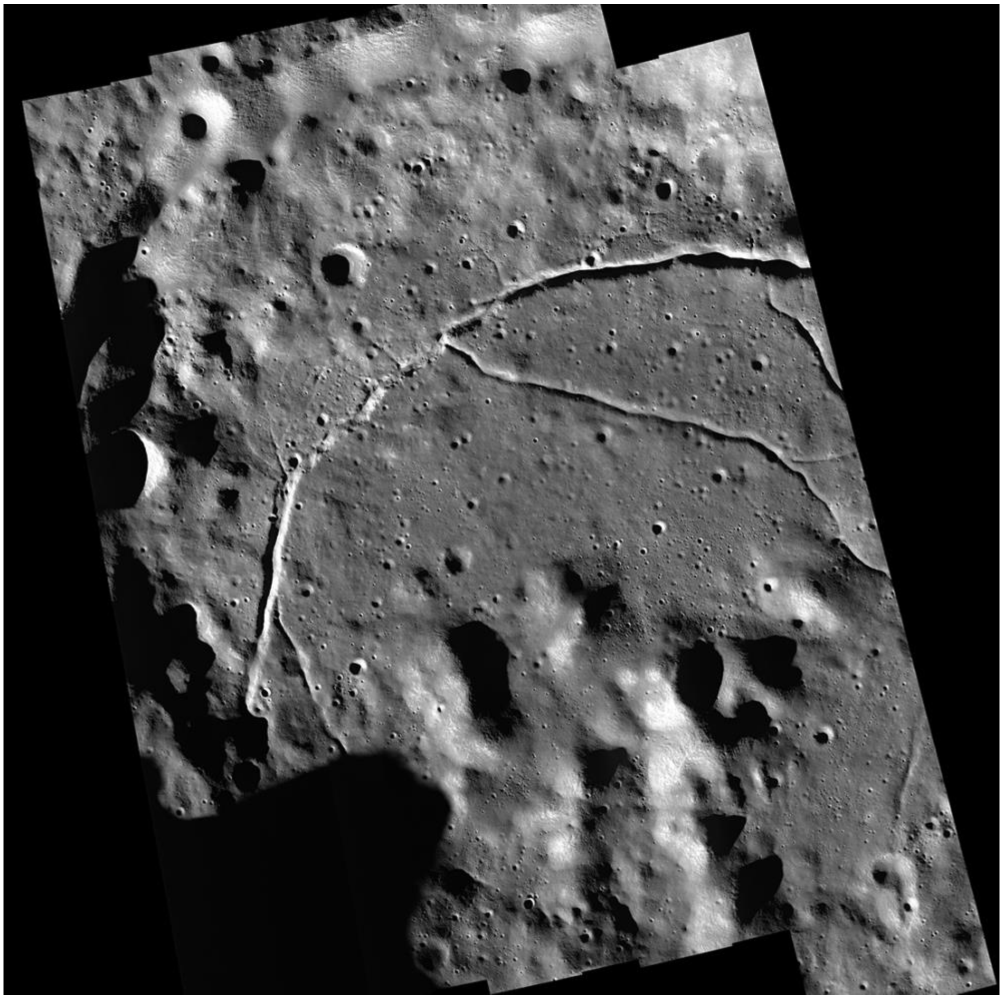

FIGURE 4.2.3.3-1 A SEAMLESS MOSAIC

Figure 4.2.3.3-1 shows part of Karpinsky Crater, located at 72.61 degrees N, 166.80 degrees East; scene is 55 km across and was processed from NAC images M130949659L/R, M1309503618L/R, M1309510644L/R, and M1309517669L/R.

4.2.4 Topographic Data Products

The shape of the lunar surface is described within several complementary topographic data products. Several high-quality topographic products are available for the lunar south pole described below. Topography is one of three primary classes of foundational data products as described in Laura and Beyer (2021).

Generally, there are three categories of terrain models, defined as follows:

- **Digital Elevation Model (DEM):** A digital representation of the topographic surface of a body that excludes natural or built surface objects.

- **Digital Terrain Model (DTM):** A digital representation of the topographic surface of a body that excludes natural or built surface objects but does include natural/built features as vector features.

- **Digital Surface Model (DSM):** A digital representation of the topographic surface of a body, including natural or built surface objects.

Currently, the lunar south pole does not host built surface objects. Preliminary mapping of natural surface objects has begun but is not yet formalized. For this reason, current topographic products are typically DEMs, although this is expected to change with future surface characterization and activity. Topographic products from several sources are described in the following subsections. Where topographic products are not available or do not provide sufficient resolution, synthetic terrain models may be generated using the statistical descriptions of the lunar surface found in DSNE Section 3.4.1.

4.2.4.1 South Pole LOLA DEM Mosaic

The shape of the lunar surface is directly measured from orbit by the Lunar Orbiter Laser Altimeter. Point measurements are then interpolated into gridded data products. Because of the orbit of LRO, LOLA points are densely clustered at high latitudes, enabling gridded topographic maps at 5 meters per pixel resolution covering much of the South Pole.

This 5 m/pixel product represents a significant improvement over previous LOLA releases. By iteratively co-adjusting the LOLA tracks in a self-consistent fashion, orbital errors were reduced by over a factor of 10 such that the new track geolocation uncertainty is about 10 to 20 cm horizontally and about 2 to 4 cm vertically over each region. The new 5 m/pixel Lunar Digital Elevation Model (LDEM) is substantially more realistic than previous products with fewer artifacts due to orbital errors and fewer spurious noise points. While the fraction of interpolated 5-meter pixels in this polar LDEM is necessarily large (about 90%) due to LOLA's cross-track and inter-spot spacing, this LDEM has the advantages of having accurate geodetic control and being unaffected by shadows, and, thus, will be complementary to higher-resolution topographic models derived solely from imagery.

This product was constructed from 97 individual 20 x 20 km fields with 2 km overlaps. Each field was processed with the same method as described in Barker et al. (2021). The fields were then individually aligned to the original DEM with a rigid 3-D translation and blended with a cosine taper weight in the overlap regions. The LOLA count maps of the individual fields were blended in the same way. Hence, non-integer counts exist in the overlap regions of the final assembled mosaic product.

The LDEM height and slope uncertainties have a median RMS-Z error 0.30 to 0.50 m (see Barker et al (2021) for a full description of source data and error deviation). Interpolation error depends primarily on gap size, or areal density of the LOLA points, with a secondary dependence on terrain slope that becomes more important over highly sloped terrain. Hence, the interpolation error will be larger at greater distances from the pole for the same pixel scale, because of the lower point density and poorer effective resolution.

Metadata products such as count maps and RMS error maps are available. Interpolation errors are quantifiable and manageable.

The LOLA DEM products are the foundation for all LRO data products; all LROC images are controlled to the LOLA dataset.

A mosaic covering all latitudes poleward of 87 degrees S is available in the Planetary Geodesy Data Archive (PGDA), here:

PGDA - South Pole LOLA DEM Mosaic (https://pgda.gsfc.nasa.gov/products/81, referred to hereafter as the South Pole LOLA DEM, short name and link also listed in Appendix C, Table C1-3.)

Large-Area DEMs are now also available on PGDA, https://pgda.gsfc.nasa.gov/products/90.

Several additional sites of interest are available here:

PGDA - High-Resolution LOLA Topography for Lunar South Pole Sites (https://pgda.gsfc.nasa.gov/products/78), hereafter referred to as the South Pole LOLA Hi-Res, referred to hereafter as the South Pole LOLA Hi-Res, short name and link also listed in Appendix C, Table C1-3..

A full description of data source calibration/corrections and error deviations is available in Barker et al (2021).

Additional LOLA DEM products covering the wider polar regions are available through the Planetary Data System (https://pds-geosciences.wustl.edu/lro/lro-l-lola-3-rdr-v1/lrolol_1xxx/data/lola_gdr/polar/), Polar LOLA DEM.

4.2.4.2 LROC NAC DTM: Stereo Observations

The two Narrow Angle Cameras aboard LRO were not designed as a stereo imaging system. However, stereo observations can be acquired over two or more orbits by slewing the spacecraft (Robinson et al., 2010). Globally, a number of these “stereo pairs" have been collected, comprising approximately 3% of the lunar surface. As described in Henriksen et al. (2017), these pairs are then reduced into Digital Terrain Models at the 2 to 4 meters per pixel scale using a consistent set of procedures leveraging the SOftCopy Exploitation Toolkit (SOCET SET) software from BAE systems in combination with the United States Geological Survey (USGS) Integrated Software for Imagers and Spectrometers (ISIS) (Anderson et al., 2004, and Keszthelyi et al., 2013). By enabling quantitative investigations of elevation, slope, volume, and roughness, complex scientific questions and engineering site suitability assessments can both be comprehensively addressed, rendering NAC DTMs invaluable for both engineering and scientific purposes.

These products offer spatial resolution of up to 2 to 4 meters per pixel, with vertical accuracy of less than 1 meter and horizontal accuracy of less than 10 meters.

As of May 2022, three LROC NAC stereo observations have been processed and published in publicly available DTMs and can be downloaded from the LROC subnode of the PDS Imaging and Cartographic Sciences data node:

Terrain Between Nobile and Malapert craters (https://wms.lroc.asu.edu/lroc/view_rdr/NAC_DTM_NOBILE01), Nobile to Malapert LROC DTM.

Peak near Spudis crater on the Shackleton-deGerlache connecting ridge (https://wms.lroc.asu.edu/lroc/view_rdr/NAC_DTM_SHACKRDGESM). (No longer available directly in September 2024, Shackleton-deGerlache Connecting Ridge DTM remains accessible, https://wms.lroc.asu.edu/lroc/view_rdr/NAC_DTM_SHACKRDGE02.)

Malapert Massif LROC DTM (https://wms.lroc.asu.edu/lroc/view_rdr/NAC_DTM_ESALL_MP1).

In addition, as a deliverable for project Constellation, NAC stereo observations for a large area comprising the rim of Shackleton over to the peak near the rim of Spudis crater have been processed and published as a large high-resolution DTM with 4 meter postings, which can be downloaded here:
https://astrogeology.usgs.gov/search/map/Moon/LRO/MOON_LRO_NAC_DEM_89S210E_4mp (No longer available directly in September 2024.)

There is limited potential to collect the additional observations required to enable the creation of additional polar DTMs in other locations near the geographic lunar south pole because of LRO orbital constraints. To request additional LROC imagery of the south polar region, use the data request process in Appendix D.

4.2.4.3 LROC NAC DEM: Photoclinometry

The principle of photoclinometry, also called "Shape from Shading" or SfS, is that nadir images with different lighting conditions (solar incidence and azimuth) can enable mathematical solutions to determine the shape and topography of the illuminated surface. As described by Alexandrov and Beyer (2018), SfS can be used to establish Digital Terrain Models from NAC frames with consistently higher spatial resolution (about 1-2 m/pixel) than that provided by the conventional SOCET SET approaches described in Section 4.2.4.2. These are produced using NAC images and photoclinometry processing, with the LOLA 5 m/pixel product as a basis. This product reverts to LOLA data for unilluminated areas in NAC images.

The quality of this product, which includes an SfS DTM, a maximally lit orthomosaic, and individual orthoimages of each imported NAC image, is limited by the availability of NAC coverage and illumination conditions. A small number of SfS models have been created to support uncrewed NASA missions to the poles. Creation of additional SfS models can be supported if sufficient NAC images with appropriate properties are available for the region of interest; please contact the Artemis Spatial Data Lead, or the SfS model development lead, for additional information, using the data request process in Appendix D.

4.2.5 Compilations

Due to advancements in computing over the decades spanned by collection of these data sets, we now have the ability to layer data from several missions. See ACT Lunar/LROC Quickmap, https://quickmap.lroc.asu.edu/?prjExtent=-3555341.7218543%2C-1737400%2C3555341.7218543%2C1737400&layers=NrBsFYBoAZIRnpEBmZcAsjYIHYFcAbAyAbwF8BdC0yioA&proj=10, and Moon Trek hosted by JPL https://trek.nasa.gov/moon/ for user-friendly mapping.

4.3 DERIVED IMAGERY & ALTIMETRY PRODUCTS

Derived products are created by leveraging foundational products to interrogate or emphasize specific attributes of the surface. Software packages exist, such as Geospatial Data Abstraction Library (GDAL (https://gdal.org/index.html), GDA Library), that can programmatically generate the products from topographic data. For example, see GDAL DEM (https://gdal.org/programs/gdaldem.html) for instructions on how to create the products discussed in this section. Products and methods that are already created for the lunar south pole are provided where available.

4.3.1 Slope Map

Slope maps are raster products that capture the angle between the observed surface and a horizontal reference plane. These can be derived from any topographic data product using a variety of algorithms at the desired spatial baseline. Slope maps can be used to identify surface hazards relevant to terrain use as well as to characterize geological attributes.

Slope maps for the lunar south pole (latitudes > 87 deg. S) are currently available at 5 m/pixel and are accessible as the South Pole LOLA DEM. Additionally, the LRO has made regional variations of the larger 5m/pixel product covering only specific regions of interest. These regional products are available at the PGDA South Pole LOLA Hi-Res. These slope products have median RMS errors of 1.5 to 2.5 degrees. Slope derivation and error analyses are fully described in Barker et al (2021).

4.3.2 Shaded Relief Map (Hillshade)

Shaded Relief Maps, also known as Hillshade Maps, are raster images generated by modeling illumination from an artificial light source across a topographic data product. These depict surface relief using shading to emphasize changes in surface elevation using artificial light and shadows on terrain from a specified angle and altitude of the sun.

Hillshade maps can be generated from any available topographic data product using standard tools in GIS software, including commonly used software packages such as the Geospatial Data Abstraction Library, ESRI’s ArcGIS, and QGIS. Hillshade maps for the lunar south pole (latitudes poleward of 87 degrees) generated from the South Pole LOLA DEM Mosaic are available at the PGDA - South Pole LOLA DEM.

This 5 m/pixel hillshade product was generated using the GDAL hillshade tool (GDAL DEM) with a solar incidence angle of 45 degrees from vertical and an azimuth angle of 45 degrees. Note: This is a physically unrealistic solar incidence angle for lunar polar regions but provides a good overview of local topographic relief.

For more information on illumination modeling, refer to Section 5.1.

4.3.3 Surface Roughness Analyses

Surface Roughness analyses encompass a broad array of surface characterization techniques relevant to describing the degree of variation in elevation across local scales. It is useful for understanding terrain hazards and traversability, as well as geological unit differentiation.

Surface Roughness can be estimated and reported through a variety of techniques and spatial scales. In general, surface roughness is either calculated directly from topographic data, or determined through either photometric assessment of imagery data or determined from radar data. Here, we summarize applications of various techniques.

4.3.3.1 Surface Roughness Products

Surface roughness can be estimated directly from topographic data products using a variety of techniques. The minimum spatial resolution and baseline for the roughness product is limited by the resolution of the topographic data. In general, estimates of surface roughness derived from topographic data are closely correlated with the slope determined for a terrain.

A commonly used metric to assess surface roughness is the Terrain Ruggedness Index (TRI), a measure of elevation variability between a central pixel and its neighboring eight pixels, using a technique similar to Horn’s method. Current pixel resolutions are not yet sufficient for TRI to be useful to lunar surface mission planning.

4.3.3.2 Estimates from Imagery

Surface roughness can also be estimated from imagery and radar measurements, offering measurements at different spatial resolutions independent of topographically derived products. Roughness estimates can be determined in several ways:

<u>Phase ratio observations:</u> Planetary surfaces exhibit light backscattering and forward scattering properties based on particle size, distribution, and orientation. In other words, surface roughness affects the phase function of a material, meaning that surfaces with different roughness characteristics will scatter light differently. Ratios of images taken at different phase angles (co-registered images captured with different incident / emission angles) suppress the signal from albedo variations, emphasizing differences in roughness and related physical properties. This technique is sensitive to roughness differences at the scale of the incoming light wavelength, which in principle can enable characterization of roughness on spatial scales significantly smaller than the spatial resolution of imagery data (e.g., Kaydash et al., 2012).

<u>Large incidence angle imagery:</u> Imagery taken with large solar incidence angles (about 55 to 80 degrees) includes significant shadowing and shading from topographic facets. Assuming similar

albedo distributions, measurements of standard deviation in pixel values correlate with surface roughness, i.e., a rougher surface will include more shadows than a smoother surface and therefore be associated with a higher standard deviation in pixel brightness. This technique estimates surface roughness at spatial scales tied to imagery data. For instance, LROC WAC images can be used as a proxy for roughness at 500 m scales, while LROC NAC images can be used as a proxy or roughness at 2.5 m scales. This technique is useful where stereo pairs and/or phase ratio observations are unavailable.

Radar Measurements: Radar instruments measuring the lunar surface detect changes in signal polarization, which can be modified by interaction of the radar wave with the lunar surface during surface reflection and subsurface scattering. The Circular Polarization Ratio (CPR) provides a quantitative measure of changes in polarization, and is strongly correlated with surface roughness at various scales, most strongly at about 100 m (e.g., Jawin et al., 2014)

4.3.4 Aspect-Slope Map

Aspect-Slope maps simultaneously show the aspect (direction) and degree (steepness) of slope for a terrain. These can be derived from any topographic product using standardized functions such as the gdaldem routines that are built into the GDAL software (https://gdal.org/programs/gdaldem.html?highlight=aspect+slope), GDAL Aspect Slope Map.

4.3.5 Illumination Maps

Reserved. **<FWD-30044-001>**

4.3.6 Earth Visibility Maps

Reserved. **<FWD-30044-002>**

4.3.7 Hazard Maps

Reserved. **<FWD-30044-003>**

4.4 LUNAR SURFACE GEOPHYSICAL PROPERITES

Geophysical properties are detailed in SLS-SPEC-159 Design Specifications for Natural Environments (DSNE) sections 3.4.1-3.4.2.

4.5 LUNAR SURFACE PLASMA ENVIRONMENT

The surface plasma environment is detailed in DSNE section 3.4.3.

4.6 LUNAR REGOLITH ELECTRICAL PROPERTIES

Electrical properties of the lunar regolith are listed in DSNE section 3.4.4.

4.7 LUNAR REGOLITH OPTICAL PROPERTIES

Optical properties of the lunar regolith are listed in DSNE section 3.4.5.

4.8 LUNAR THERMAL ENVIRONMENT

The lunar thermal environment for assets on the surface is driven by radiation from the sun, reflection and re-radiation from the lunar surface, and conduction of the surface in contact with hardware. At high latitudes, especially at the north and south pole, local topography and seasonal variations drive the thermal environment to extremes. General thermal properties of the lunar regolith are provided in DSNE section 3.4.6 to be used in analysis of thermal behavior of systems operating on the lunar surface. The provided tables of values are intended to be used as bounding design-to cases; the figures are provided for qualitative understanding.

Section 3.4.6.1 provides equations to be used to calculate the specific thermal properties at the location (latitude) of interest to the user: reflected sunlight, solar albedo, absorptivity and emissivity of the regolith, emitted longwave infrared radiation of the regolith (re-radiation of heat from sun), and how to best approximate daytime surface temperatures in any given location. A table of extremes is provided in section 3.4.6.3, ranging from 18 K (-255 C, -427 F) in permanently shadowed regions to 394 K (121 C, 250 F) at noon at the equator.

Section 3.4.6.2 describes lunar regolith in parameters necessary for analysis of heat transfer to and from the regolith. Values for conductivity, heat capacity, diffusivity, and bulk density are provided.

Section 3.4.6.3 goes into deeper detail about the ambient surface temperature, and 3.4.6.4 provides a qualitative discussion of the variation of temperature with depth into the regolith.

4.9 LUNAR IONIZING RADIATION ENVIRONMENT

The ionizing radiation environment is described in DSNE section 3.4.7. **<FWD-30044-012>**

4.10 LUNAR METEOROID & EJECTA ENVIRONMENT

The meteoroid and ejecta environment is described in DSNE section 3.4.8. **<FWD-30044-013>**

4.11 GEOLOGICAL MAPS

Reserved. **<FWD-30044-004> <TBD-30044-001>**

4.12 MINERALOGICAL MAPS

Reserved. **<FWD-30044-005>**

5.0 MODELING ANALYSES AND ASSUMPTIONS

Direct observational knowledge of surface features at proposed landing sites remains at the scale of meters per pixel. Every lander has a limit to the size of feature on which it can safely land. Given enough data from landing site observations and lander capability, feature measurements and lander robustness could be brought to agreement; this is shown qualitatively in Figure 5.0-1 below.

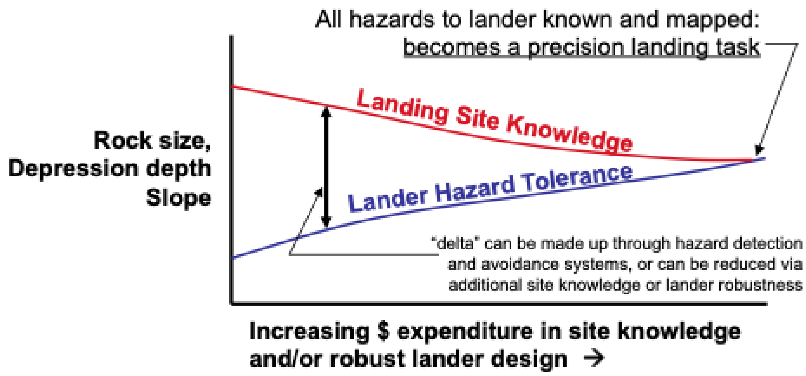

Site Knowledge vs. Lander Tolerance Continuum

FIGURE 5.0-1 SITE KNOWLEDGE VS. LANDER TOLERANCE

The difference between the size of feature a lander can safely set down on and the resolution of features at the landing site can be mitigated in three ways: either the lander can be made more robust, the feature size can be further resolved, or the lander can implement hazard detection and avoidance.

The capability to process lunar surface data to a resolution that provides adequate hazard mapping varies by location on the surface. Some regions will require a lander to have a higher hazard tolerance, or higher hazard avoidance capability, than others, even with tightly resolved feature size, due to the size of the features present. To resolve feature size, models are refined and analyzed, and assumptions are made, as described in the subsections below.

5.1 LOLA ILLUMINATION ANALYSIS

The LRO LOLA Instrument team has leveraged the LOLA dataset to simulate average illumination conditions over the 18.6-year lunar precession cycle (Mazarico et al., 2011). Illumination models leverage local topography with the orbital positions of the Earth, Moon, and Sun to derive illumination conditions across the lunar surface at a specified time or time range. These models may also consider surfaces that are illuminated through "double-bounce" photons (i.e., a surface may not experience direct illumination but may be secondarily illuminated by light reflected from local terrain). LOLA south polar models and additional background information are available at the
PGDA – Lunar Polar Illumination (https://pgda.gsfc.nasa.gov/products/69)

These models are available at 240 meters per pixel for latitudes above 65, 120 m/pixel for latitudes above 75, and 60 m/pixel for latitudes above 85. Currently, several types of illumination model are available at the PGDA link supplied above:

- **Solar Illumination:** This product indicates the percentage of model timesteps where a pixel was sunlit by any fraction of the solar disc.
- **Earth Visibility:** This product indicates the percentage of model timesteps where a pixel was lit by any fraction of the Earth disc.
- **Sky Visibility:** This product indicates the solid angle of sky not obscured by topography visible from each pixel.
- **Permanent Shadow:** This product indicates areas receiving no sunlight over the 18.6-year lunar precession cycle.

Using similar techniques, higher-resolution products (5 m/pixel) can be requested for a specified time or time range and/or elevation above the surface (please contact the SMD Artemis Spatial Data Lead, for additional information using the process in Appendix D). For example, solar illumination at 5 m above the surface of the local and surrounding terrain may be a relevant product for planning solar power arrays. More nuanced models can also be produced accounting for scattered light, percentage of visible solar/Earth disc, and/or accounting for time variability in Earthshine or solar flux.

The revised LOLA DEM products and processing methodology are described in Barker et al., (2021). More information about the derivation and properties of these models including detailed data descriptions are in the database label (LBL) files on the PDS available at the PGDA – South Pole LOLA DEM.

5.2 EARTHSHINE MAP

Earthshine is affected both by position relative to the local horizon and time-variable intensity. As defined in Glenar et al. (2019), in the context of lunar exploration, earthshine is the combined irradiance from reflected sunlight and thermal emission from Earth that illuminates the Moon. See Figure 5.2-1 for an example of an earthshine map.

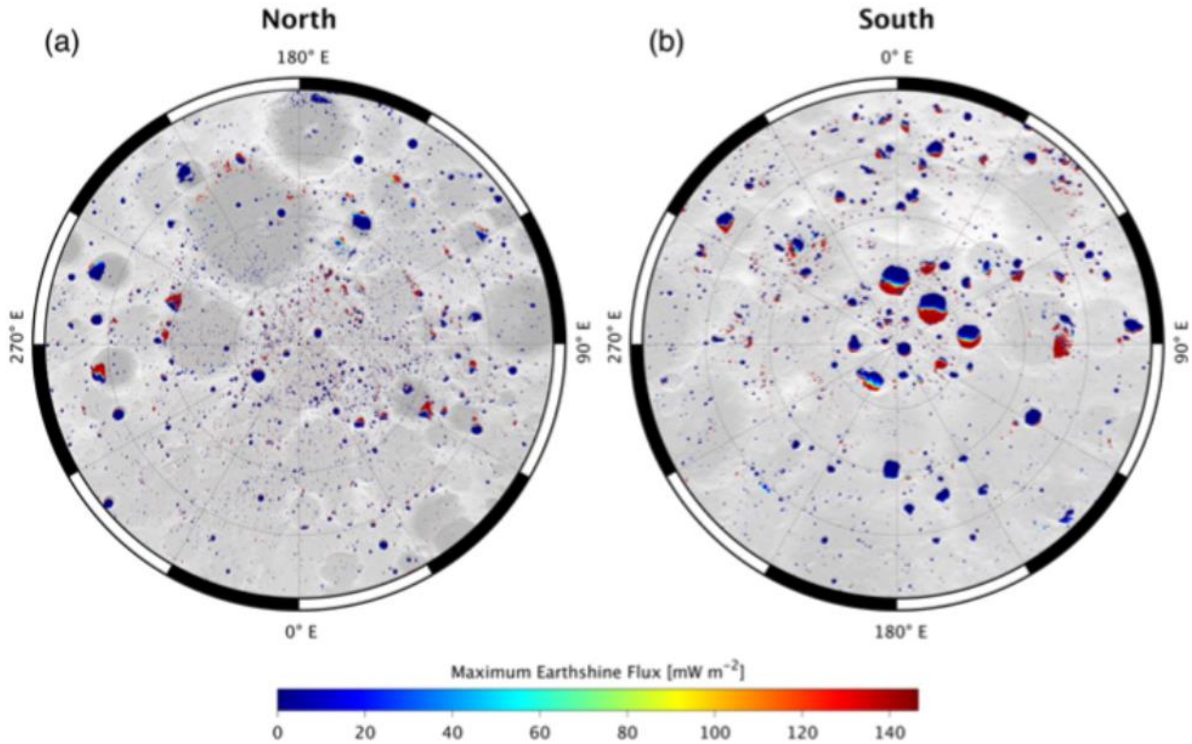

FIGURE 5.2-1 MAXIMUM EARTHSHINE FLUX INCIDENT ON POLAR PSRS

Figure 5.2-1 shows the Maximum Earthshine Flux incident on Lunar PSRs at the North Pole (a) and South Pole (b) across one 18.6-year Lunar Precessional Cycle, reproduced from Kloos & Moores (2019). The earthshine flux is overlaid on topography (grayshade).

5.3 ASSUMPTIONS

Where analytical data is not available, assumptions must be made. Common generalizations are listed here:

1. Crater diameter-to-depth ratio is 1m:10cm, or 10 cm of depth for every 1 meter of width (diameter) for craters smaller than 40m across. Larger craters are described in the DSNE, Table 3.4.1.2-1. Crater lifetimes are explored by Fassett et al (2022).

2. Boulders – referred to as “blocks” on the Moon – appear as bright, sun-facing, positive relief features; the smallest identified with confidence are 1-2 meters. Refer to Watkins et al. (2019). Lunar Surface Rock and Rock Size Distributions for > 1m rocks are defined in DSNE Section 3.4.1.4.

3. Debris size varies predictably from the rim of a crater going out from the crater, with larger blocks and more coarse debris at the rim of each impact crater, and smaller blocks and less coarse debris radiating out. (Melosh, 2011)

4. Current knowledge or data from previously explored portions of the moon will be used as assumptions when detailed information for unexplored areas is missing/unavailable.

6.0 LUNAR TERRAIN CHARACTERISTICS

Please refer to NASA-STD-1008, Classifications and Requirements for Testing Systems and Hardware to be Exposed to Dust in Planetary Environments, for test guidelines and other collated data throughout its sections. NASA-STD-1008 speaks to plume surface interactions, trafficability, and characteristics of hazards, supplementing the discussions in this section.

6.1 GENERAL CHARACTERISTICS

The following tables describe characteristics inherent to the lunar south pole region, defined in the 2020 NASA Lunar Exploration Plan (more formally, NASA's Lunar Exploration Program Overview, https://www.nasa.gov/sites/default/files/atoms/files/artemis_plan-20200921.pdf) as the region within six degrees of latitude of the geographic lunar south pole, and are provided as a reference for vehicle design in correlation with system requirements. Global slope distribution data, that is also applicable at the south pole, is available in SLS-SPEC-159, Design Specifications for Natural Environments, for design purposes.

The lunar south pole terrain incorporates the following discrete features, in Tables 6.1-1 and 6.1-2, where (+ or -) means upslope/downslope.

TABLE 6.1-1 SLOPES INHERENT TO LUNAR SOUTH POLE REGION

Max Slopes (°)	% South Pole Surface Area with these Slopes
0-5 (+ or -)	25%
5-10 (+ or -)	32%
10-15 (+ or -)	23%
15-20 (+ or -)	12%
20+ (+ or -)	8%

Approximate areal extent of terrain with stated slopes (over a 5 m baseline) are derived from the South Pole LOLA DEM Mosaic covering latitudes poleward of 87 deg. S. The derivation of this slope map is discussed in greater detail in section 4.3.1, and the DEM is described in section 4.2.4.1. The slope map was derived using Horn’s method and is available at 5 m/pixel with a median RMS slope error 1.5 - 2.5°. More information on source data, slope derivation, and error estimation is available in Barker et al (2021) and at PGDA - South Pole LOLA DEM and PGDA - South Pole LOLA Hi-Res.

TABLE 6.1-1 LUNAR REGOLITH TRAFFICABILITY PARAMETERS FOR APOLLO LRV SIMULATIONS

Symbol	Description	Value from Lunar Sourcebook
n	Exponent of sinkage	1
kc	Cohesive modulus	1400 N/m2
kϕ	Frictional modulus	830,000 N/m3
ϕ	Angle of internal friction	35 degrees
c	Cohesive strength of soil	170 N/m2
γ	Soil weight density	2470 N/m3
K	Coefficient of soil slip	0.018 m
NOTE: These values were produced to support model analysis of the Apollo Lunar Roving Vehicle from equatorial region Surveyor data. Their orders of magnitude were confirmed by the Apollo missions. These are not actual measured values and are here as reference only. Actual design and analysis values are dependent on vehicle size and load, therefore it is incumbent on mission designers and vehicle developers to identify the appropriate model parameters for their own applications, such as Plescia (2016) and Connolly (2023). The DSNE Table 3.4.2.3-1 provides measured mechanical properties of lunar regolith which can serve as a source to help derive appropriate model parameters.		

Tables are derived from Lunar Sourcebook (Heiken et al., 1991), Bulk geotechnical properties of regolith at the South Pole are so far observed to be in-family with the Equatorial Region. Lunar regolith characteristics vary, including the potential for ice mixing with regolith in/near Permanently Shadowed Regions (PSRs), and from crater rim to slope to floor. For further clarification reference the Cross-Program Design Specification for Natural Environment (DSNE), SLS SPEC-159, Section 3.4.2 Lunar Regolith Properties.

The Trafficability Parameters presented in Table 6.1-2 are “Bekker values” derived for terramechanics modeling of rovers on the lunar surface: these represent one case and are not encompassing of the range of conditions expected on the Moon. They were selected to create a virtual terrain case for modeling the Apollo Lunar Roving Vehicle, derived from Surveyor data and simulants in use at that time for the equatorial region. As of yet, no true “Bekker values” have been collected on the lunar surface. The terrain at the south pole may be different, and Bekker values are highly dependent on wheel sizes and loads, not just the terrain itself. There is high variability from test to test, so even when we do get measured values, it will be important to account for a range.

6.2 CHARACTERISTICS SPECIFIC TO INTERACTION WITH THE SURFACE

Actions such as vehicles landing, rovers traversing, or crew walking change the physical characteristics of lunar regolith.

6.2.1 Plume-Surface Interaction

Vehicles that make use of rocket engines during landing, ascent, or near-surface operations create an exhaust plume that will interact with the surface beneath the vehicle. These Plume-Surface Interactions (PSI) are affected by local surface properties (e.g., regolith particle-size distribution, porosity), vehicle configuration (e.g., number and location of engines), and vehicle operations (e.g., actual descent trajectory or engine throttling). PSI may pose hazards to the lander itself, crew, and nearby assets. PSI may modify surface topography, alter the physical properties of regolith, and deposit chemical products in the vicinity of the lander. These effects have implications for traverse planning, sampling, and the deployment of surface payloads. Use the process defined in Appendix D to request communication with the teams that model PSI.

The Moon is covered in rocky, unconsolidated, granular material called regolith. It consists of dust, sand, gravel and cobble-sized objects. Particle-size distributions for the lunar regolith may be found in the DSNE, Section 3.4.2.2.1 for particles from one micrometer to one centimeter (derived from Apollo samples, many of which are documented in the 1993 Graf Lunar Soils Grain Size Catalog) and Section 3.4.1.4 for rocks from one millimeter to two meters (derived from Surveyor imagery). While lunar regolith geotechnical properties vary point-to-point and at areas such as crater rims, their variance is less than geotechnical properties of soils on Earth. Rocks and boulders are not evenly distributed and are more likely to be found near fresh craters. Specific guidance on assessing rock abundance is found in DSNE 3.4.1.4. The lunar South Pole consists of highlands terrain; unless otherwise specified in DSNE, highlands regolith properties may be used for the Lunar South Pole. Plume-surface interaction analyses should account for the broad range of lunar particle sizes. Smaller particles tend to achieve higher velocities, and plume-interaction events may result in a "sandblasting" effect on hardware.

While erosion is often the focus of plume-surface interaction analyses, engine exhaust plumes can impinge on and interact directly with nearby objects. Objects with large surfaces, such as solar arrays, may be particularly susceptible to these effects. The resulting impingement pressure and associated heat flux depends on the lander's engine configuration and thrust level, and generally decreases as distance from the landing site increases.

Rocket plume effects vary based on lander configuration and concept of operations. Plume structure depends on the number and placement of engines on a vehicle. As an engine approaches a surface, the pressure distribution resulting from its exhaust will tend to narrow in spatial extent and increase in peak pressure. Erosion modes and the instantaneous erosion rate will vary accordingly but tend to be less benign as a lander approaches the surface. Multi-engine configurations have been used to reduce plume-surface interactions, but plume-plume interactions can also enhance PSI effects.

In the absence of surface infrastructure such as landing pads or berms that sufficiently mitigate landing hazards, detailed analyses must be conducted to assess plume-surface interaction effects for each vehicle, mission, and landing site. Plume-surface interaction analyses are limited by current modeling capabilities, natural environments knowledge gaps, and vehicle performance variability. The quantitative and qualitative outcomes of predictive PSI models are subject to varied levels of uncertainty. PSI outcomes depend on the specific vehicle landing, local topography, and variation in local geotechnical properties. Allowances for these modeling and environmental uncertainties should be made when conducting landing hazard assessments.

Rocket exhaust plumes may eject regolith particles during landing or initial ascent. These particles can be accelerated to a significant fraction of the plume gas velocity and pose hazards to the vehicle itself or surrounding assets. Particle velocities are roughly anticorrelated with particle mass; that is, smaller particles will tend to have the highest velocities, some of which may exceed the lunar gravitational escape velocity. As the Moon has no atmosphere to cause drag, and neglecting the effects of lunar terrain which may block certain trajectories, particles that achieve high enough velocities can theoretically reach arbitrary locations on the lunar surface.

The effects of a given plume-surface interaction event will depend on the topography surrounding the lander and any affected asset. Landing events which occur on hills may affect a broader area than those located in valleys. Assets may want to take advantage of local topographic features to block particles originating from a landing event. Mobile assets may choose to relocate during later vehicle landing or ascent to minimize risk exposure.

At present, plume-surface interaction predictions for the lunar environment are anchored to estimates of Apollo Lunar Module erosion. These estimates are subject to high uncertainty and have been revised upward in more recent analysis (Metzger et al. 2009; Lane and Metzger 2015; Metzger 2024) and range from 2 to 26 mT. Mission planners must consider PSI effects in their own landing and ascent trade spaces (both effects on their own vehicles or nearby assets), and in operations near landing or ascending spacecraft.

Expected effects of the lunar dust portion of the regolith include and are not limited to: slipping or falling of crew; dust ejecta due to spinning wheels causing further downstream effects; jamming or binding of mechanisms in vehicles such as landing legs; obscuration of crew visuals or other optics; obscuration of camera lenses, windows, or other optical components; and ejection of dust upwards towards the EVA hatch of the landing vehicle.

It is not solely ejecta force that can be the hazard from plume surface interactions; there are mechanical, optical, and other potential hazards that may arise from dust from the PSI settling onto the spacecraft. As referenced by Gaier in The Effects of Lunar Dust on EVA Systems During the Apollo Missions, 2005, the lunar dust transported during the takeoff and landing stages of lunar surface missions obscured crew vision during landing, clogged mechanisms (such as landing legs), and gave false instrument readings during landing. While the magnitude of the effects and hazards due to lunar dust contamination from PSI varied between missions, crew on every mission noted multiple off-nominal effects due to lunar dust from PSI. As shown in Metzger, 2020a, during landing, there are multiple tons of regolith that have been displaced, and the settling of this regolith on the spacecraft can cause numerous off-nominal effects, many of which are covered by Gaier, 2005 and NASA-STD-1008.

6.2.2 Trafficability

The top layer of the lunar surface is the regolith; it ranges in thickness from meters to tens of meters and ranges in content from large rocks to microscopic particles. Lunar regolith properties including composition, particle size distribution and morphology, and geotechnical properties are defined in the DSNE Sections 3.4.2, 3.4.4, and 3.4.5. Far below the surface is the lunar crust. Figure 6.2.2-1 shows the lunar surface layers (Plescia, 2016):

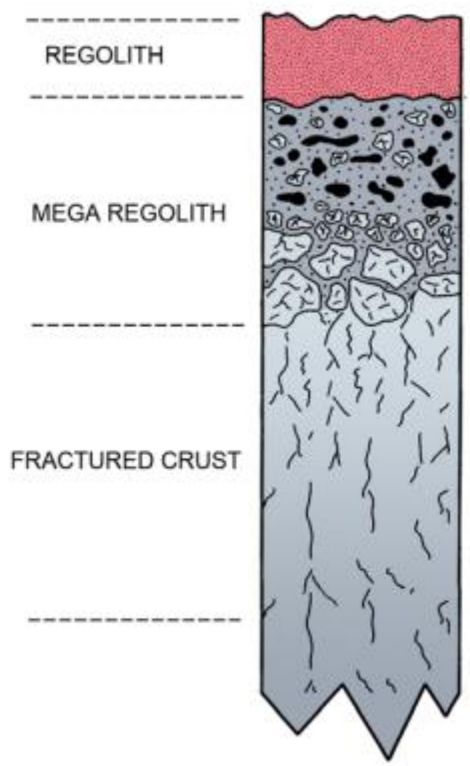

FIGURE 6.2.2-1 LUNAR SURFACE STRATA

Layers beneath and within the regolith are not uniform or universal across the surface. Impacts and thermal stress break down larger particles into smaller ones, impacts throw smaller particles out from the impact site, the heat of impact fuses smaller particles into larger ones, and the process of amalgamation bonds smaller particles together to reform larger ones again. These ongoing processes are constantly changing the surface and breaking down and remixing the composition. No single sample returned has yet been completely characterized (Plescia, 2008). The regolith in general is less compact, more deformable, more compressible, and generally less load bearing at the surface, and gets progressively more compact, less deformable, less compressible, and better able to support loads the deeper it is.

The trafficability – the ability of terrain to allow passage of vehicles or personnel – of the lunar surface varies with the size of particles in the path to be traveled and the depth of the finest particles. The low-density, uppermost layer of the regolith varies in depth and cohesion; it is less dense and deeper near the rims of young craters and more dense and shallower farther away (Plescia, 2008). The nondimensional bearing capacity of lunar soil increases as the impacting foot width goes up: wider feet (or wheels or tracks) do not sink as much as narrower ones holding the same weight. Bearing capacity as a function of footing size and the modulus of subgrade reaction are defined in DSNE section 3.4.2.4.5. Refer to Prabu et al, 2022, for an explanation of how the foot size and low gravity together impact the bearing capacity of lunar soil.

Expect a path traveled by foot, wheel, or track to change over repeated use as the act of stepping on or rolling over the regolith mixes, breaks down, casts aside, and packs down that top layer.

A general overview of the characteristics of the surface presented by Dr. Plescia is available via the Lunar Planetary Institute Moon 101 Lecture Series, https://www.lpi.usra.edu/lunar/moon101/#surface (Plescia, 2008). The summary trafficability chart from that lecture is also included by Dr. Metzger in the Lunar Geology presentation, https://sciences.ucf.edu/class/wp-content/uploads/sites/23/2020/02/2020-Lunar-Geology_Metzger.pdf, where it is much more legible as slide 35 (Metzger, 2020b).

A discussion of when, and in what conditions it is or is not advantageous, to travel the same path or land at the same location repeatedly will be added in a later revision. **<TBD-30044-003>**

Crew on the lunar surface have experienced slipping, particularly on ladders and other manmade structures that have been coated with or exposed to dust. As reported in Gaier, 2005, Neil Armstrong reported lunar dust adhering to the soles of his boots, causing slippage on the ladder during ingress to the LM. Additionally, it was noted in Apollo 12 that skinny tires had slippage problems, and the LRV in Apollo 15 noted about 10% slippage during transit. In addition to slipping, dust rapidly covered and obscured trip hazards, such as the TV cable from Apollo 11, and caused numerous trips by crew. Furthermore, the dust kicked up by walking and rotating wheels can cause similar issues to the dust lofted by PSI, including clogged mechanisms, optical obscuration, and false instrument readings. During most nominal operations of the LRV, noticeable quantities of lunar dust were not kicked up; the highest quantities were lofted during sharp turns and times of rapid acceleration and deceleration, such as during the “Grand Prix” performance trial. In both Apollo 16 and 17, when the rear fender extensions were knocked from the LRV (due to being tripped over by crew), dust “rooster tailed” and “showered” the crew during transit. This problem ended up being so difficult for the crew to deal with that they made a temporary fender from maps and tape and clamped it down into position where the original fender had been located.

6.3 CHARACTERISTICS OF ILLUMINATION

Lunar south pole illumination is dependent on lunar seasons, topography, specific location, and specific height above the surface. Timing of a lunar traverse must be considered with utilization objectives. For example, the lunar south pole summer provides an increased number of interconnected illuminated pathways compared to the lunar south pole winter.

6.3.1 Seasonal Variation

On a seasonal scale, the capability of a lunar asset to survive the night/shadow will define the exploration range throughout the year. A lower tolerance to survive darkness increases limitations such as being tethered to an illuminated location, or the need to rely on an external energy source (e.g., separate utility pallet). **<FWD-30044-017>**

As an example, a lunar asset in a lunar south pole winter can experience up to 150 continuous hours of darkness at least once annually without exposure to sunlight at a certain small surface area location at a height >5m above the surface. Such information can be used by some subsystems or operational planning; however, it should not be used for subsystems such as power. Larger than 150 hours will be experienced outside the small surface area location and at lower than 5m height above the lunar surface. The derivation of the 150-hour continuous darkness duration is documented in Appendix E. This continuous darkness duration does not include the darkness or illuminated periods immediately before and after this continuous period. Figure 6.3.1-1 shows a sample illumination profile that illustrates this issue. It shows the fraction of the sunlight that reaches a specific location in the polar region with good illumination at a height of 10 meters above the surface for a one-year period and 1 hour time step. The figure shows how illumination varies during the Winter period and summer period. It also shows how the horizon varies over each lunation and how the Sun elevation changes, which is why the Illumination Fraction is created. Analysis includes the width of the Solar Disk (.52 deg diameter), which is why the Illumination Fraction is not binary. The reason the horizon is repeated every lunation is because the Sun azimuth varies 360 degrees every lunation. The Figure illustrates how illumination and darkness are somewhat random appearing making the maximum continuous darkness of limited use for subsystems like power. A new metric called Effective Energy Storage Duration (EESD) has been developed to account for power system characteristics and addresses the periods of illumination and darkness before and after the maximum continuous darkness duration.

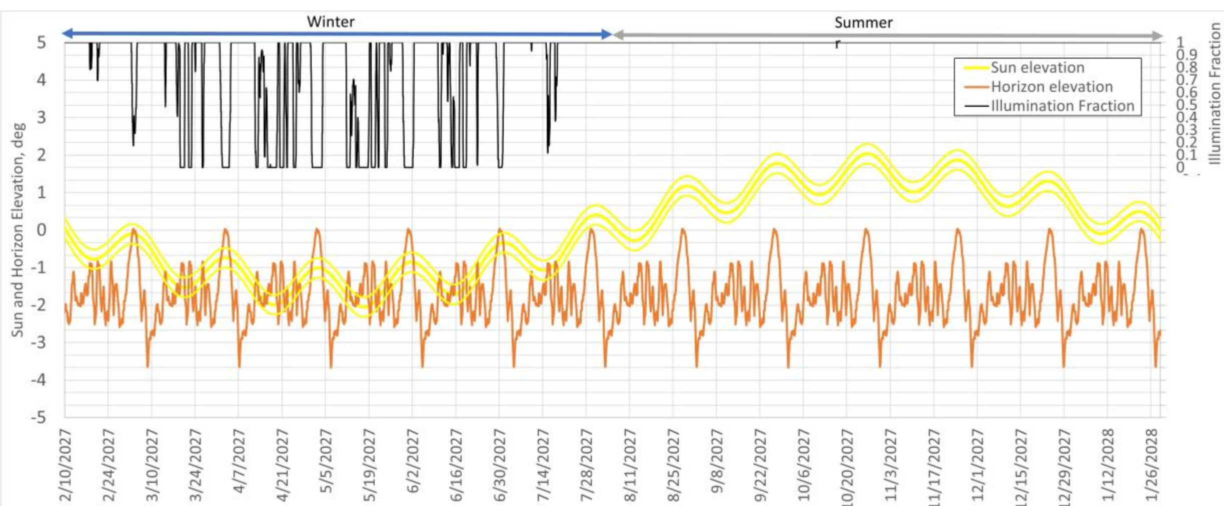

FIGURE 6.3.1-1 LUNAR ILLUMINATION AND ELEVATION ANGLES OVER A LUNAR YEAR

On the timescale of a mission, it is necessary to note that the sun moves across the sky at the rate of approximately 12.07 to 12.31 degrees in 24 hours: shadows are long due to the shallow Sun elevation, sharply defined, and move extensively. The lack of atmospheric diffusion significantly minimizes light in shadows to the effects of Earthshine and solar reflection/scattering as local topography and seasonal conditions allow. Glare will be a factor any time the sun is in the field of view, in addition to bright light and deep shadow. Rapidly appearing thermal impacts of shadows can result in very cold areas that affect hardware or crew. Refer to Gläser et al, 2014.

On the timescale of a single task or EVA, it is necessary to note that the highest the sun gets above the horizon in the lunar south polar region is 7.5 degrees. This very low angle of solar illumination means that even on the side facing the sun, there is too much light aligned to vertical surfaces, and too little light aligned to horizontal surfaces, for either cameras or human eyes to adjust to see details in both at once. Minor variations of the lunar surface (rocks/boulders and craters) can create complicated surfaces for mobility and crew to navigate. These variations cannot be known a priori. Without assistance, the low angle of illumination, and the light glare and reflectance on some surfaces may affect human interaction and camera settings. Considerations for potential adaptation, shielding, etc. are suggested.

Earthshine also illuminates the surface of the Moon at the south pole from a very low angle (Metzger, 2020b).

Complicating the design of task lighting, the reflectivity of lunar soil depends on the angle between the source and the observer: it reflects more light back in the direction from which it came, like a retroreflector. When looking from the same direction of the light source, details will be washed out. (Metzger, 2020b). A description and visual reference for phase-dependent reflectivity can be found here on slides 16-19: https://ntrs.nasa.gov/citations/20220008695, Lighting Environment. The scattering function of light for lunar regolith is defined in DSNE Section 3.4.5.1.

Lighting is an important technical and integration challenge, and Human Health & Performance is actively engaged in ongoing maturation of concepts and requirements for lighting systems, lighting architecture, lamps, lighting environments, and the like. While it is not feasible to add all lighting considerations in this relatively brief lunar surface data book, it can provide reference to other existing data sources and guidelines to provide users with a more comprehensive perspective. Accordingly, refer to NASA Standard 3001 Volume 2, Revision D (or latest), section 8.7 Lighting (publicly available at standards.nasa.gov).

6.3.2 Impact on Power Systems

Energy storage can be one of the most massive aspects of lunar hardware. Even using the most modern state-of-the-art batteries can result in landed masses in the metric ton range. With technology development, regenerative fuel cells are expected to offer mass savings.

In Appendix E, a discussion is presented regarding the results of one illumination metric called Maximum Continuous Darkness (MCD). A maximum of 150 hours of continuous darkness is presented as an appropriate design assumption for a mobile asset if mission specific MCD is not available. MCD is derived from the hourly illumination profile generated over a period greater than 1 lunar year at a particular height above the lunar surface and at a specific location. MCD analysis needs specific information about the landing site, or long-term parking sites, and minimal information about the vehicle itself. MCD determines the longest time period where continuous darkness exists over the course of the lunar year. This is useful for the design of some aspects of lunar surface hardware and represents a best-case condition for sizing power systems/energy storage for rovers.

Using an assumed MCD of 150 hours is not necessarily conservative. A more detailed analysis can be performed to find the Effective Energy Storage Duration (EESD). It needs not only the data about the illumination profile of the resting locations and route, but also more details of the power system: solar array power level, darkness/winter survival power level, and more. EESD is defined as the number of hours an energy storage device must be sized for, to account for the inability to fully recharge during an insolation period (i.e., the time in sunlight) before entering another period of darkness. This value is dependent on location, solar array sizing, recharge power, discharge power, and insolation profile. When this concept is applied, it accounts for all darkness and illumination periods from the time when the energy storage device is fully charged and entering into darkness until the energy storage device can be sufficiently recharged. This typically includes darkness and illumination periods before and after the MCD. With more recharge power and/or lower discharge power, a shorter energy storage duration is achievable until it approximates MCD. Using EESD to correctly size energy storage generally results in greater energy storage mass than one sized solely for the specific location's MCD.

EESD is calculated directly using power system design inputs. To compare design proposals, it can be helpful to normalize the characterization of the power system using the Power System Factor (PSF). The same PSF can represent a wide range of different power systems in terms of EESD calculation. PSF is used to represent the power system design and operation and is applied to perform an energy balance using the illumination profile. Power System Factor is the ratio of the recharge power divided by the discharge power, where discharge power is the survival user power including all losses and inefficiencies, and recharge power is the power provided from the solar array under full illumination, including all losses and inefficiencies. This factor can vary as the system degrades over years of service.

6.4 CHARACTERISTICS OF HAZARDS

Reserved. **<FWD-30044-006>**

7.0 EXAMPLE USE CASES LEVERAGING LUNAR SURFACE DATA

There are twenty-six distinct sites of interest identified at the lunar south pole. Figure 7.0-1 depicts these candidate landing regions. Refer to Appendix A, Table A 2-2 for more details.

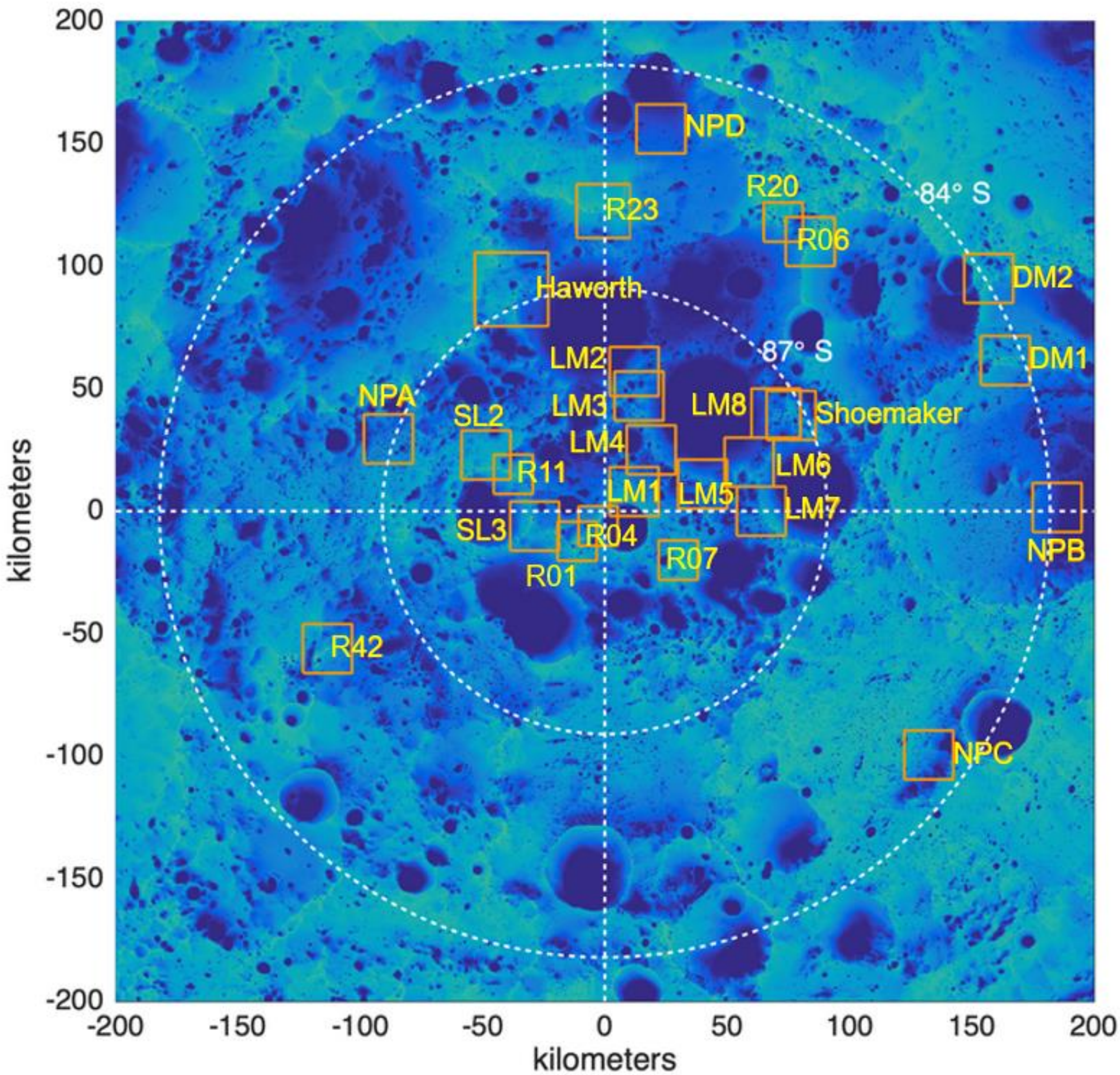

FIGURE 7.0-1 CANDIDATE LANDING REGIONS

Artemis will focus on these landmarks announced in August 2022.

7.1 SOUTH POLE EXPLORATION SITES

Reserved. **<TBD-30044-002>**

7.2 TERRAIN 101

<FWD-30044-018>: Forward work to summarize Terrain 101.

7.3 REPRESENTATIVE TRAVERSES

The following examples represent notional, representative traverses for lunar mobility assets, and were chosen to sample the variety of conditions and demands a moving vehicle may encounter. Examples include relocation of logistics around the South Pole Exploration Sites, a long uncrewed science traverse, and a traverse into a Permanently Shadowed Region. These are example traverses only and do NOT represent definitive statements of operational mission priorities or profiles, and they do NOT encompass all possible exploration activities or destinations on the surface of the Moon. A comprehensive traverse analysis will include environmental and other mission parameters in combination; the following traverses' analyses were limited primarily to slope.

These examples are not directly linked together unless explicitly stated. Details, acronyms, and labels in one example should not be assumed to be associated with another example. For example, PSR number labels are relevant to the figures in which they appear and are not universally recognized labels; they are not consistent across figures unless explicitly linked.

Furthermore, all traverses described here are assumed to be carried out during illuminated portions of the lunar year except where otherwise noted and subsequent planning efforts will have to account for when actual missions are planned, and thus are likely to change. Integrated technical solutions to meet the variety of terrain encountered will need to be developed with limited data. Most of these traverses were originally developed for HEOMD, then ESDMD and published as ESDMD-410, Lunar Surface Exploration Planning: Terrain Characteristics. Distances traversed are calculated three-dimensionally with hazardous slopes avoided unless otherwise noted. Vector data files of the traverses are available upon request; refer to Appendix D for the process by which to make a request.

When the Artemis Geospatial Data Team studies a potential traverse, assumptions must be made about the vehicle making the journey. A narrower vehicle can safely pass closer to crater edges than a wider one, for example. See Figure 7.3-1 below for mobile vehicle dimensional terminology.

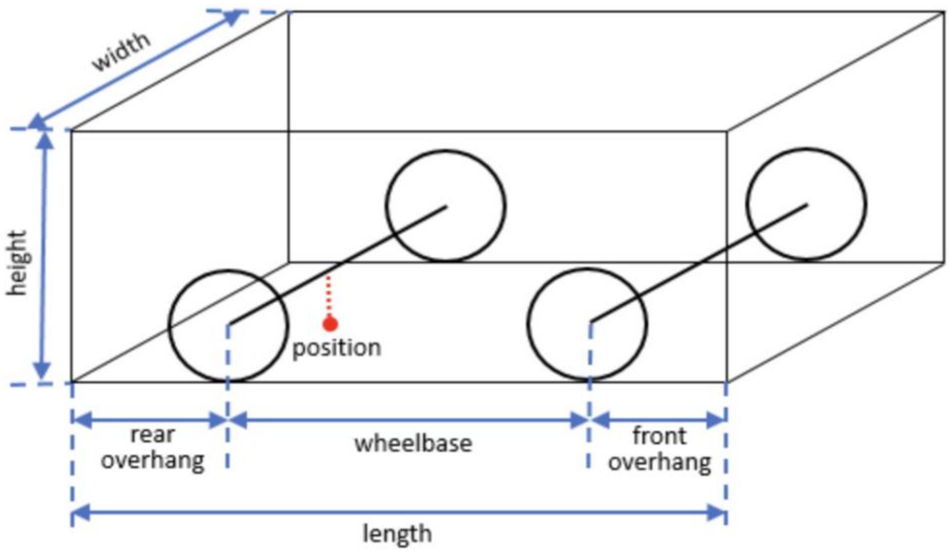

FIGURE 7.3-1 MOBILE VEHICLE DIMENSIONAL TERMINOLOGY

It is incumbent on the user to consider the needs of the vehicle when assessing any traverses described here for use by their specific vehicle. For example, users should consider if there will be enough sunlight to power the vehicle if solar arrays are used? Will there be enough light for cameras or other sensors? How will the vehicle maintain thermal balance? The traverses presented in this section are provided as examples, summarized in Table 7.3-1 below.

TABLE 7.3-1 EXAMPLE TRAVERSES

Section	**Traverse Descriptor**	**Defining Characteristics <TBR-30044-001><FWD-30044-014>**
7.3.2	Short Flat	Elevation change is less than 50m over 1.3 km
7.3.3	Illuminated Science Traverse	Emphasizes travel in sunlight between Connecting Ridge (CR), Shackleton Rim (SR), and PSR access points
7.3.4	Steep Traverses	Elevation change is greater than 1000m in less than 25km, including into PSRs
7.3.5	Long Gentle Traverse	46.6km with slopes less than 20 degrees
7.3.6	Long Challenging Traverse	47.8 km with slopes greater than 20 degrees

<FWD-30044-016>	20km or more with slopes less than 20 degrees

7.3.1 General Traverse Design Methodology

The following examples depict a few possible traverses. The design of any mobility asset should consider the asset's intended use, capability, and survivability on the lunar surface. This summary describes the methodology for designing traverses. While it is feasible to manually design each traverse, it is anticipated that the best method is to use automated processes to construct large numbers of hypothetical traverses to understand the limitations and constraints of the mobility asset to possible mission scenarios.

For the Artemis lunar south polar region (84 to 90 deg S), traverse design should start with the highest resolution digital elevation model (DEM) available. This is documented in other sections of the Lunar Surface Data Book and are also referenced in the DSNE. This could be DEMs from 1-5 m/pixel. This resolution is a relevant size scale for currently planned mobility assets. Larger resolution DEMs have pixel sizes of too large of an area and lose their applicability to traverse design. It is desirable to have height error data associated with each pixel of the selected DEM. This enables the ability to derive the slope at each pixel location and understand possible error band. The goal is to adequately characterize the slope and its worst-case estimate so the data can be used to derive a potential traverse.

Next, a slope map needs to be generated. This includes the formulation of an algorithm to estimate the slope using the DEM data and DEM height error. Methods can include simple straight-line slopes from one pixel to the adjacent pixel or can be more complex using a interpolated surface composed of all surrounding pixels. Whichever method is used, this needs to be documented in the traverse definition process.

Next, a PSR map is needed at the best DEM resolution available. This is used to help design traverses that avoid driving into PSRs for a nominal traverse. Specialized PSR focused traverses can be designed which ignore this limitation, but due to the nature of PSRs (very cold, need to preserve their state, no illumination) it is desirable to avoid them unless focused on visiting them.

The selection of starting and ending locations is a useful next step after obtaining the input DEM data. Generically, this is somewhat open ended. The distance between these two end points is unconstrained except for the latitude limit. Ideally, the selection of these end points depends on mission scope and constraints. For example, there are limited Winter Survival sites that minimize energy storage needs; summer crewed operations sites are much more frequent but presently unspecified; and there are many sites that may prove to be of interest to science and exploration.

Next, using an assumed slope limit for the mobility asset (upward and downward) and the slope and slope error data for all the pixels in the 84-90 deg S latitude area, a potential path connecting these 2 points can be generated. Such a path would have all travel between the pixels defining the path be within the acceptable slope range. PSRs would be avoided for nominal traverses. PSR specific traverses can be designed separately. Manual or automated methods can be used to do this. Achieving minimum distance is not a requirement but could be implemented. Direct to Earth communication access, Illumination, thermal or regolith properties are not considered at this phase of traverse design.

After definition of a traverse, the mobility assets can be assessed as to applicability. Modelling small rocks/boulders and craters which are not perceivable in current DEMs can be applied to the traverse in some probabilistic method. The DSNE and the Lunar Surface Data Book have data to define these. Regolith mechanical properties are also needed to do this assessment and are available in the Lunar Surface Data Book and the DSNE.

Using this method alone can be used to generate many traverses and will give a good first assessment on the versatility and applicability of a mobility asset.

Mobility assessment benefits from time phased illumination analysis over each created traverse. Such data will assist in assessing the temperature along the path at various heights (from wheels/regolith to the top), traverse path illumination (is supplemental lighting needed?), and any need for additional power augmentation and/or solar power generation (if solar arrays are deployed or recharge locations). This process involves generating the illumination at each traverse step (1-5 m pixel) at key heights above the surface and over a relevant time span (likely an entire year) and time step (hourly). After this data is obtained, it is possible to select departure times for the traverse and simulate travel along the path at a specific mobility asset speed. Distance travelled until the need for recharge of energy storage for further travel can be assessed. Note that the metric of more frequent departure times is likely beneficial.

While mobility is most likely to be used during the 30-day period the crew is present for significant exploration activities, the assets will be active throughout the entire year with various telerobotic operations when the crew is not there. Thus, even in winter, with its more frequent shadowing periods each lunation, there are opportunities for uncrewed traverses.

7.3.2 Short Flat Traverse

The Short Flat Traverse is based on the Large Logistics Transfer Traverse. This example traverse describes a logistics transfer scenario where pre-deployed supplies are transferred between two points on the Connecting Ridge between Shackleton and de Gerlache craters using any mobility asset, over a distance of 1.3 km and a total elevation change of less than 50 m. Developed initially for the Lunar Terrain Vehicle (LTV), this example traverse could include a maximum transport mass (cargo) over a shorter distance in the vicinity of fixed Artemis operating locations (known terrain), with lower speeds. Crew may be present to load/unload logistics, and the LTV may be driven by the crew during an EVA to relocate large logistics packages.

7.3.2.1 Representative Site Terrain/Elevation Profiles

Elevation and slope profiles are provided graphically in Figure 7.3.2.1-1. A table outlining slope statistics of this region is provided in Table 7.3.2.1-1.

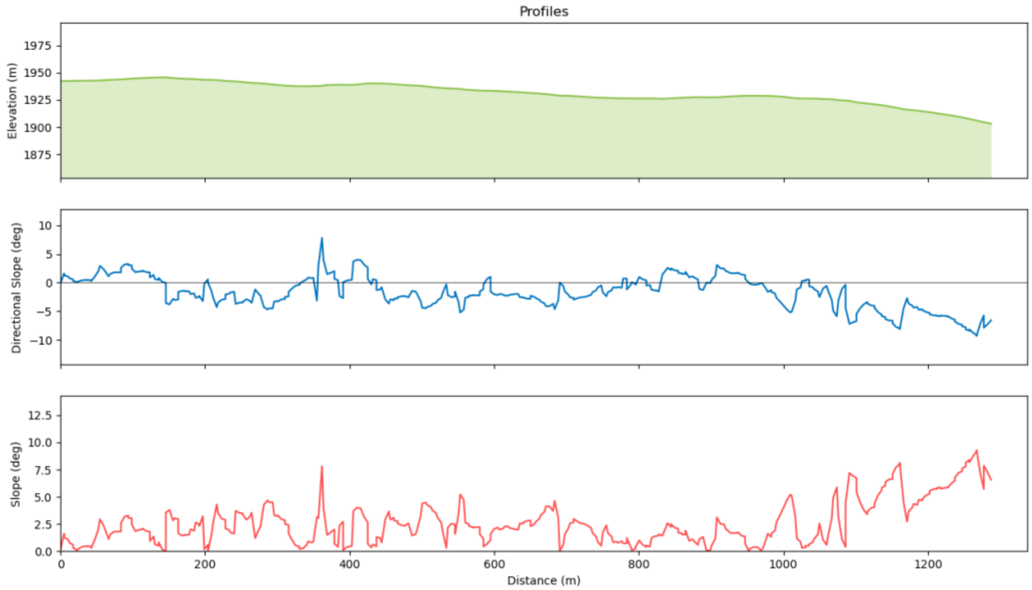

FIGURE 7.3.2.1-1 ELEVATION, DIRECTIONAL SLOPE, AND SLOPE PROFILES FOR SHORT FLAT TRAVERSE.

TABLE 7.3.2.1-1 MORPHOMETRY SUMMARY OF SHORT FLAT TRAVERSE

C1 to C2 Traverse Slope Statistics	
Minimum	0.2°
Maximum	9.8°
Mean	3.3°
Standard Deviation	1.9°

Elevation map to be added. **<FWD-30044-007>**

7.3.2.2 Representative Site Illumination

Details to be added. **<FWD-30044-007>**

7.3.2.3 Representative Site Earth Views

Details pertinent to communication to be added. **<FWD-30044-007>**

7.3.2.4 Representative Site Geological Map

Map to be added. **<FWD-30044-007> <TBD-30044-001>**

7.3.2.5 Representative Site Mineralogy and Resources

Mineralogical maps and hydrogen abundance maps to be added. **<FWD-30044-007>**

7.3.2.6 Representative Site Hazard Maps

Details of known slopes, craters, and rocks to be avoided to be added. **<FWD-30044-007>**

7.3.2.7 Representative Traverse

Figure 7.3.2.7-1 depicts the traverse between two points C1 (89.468° S, 222.6° E) and C2 (89.500° S, 222.1° E) on the Shackleton - de Gerlache connecting ridge. Base map is the slope information derived from USGS Astrogeology Science Center's Moon LRO South Pole DEM (https://astrogeology.usgs.gov/search/map/moon_lro_south_pole_dem) using Horn (3x3) algorithm. Refer to the discussion of LOLA DEM in section 4.2.4.1.

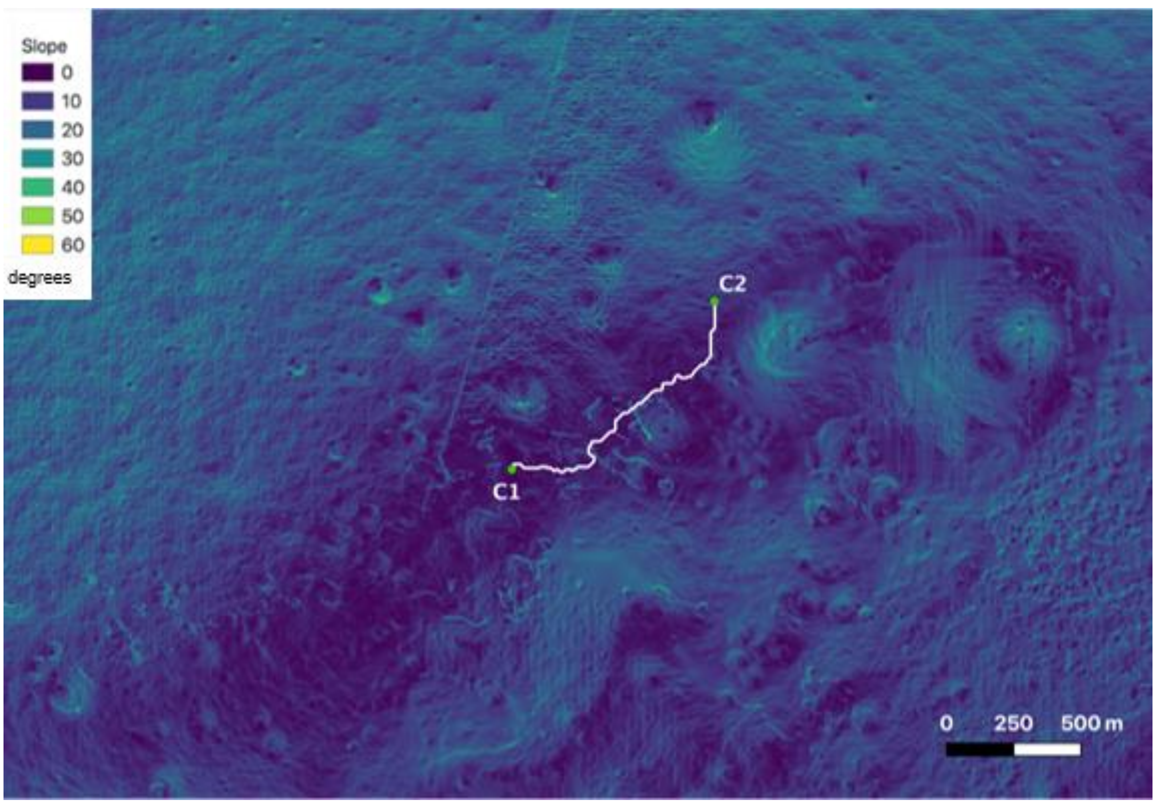

FIGURE 7.3.2.7-1 SHORT LEVEL TRAVERSE – 1.3KM WITH SLOPE UNDER 10 DEGREES

7.3.3 Illuminated Science Traverse

The Illuminated Science Traverse is a prospective traverse using a rover with a body width of 3 meters, originally developed for an autonomous or remotely operated vehicle traveling at low speed. It is based on the traverse developed in Speyerer et al, 2016 (Figure 7.3.3-1), as a representative example to provide options for Lunar Terrain Vehicle utilization that enables a variety of science and prospecting use cases and maximizes movement time between Connecting Ridge (CR), Shackleton Rim (SR), and PSR points. As noted by Speyerer et al, 2016 (summarized here: [http://lroc.sese.asu.edu/posts/937,](http://lroc.sese.asu.edu/posts/937) LROC Next Steps) this traverse does not include specific science station stops and does not assume a specific instrument suite on the vehicle; it is instead designed to maximize opportunities to achieve science and exploration objectives subject to future instrument selection and operations plan development, while keeping the vehicle illuminated for most of a calendar year.

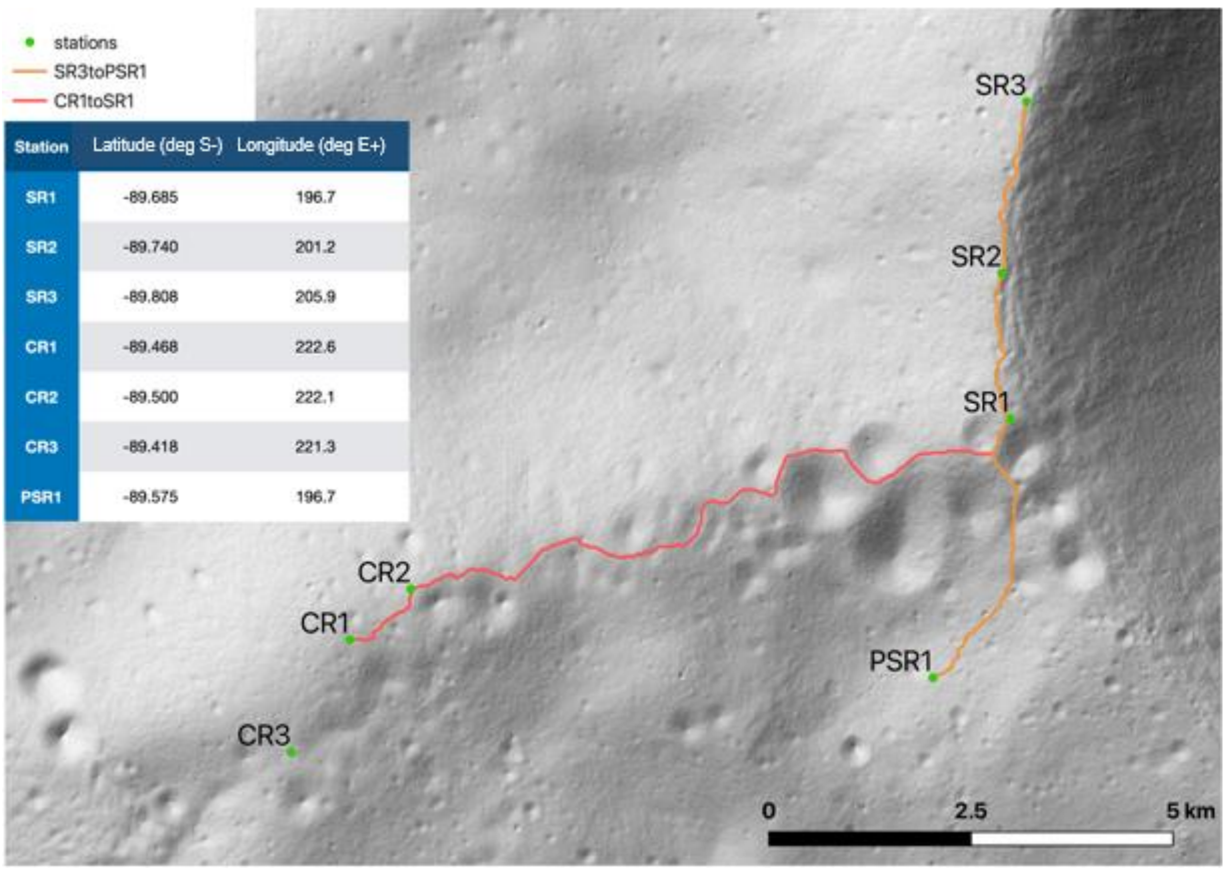

Station	Latitude (deg S-)	Longitude (deg E+)
SR1	-89.685	196.7
SR2	-89.740	201.2
SR3	-89.808	205.9
CR1	-89.468	222.6
CR2	-89.500	222.1
CR3	-89.418	221.3
PSR1	-89.575	196.7

FIGURE 7.3.3-1 EXAMPLE WELL-ILLUMINATED SCIENCE TRAVERSE

The Illuminated Science Traverse is an example of an uncrewed traverse focused on achieving science and exploration objectives and maximizing mobility in the absence of human crews, derived from Speyerer et al, 2016. Slopes along the path of this traverse do not exceed 11 degrees at the pixel level; the maximum distance from the origin is 8.6 km. The total distance traveled along the red path labeled CR1 to SR1 is 11.15 km and the orange path SR3 to PSR1 is 8.66 km. The line plot in Figure 7.3.3.1-1 below corresponds to the red path from CR1 to SR1. The grayscale basemap used for Figure 7.3.3-1 is a synthetic hillshade image derived from the 5 m/pixel LOLA polar data product. Hillshade was generated with default parameters (solar azimuth: 315°; solar elevation: 45°) to quickly view terrain and is not intended to represent realistic illumination conditions.

The PSR number labels are relevant to the traverse discussions in which they appear and are not universally recognized labels.

7.3.3.1 Representative Site Terrain/Elevation Profiles

Elevation and slope profiles are provided graphically in Figures 7.3.3.1-1 and 7.3.3.1-2-6; slope statistics are provided in Tables 7.3.3.1-1 and 7.3.3.1-2.

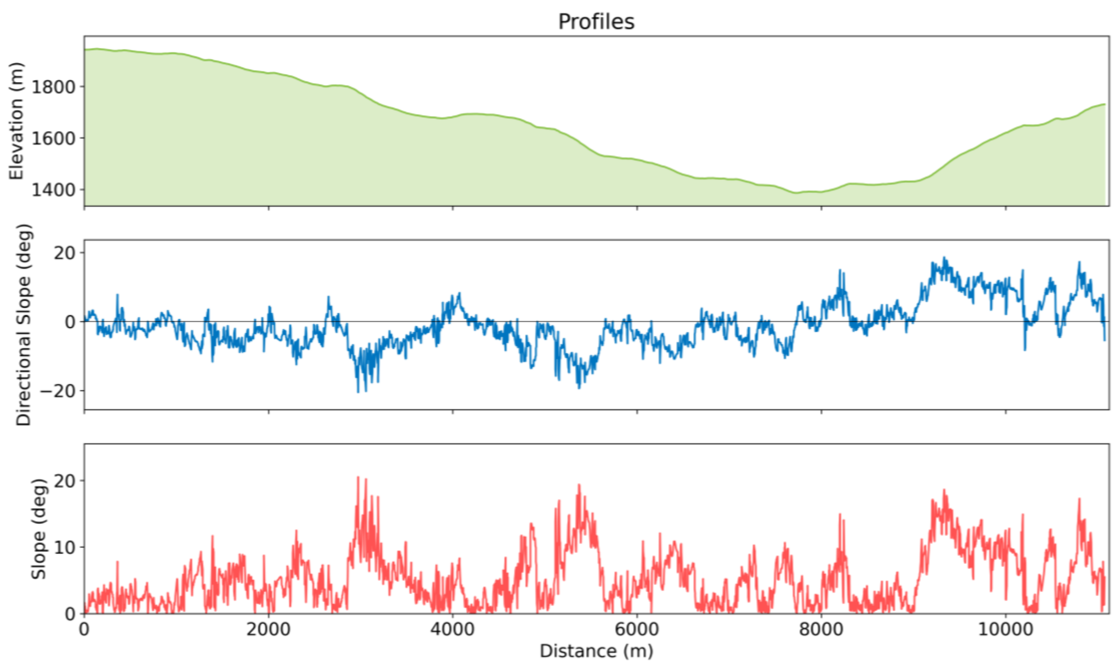

FIGURE 7.3.3.1-1 ELEVATION, DIRECTIONAL SLOPE, AND SLOPE PROFILES FOR TRAVERSE PATH FROM CR1 TO SR1 OF THE SHACKLETON - DE GERLACHE REGION

TABLE7.3.3.1-1 MORPHOMETRY SUMMARY TRAVERSE FROM CR1 TO SR1

CR1 to SR1 Slope Stats	
Minimum	0°
Maximum	20.5°
Mean	5.2°
Standard Deviation	4.0°

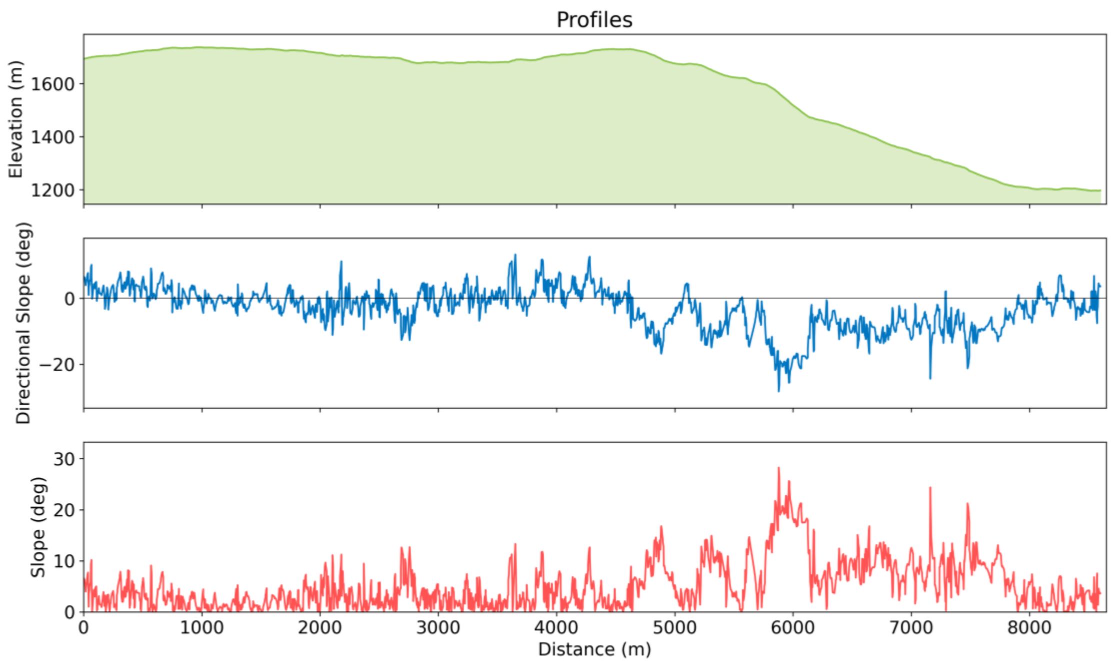

FIGURE 7.3.3.1-2 ELEVATION, DIRECTIONAL SLOPE, AND SLOPE PROFILES FOR TRAVERSE PATH SR3 TO PSR1 OF THE SHACKLETON - DE GERLACHE REGION.

TABLE 7.3.3.1-2 MORPHOMETRY SUMMARY TRAVERSE FROM SR3 TO PSR1

SR3 to PSR1 Slope Statistics	
Minimum	0°

SR3 to PSR1 Slope Statistics	
Maximum	28.3°
Mean	5.2°
Standard Deviation	4.7°

Elevation map to be added. **<FWD-30044-008>**

7.3.3.2 Representative Site Illumination

In this representative Illuminated Science Traverse, the vehicle lands at the site designated CR1 and may rove between CR2 and CR3 to minimize nighttime duration. The total traverse distance is 38 km and was assumed to be fully illuminated. Traverses to SR-1, SR-2, SR-3, and into PSR-1 from the CR-1 location are feasible during illuminated periods, examples of which are provided in Figures 7.3.3-1, 7.3.3.7-1, and 7.3.3.7-2.

Details to be added (figure showing this area's version of "fully illuminated" would be ideal – frame from movie?). **<FWD-30044-008>**

7.3.3.3 Representative Site Earth Views

Details pertinent to communication to be added. **<FWD-30044-008>**

7.3.3.4 Representative Site Geological Map

Map to be added. **<FWD-30044-008> <TBD-30044-001>**

7.3.3.5 Representative Site Mineralogy and Resources

Mineralogical maps and hydrogen abundance maps to be added. **<FWD-30044-008>**

7.3.3.6 Representative Site Hazard Maps

Relevant to LTV or any mobile asset that travels this route, this example includes representative traverse paths designed to avoid o known hazards, with smaller transport mass (science payloads, no crew/cargo), over relatively long distances and long durations. Hazards include craters larger than 15 meters in diameter, blocks greater than 1 meter in diameter, and slopes greater than 20 degrees as much as deemed practical; when avoiding such routes, lower slopes are actively prioritized.

Details of known slopes, craters, and rocks to be avoided to be added. **<FWD-30044-008>**

7.3.3.7 Representative Traverse

This Illuminated Science Traverse illustrates a viable Connecting Ridge scenario where the vehicle lands at the location identified here as CR-1 and can then rove freely between CR-2 and CR-3 with minimal nighttime duration year-round. Traverses to sites identified here as SR-1, SR-2, SR-3, and PSR-1 are also feasible during illuminated periods from the starting point CR-1. The total traverse distance shown is 38 km, detailed in Figures 7.3.3.7-1 and 7.3.3.7-2.

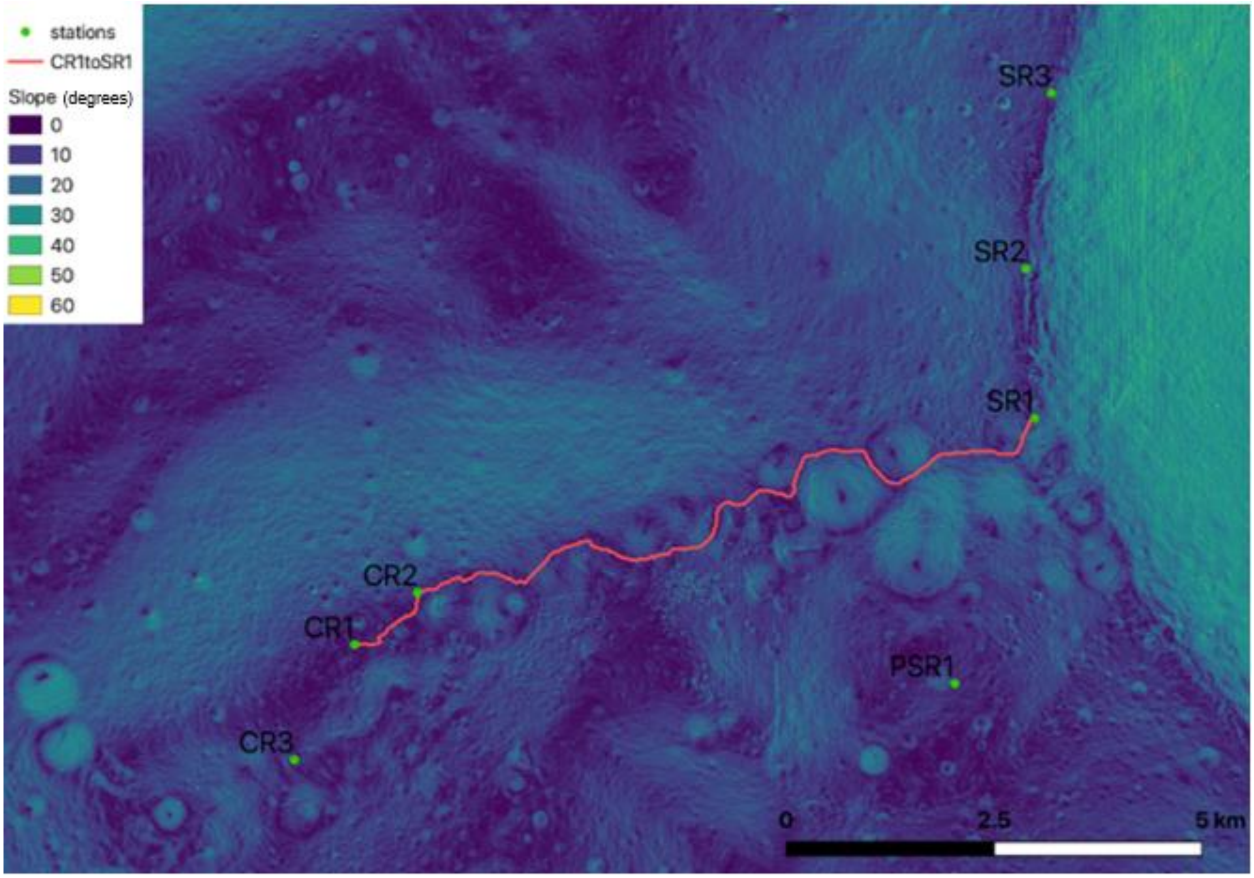

FIGURE 7.3.3.7-1 REPRESENTATIVE TRAVERSE FROM STATIONS CR1 TO SR1 ON A SLOPE MAP OF THE SHACKLETON - DE GERLACHE REGION.

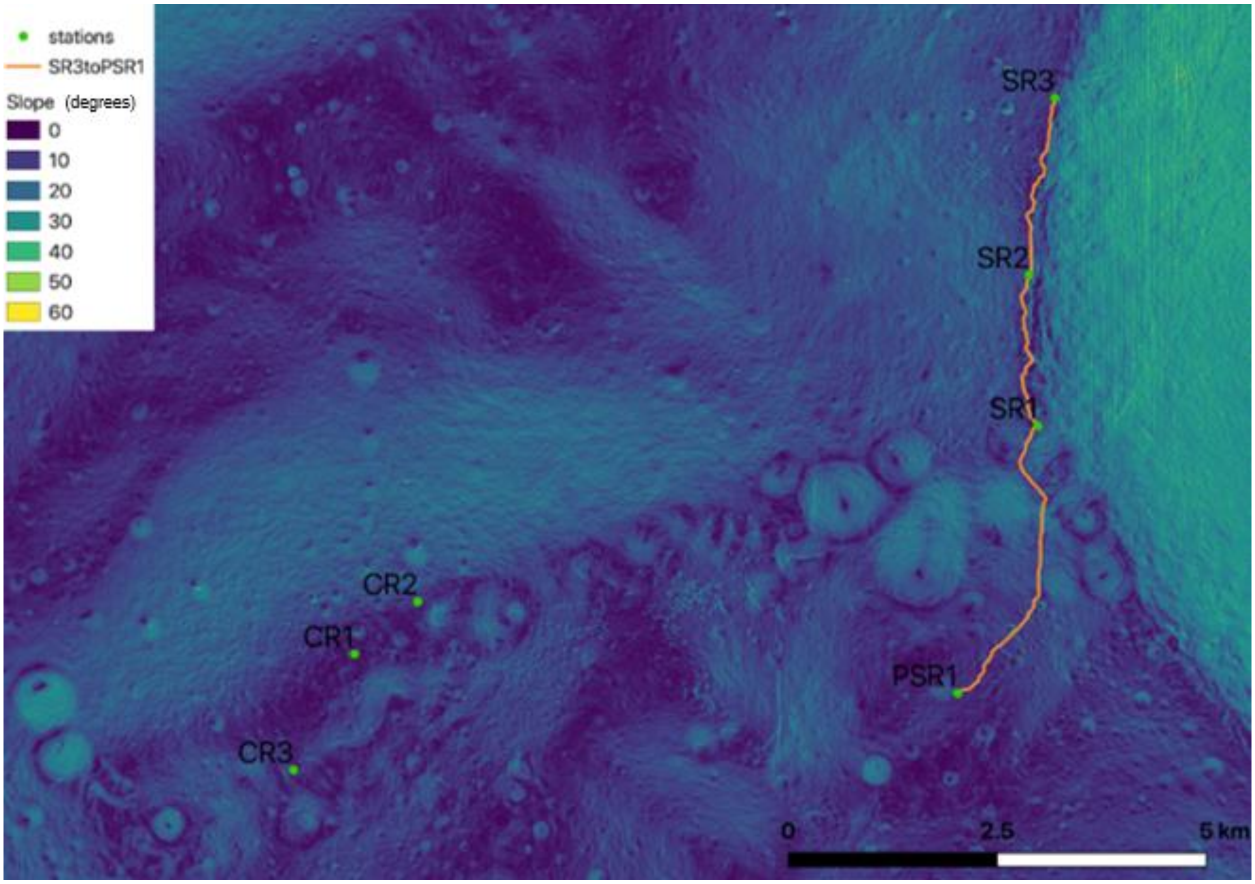

FIGURE 7.3.3.7-2 REPRESENTATIVE TRAVERSE FROM STATIONS SR3 TO PSR1 OVERLAIN ON A SLOPE MAP OF THE SHACKLETON - DE GERLACHE REGION.

The PSR number labels are relevant to the traverse discussions in which they appear and are not universally recognized labels.

7.3.4 Steep Traverses

These example Steep Traverses serve as examples of prospective traverses designed to enable the exploration of cold traps near the Shackleton - de Gerlache Connecting Ridge near Spudis crater. They were originally developed for the LTV. Relevant to LTV or any mobile asset that travels these routes, they include challenging terrain (steep slope), appropriate for a smaller transport mass, vehicle width on the order of 3 meters, with crew and/or science payloads on board, including deployed experiments and sample collection and acquisition hardware elements, traveled at higher speeds over a shorter distance than that outlined in the Well-Illuminated Science Traverse, Section 7.3.3. The elevation change is over 1000 meters and slopes exceed 20 degrees positive and negative.

7.3.4.1 Representative Site Terrain/Elevation Map

Elevation and slope profiles are provided graphically in Figures 7.3.4.1-1 and 7.3.4.1-2; slope statistics are provided in Tables 7.3.4.1-1 and 7.3.4.1-2.

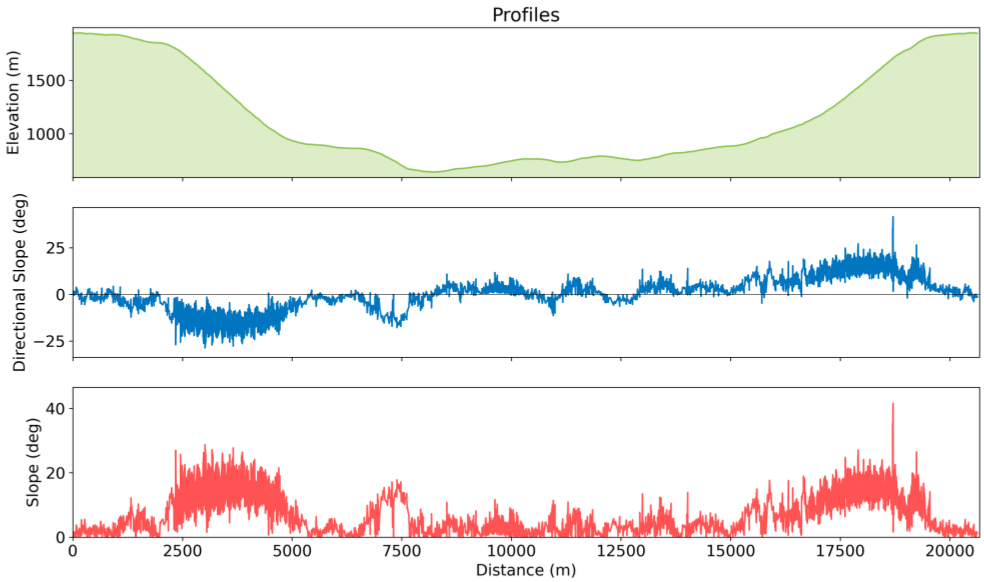

FIGURE 7.3.4.1-1 ELEVATION, DIRECTIONAL SLOPE, AND SLOPE PROFILES FOR TRAVERSE PATH SHOWN FROM CR1 TO PSR1 AND PSR2 OF THE SHACKLETON - DE GERLACHE REGION.

TABLE 7.3.4.1-1 OF MORPHOMETRY SUMMARY TRAVERSE FROM CR1 TO PSR1 AND PSR2

Slope Stats	CR1 to PSR1	PSR1 to PSR2	PSR2 to CR1
Minimum	0°	0°	0°
Maximum	28.7°	11.7°	41.6°
Mean	8.4°	3.3°	7.8°
Standard Deviation	7.2°	2.0°	6.0°

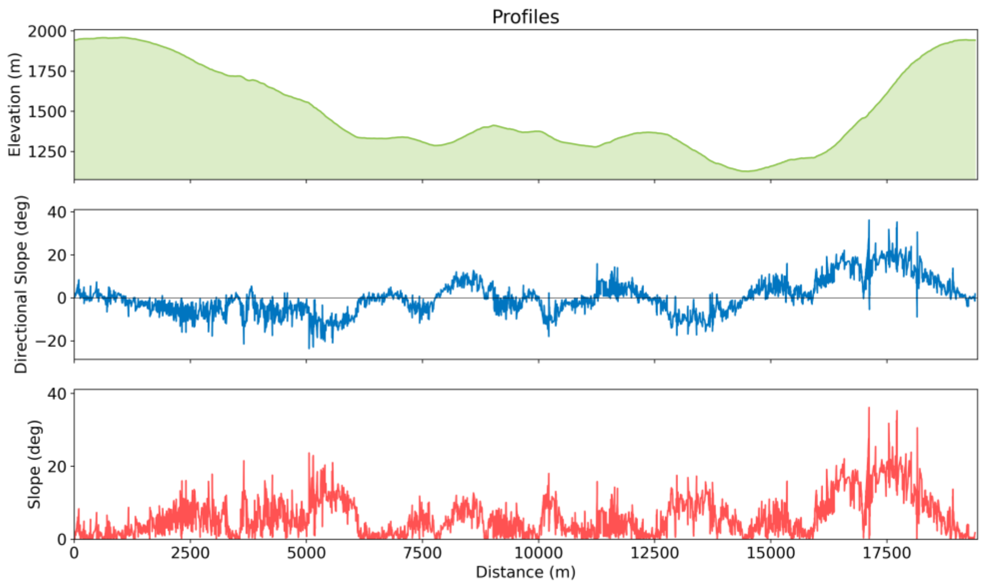

FIGURE 7.3.4.1-2 ELEVATION, DIRECTIONAL SLOPE, AND SLOPE PROFILES FOR TRAVERSE PATH FROM CR1 TO PSR3 OF THE SHACKLETON - DE GERLACHE REGION.

TABLE 7.3.4.1-2 MORPHOMETRY SUMMARY OF TRAVERSE FROM CR1 TO PSR3

Slope Stats	CR1 to PSR3	PSR3 to Midway	Midway to CR1
Minimum	0°	0°	0°
Maximum	23.6°	17.5°	36.1°
Mean	5.3°	5°	11.7°
Standard Deviation	4.0°	3.7°	6.9°

A more detailed (easier to read) elevation map to be added. **<FWD-30044-009>**

7.3.4.2 Representative Site Illumination

Details to be added. **<FWD-30044-009>**

7.3.4.3 Representative Site Earth Views

Details pertinent to communication to be added. **<FWD-30044-009>**

7.3.4.4 Representative Site Geological Map

Map to be added. **<FWD-30044-009> <TBD-30044-001>**

7.3.4.5 Representative Site Mineralogy and Resources

Mineralogical maps and hydrogen abundance maps to be added. **<FWD-30044-009>**

7.3.4.6 Representative Site Hazard Maps

Details of known slopes, craters, and rocks to be avoided to be added. **<FWD-30044-009>**

7.3.4.7 Representative Traverse

This scenario assumes a landing at the CR1 (89.468° S, 222.6° E) location originally described in Section 7.3.3. This scenario also assumes that the surface mission enables at least two rover-based traverses per mission. The PSR number labels are relevant to the traverse discussions in which they appear and are not universally recognized labels.

Figure 7.3.4.7-1 below is the topographical map for the round-trip from CR1 to PSR1, PSR2, and back. The Figure 7.3.4.1-1 above shows representative elevation and slope profiles, summarized in Table 7.3.4.1-1.

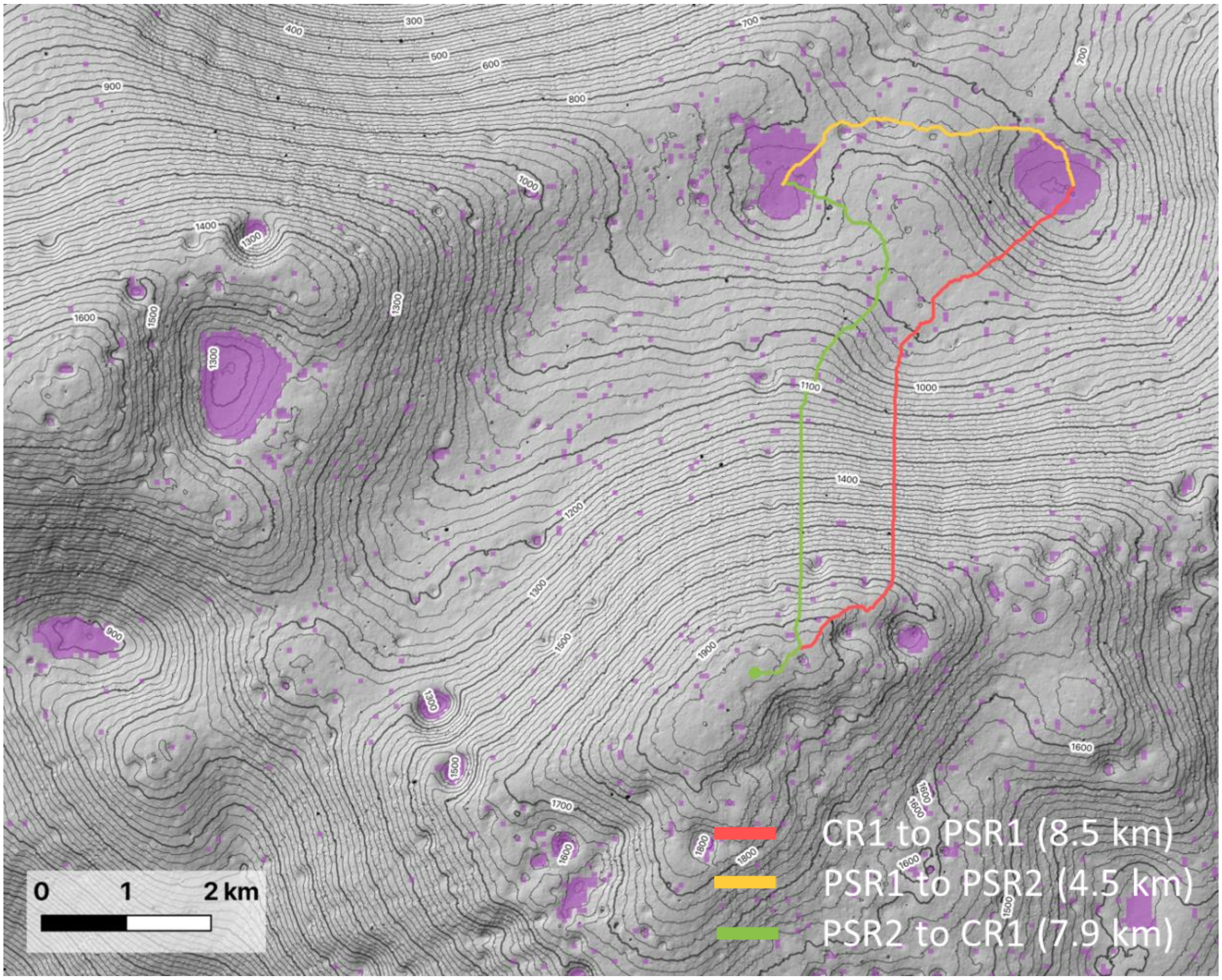

FIGURE 7.3.4.7-1 TOPOGRAPHIC MAP OF THE SHACKLETON - DE GERLACHE CONNECTING RIDGE, SHOWING A ROUND-TRIP TRAVERSE FROM CR1 TO PSR1 AND PSR2.

Figure 7.3.4.7-2 shows a representative round-trip traverse from CR1 to PSR3. The elevation and slope profiles are detailed in Figure 7.3.4.1-2 and summarized in Table 7.3.4.1-2 above.

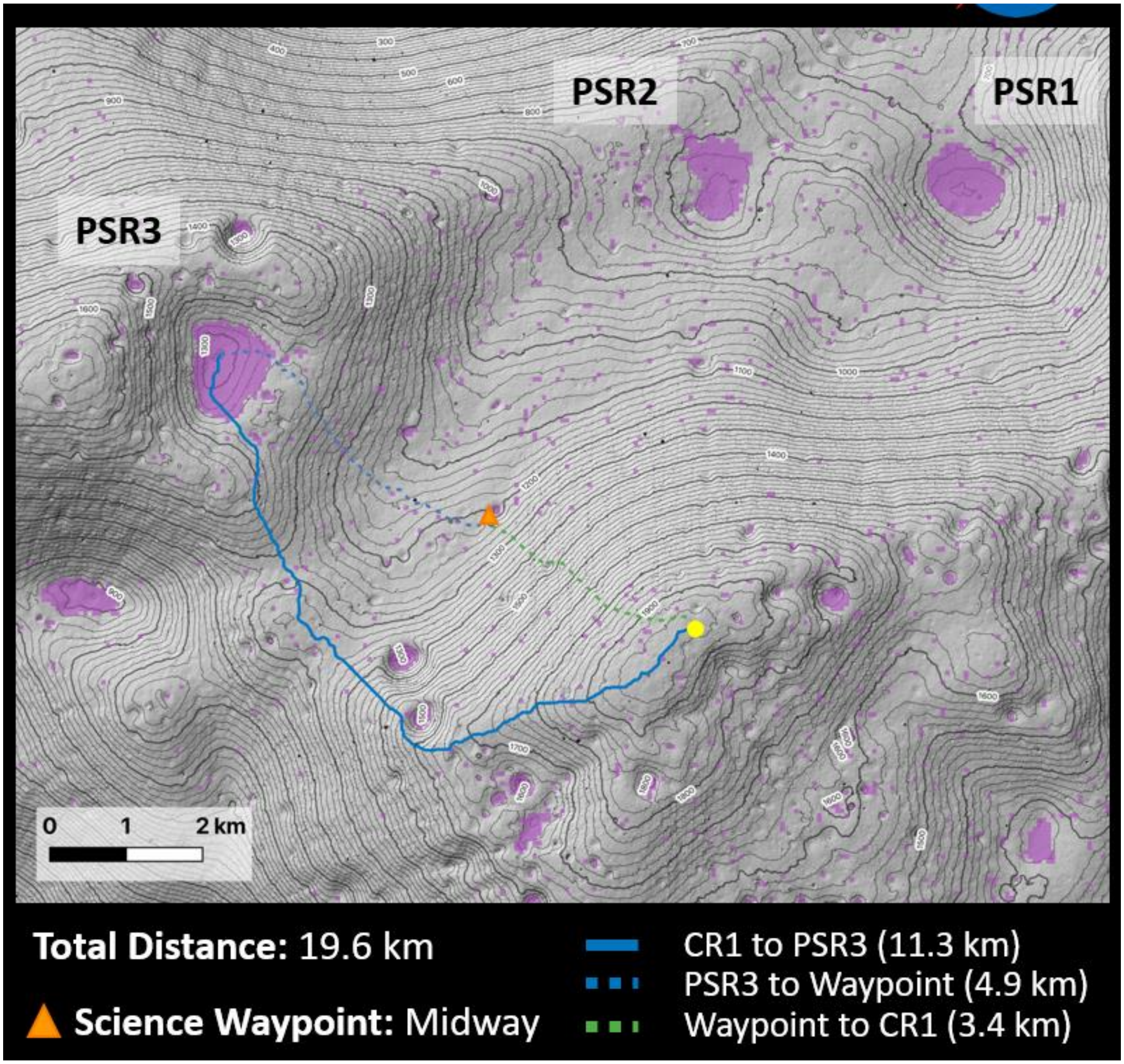

FIGURE 7.3.4.7-2 TOPOGRAPHIC MAP OF THE SHACKLETON – DE GERLACHE CONNECTING RIDGE SHOWING A ROUND-TRIP TRAVERSE FROM CR1 TO PSR3.

7.3.5 Long Gentle Traverse

The Artemis Geospatial Data Team is responsible for helping plan traverses for mobile assets that will be landed as part of the Artemis mission campaign. The AGDT has plotted a new long and gentle traverse for a vehicle three meters wide, avoiding hazards to allow for a higher mass and/or center of gravity. The Long Gentle Traverse connects Connecting Ridge and Peak near Shackleton and was inspired by Path 2 from the paper “Sunlit Pathways between South Pole Sites of Interest for Lunar Exploration” by Mazarico, 2023, a traverse of 47.8 km. It is both very long and a challenging traverse, passing along crater limbs and areas of high slope. The Long Gentle Traverse is 46.6 km and avoids both crater limbs and slopes greater than 20 degrees.

7.3.5.1 Representative Site Terrain/Elevation Map

Elevation and slope profiles for the Long Gentle Traverse are provided graphically in Figure 7.3.5.1-1 with slope statistics provided in Table 7.3.5.1-1.

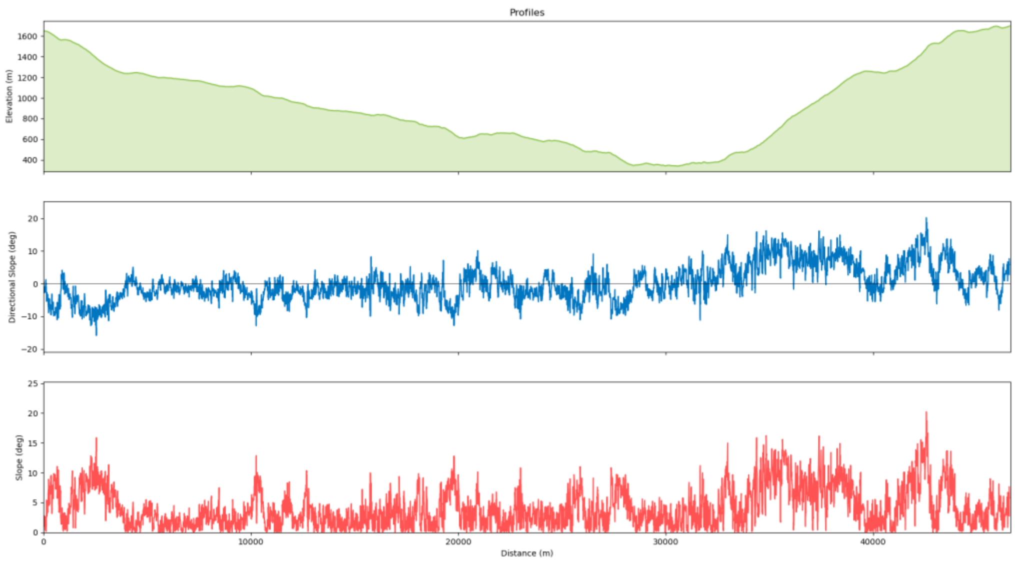

FIGURE 7.3.5.1-1 ELEVATION, DIRECTIONAL SLOPE, AND SLOPE PROFILES FOR LONG GENTLE TRAVERSE PATH FROM CONNECTING RIDGE TO PEAK NEAR SHACKLETON

TABLE 7.3.5.1-1 MORPHOMETRY SUMMARY OF LONG GENTLE TRAVERSE

Slope Stats	CR to PS
Minimum	0°
Maximum	20.2°
Mean	4.0°

Slope Stats	CR to PS
Standard Deviation	3.2°

Elevation map to be added. **<FWD-30044-010>**

7.3.5.2 Representative Site Illumination

Solar illumination has not yet been considered. Details to be added. **<FWD-30044-010>**

7.3.5.3 Representative Site Earth Views

Details pertinent to communication to be added. **<FWD-30044-010>**

7.3.5.4 Representative Site Geological Map

Map to be added. **<FWD-30044-010> <TBD-30044-001>**

7.3.5.5 Representative Site Mineralogy and Resources

Mineralogical maps and hydrogen abundance maps to be added. **<FWD-30044-010>**

7.3.5.6 Representative Site Hazard Maps

This Long Gentle Traverse avoids craters larger than 10 meters in diameter and blocks greater than 1 meter in diameter. It was specifically designed to avoid known hazards.

7.3.5.7 Representative Traverse

Figure 7.3.5.7-1 below shows two traverses between the Artemis landing regions Connecting Ridge (pink circle) and Peak near Shackleton (blue circle).

The purple traverse is provided for reference only: it is Path 2 from Mazarico (2023), a traverse of 47.8 km. It is both very long and a challenging traverse, passing along crater limbs and areas of high slope. That traverse is detailed at great length in the paper, Sunlit Pathways between South Pole Sites of Interest for Lunar Exploration.

The white traverse shows a hazard-cleared path that accounts for a mobile vehicle 3 meters wide. Hazards mapped and avoided included craters larger than 10 meters in diameter and blocks greater than 1 meter in diameter. The Long Gentle Traverse (white line) also avoids slopes greater than 20 degrees and prioritizes lower slopes as much as possible. This example Long Gentle Traverse is about 1 km shorter than the traverse created by Mazarico et. al., (2023) and avoids driving along the rims of large craters. Hazards larger than 1m diameter were identified in the LRO NAC images and avoided in the traverse shown; there is no way to eliminate the risk that hazards up to 1m diameter still exist on the traverse and capability to make real-time adjustments is recommended.

This Long Gentle Traverse was developed specifically for a larger vehicle such as a Pressurized Rover. Unlike the Mazarico traverse, solar illumination has not yet been considered for this Long Gentle Traverse. The background image is the 1m/pixel mosaic created from LROC NAC frames by ASU and the USGS.

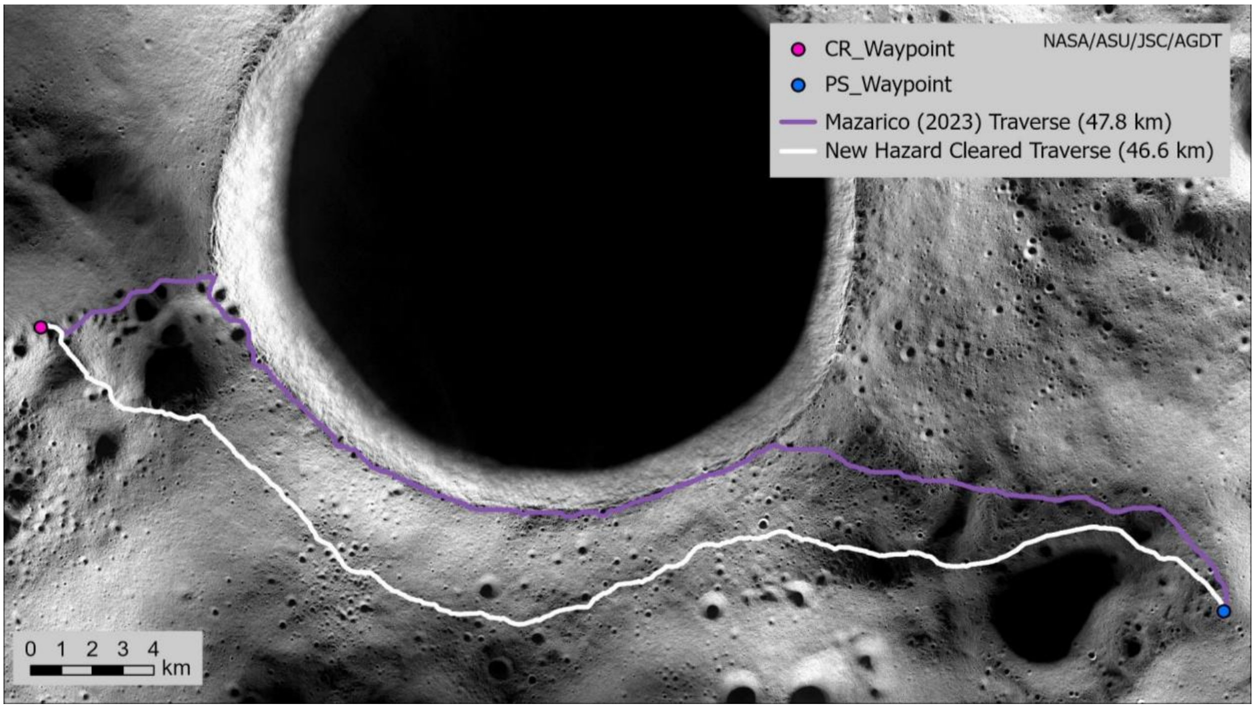

FIGURE 7.3.5.7-1 LONG GENTLE TRAVERSE BETWEEN CONNECTING RIDGE (CR) AND PEAK NEAR SHACKLETON (PS)

7.3.6 Long Challenging Traverse

The traverse presented by Mazarico et al (2023) as Path 2 from Connecting Ridge to Slater represents a long and challenging traverse for any rover that is well illuminated year-round. Details will be compiled here for ease of access by the users of this data book. **<FWD-30044-014>**

7.3.6.1 Representative Site Terrain/Elevation Map

Elevation map to be added. **<FWD-30044-011>**

7.3.6.2 Representative Site Illumination

Details to be added. **<FWD-30044-011>**

7.3.6.3 Representative Site Earth Views

Details pertinent to communication to be added. **<FWD-30044-011>**

7.3.6.4 Representative Site Geological Map

Map to be added. **<FWD-30044-011> <TBD-30044-001>**

7.3.6.5 Representative Site Mineralogy and Resources

Mineralogical maps and hydrogen abundance maps to be added. **<FWD-30044-011>**

7.3.6.6 Representative Site Hazard Maps

Details of known slopes, craters, and rocks to be avoided to be added. **<FWD-30044-011>**

7.3.6.7 Representative Traverse

New figure. **<FWD-30044-011>**

APPENDIX A
ACRONYMS, ABBREVIATIONS, AND GLOSSARIES

A1.0 ACRONYMS AND ABBREVIATIONS

TABLE A1.0-1 ACRONYMNS AND ABBREVIATIONS

ACD	Artemis Campaign Development
AIAA	American Institute of Aeronautics and Astronautics
ArcGIS	(a name of a software package)
BAE	British Aerospace / Marconi Electronic Systems
CCD	Charge Coupled Device
CONOPS	Concept of Operations (may also appear as ConOps)
CPR	Circular Polarization Ratio
CR	Change Request (in reference to documents)
CR	Connecting Ridge (in reference to lunar topography)
CRaTER	Cosmic Ray Telescope for the Effects of Radiation
DEM	Digital Elevation Model
DLRE	Diviner Lunar Radiometer Experiment (usually referred to as Diviner)
DOD	Department of Defense (may also appear as DoD)
DSM	Digital Surface Model
DSNE	Design Specification for Natural Environments
DTM	Digital Terrain Model
EESD	Effective Energy Storage Duration
ESA	European Space Agency
ESDMD	Exploration Systems Development Mission Directorate
ESMD	Exploration Systems Mission Directorate
ESRI	Environmental Systems Research Institute
GDAL	Geospatial Data Abstraction Library
GIS	Geospatial Information System
GRAIL	Gravity Recovery and Interior Laboratory
HEND	High Energy Neutron Detector
IJMF	International Journal of Multiphase Flow
ISIS	Integrated Software for Imagers and Spectrometers
ISRO	Indian Space Research Organisation
JAXA	Japan Aerospace eXploration Agency
JFM	Journal of Fluid Mechanics
JPL	Jet Propulsion Laboratory
LADEE	Lunar Atmosphere and Dust Environment Explorer

LAMP	Lyman Alpha Mapping Project
LBL	(a file extension)
LCROSS	Lunar Crater Observation and Sensing Satellite
LDEM	Lunar Digital Elevation Model
LEAG	Lunar Exploration Analysis Group
LEND	Lunar Exploration Neutron Detector
LIDAR	LIght Detection And Ranging
LOLA	Lunar Orbital Laser Altimeter
LRO	Lunar Reconnaissance Orbiter
LROC	Lunar Reconnaissance Orbiter Camera
LTV	Lunar Terrain Vehicle
M2M	Moon to Mars
MAPSIT	Mapping and Planetary Spatial Infrastructure Team
MCD	Maximum Continuous Darkness
NAC	Narrow-Angle Camera
NASA	National Aeronautics and Space Administration
NSSDC	NASA's Space Science Data Coordinated Archive
OPR	Office of Primary Responsibility
PDS	Planetary Data System
PGDA	Planetary Geodesy Data Archive
PSF	Power System Factor
PSI	Plume Surface Interaction
PSR	Permanently Shadowed Region
QGIS	(a name of a software package)
RF	Radio Frequency
RMS	Root Mean Square
SE&I	Systems Engineering & Integration
SfS	Shape from Shading
SLS	Space Launch System
SMD	Science Mission Directorate
SOCET SET	SOftCopy Exploitation Toolkit (a software package)
SR	Shackleton Rim
TRI	Terrain Ruggedness Index
USGS	United States Geological Survey
UV	Ultraviolet
WAC	Wide-Angle Camera

A2.0 GLOSSARY OF TERMS: LUNAR SURFACE TERMINOLOGY

The following terminology provides a common set of definition with respect to lunar terrain features that must be navigated and traversed by lunar mobility assets.

TABLE A2.0-1 LUNAR SURFACE TERMINOLOGY

3-Dimensional Distance	Measure of the cumulative distance along the elevation profile between two points to account for elevation gain and loss along a Euclidean or spherical distance
Cold Trap	An area cold enough to trap normally volatile gasses in the solid state
Coordinate Reference Frame	A solution that defines from observational data the specific numerical location of given points in the reference system (See Appendix F)
Crewed	Operations performed with local crew involvement
Datum	A reference point of set of reference points on the surface against which position measurements are made
Digital Elevation Model (DEM)	A digital representation of the bare ground topographic surface of a body that excludes a natural or built surface objects
Digital Terrain Model (DTM)	A digital representation of the bare ground topographic surface of a body that excludes natural or built surface objects but does include natural/built features as vector features
Digital Surface Model (DSM)	A digital representation of the bare ground topographic surface of a body and includes natural or built surface objects
Elevation	Vertical distance of a point or object above or below a reference surface or datum
Elevation Profile	Measure of elevation gain and loss along a line between two or more points
Equatorial Circumference of Moon	10916.4 km
Euclidean Distance	Measure of the straight-line distance from one point to another in the Euclidean space in cartesian coordinates. Also known as the Pythagorean distance
Figures of Merit (FOM)	Characteristics used to quantify the relative utility of a site (or other parameter), and form a basis of comparison between multiple factors
GIS	A Geospatial Information System (GIS) is a digital system designed to capture, store, manipulate, analyze, manage, and present spatial data
Gradient	The magnitude of a slope in the steepest direction. Defined as Change in Z / Change in X. A slope relative to the LTV is described by a max slope gradient and a gradient relative to the LTV planed direction of motion or angle of attack (LTV relative slope gradient)
Hazard	Physical feature on the lunar surface that generates a risk for the crew and mobile assets by preventing progress. *Note: Hazardous obstacles are not defined here because mobile asset design (traverse threshold, traverse threshold angle, etc.) will dictate which obstacles are safe or hazardous
Height	Vertical distance above the local surface

TABLE A2.0-1 LUNAR SURFACE TERMINOLOGY

Horn Method	An averaging method to calculate slope from eight neighboring cells/pixels about a center cell/pixel where a third-order finite difference equation is used to produce an estimate of an average slope within an 8-cell neighborhood of a central cell
Landing Ellipse	The dispersed area (either 3 sigma or 99%-tile) on the lunar surface where the is vehicle is estimated to land with the landing site at the center of the ellipse
Landing Site	A vector point data type use to indicate the exact surface location of the landing site
Lunar Digital Elevation Model (LDEM)	Topographic dataset providing an elevation (km) above fixed lunar radius of 1737.4 km
Map Points	Vector data type used to symbolize coordinates of a single object or location at the surface
Negative Obstacle	Defined by a diameter (Ø) and a negative slope. On the lunar surface they are mostly craters.
Obstacle	Physical feature that can hinder LTV progress on the lunar surface (e.g., rock, crater, slope)
Offset	Shift in datasets relative to each other due to differences in processing or data preparation
Parking Lot	Larger area that can accommodate multiple landing ellipses
Permanently Shadowed Region (PSR)	An area that sunlight does not reach despite the changing seasons of the year. On the Moon, there are many such areas in craters near the South Pole where the walls cast shadows all the time, allowing the temperature to remain low enough to trap volatiles in solid form.
Pixel	The smallest addressable element in a raster image
Positive Obstacle	Defined by a step height and a positive slope. On the lunar surface they are mostly rocks. The positive obstacle step height is the distance between the surface and the maximum height of an obstacle
Radius of Moon	1737.4 km
Raster	Data which has been processed into the form of a two-dimensional image, frequently associated with geographic data.
Region	A geographic territory that encompasses a range of features, bound together by shared characteristics, either natural or connected to the territory explored during a mission
Region of Interest	Portions of a region of expected potential scientific or other exploration value
Regolith	The surficial layer of fragmented material (rocks, soil, and dust) that covers virtually the entire surface of the Moon
Selapoid	A smooth but irregular surface whose shape results from the uneven distribution of mass within and on the surface of the Moon

TABLE A2.0-1 LUNAR SURFACE TERMINOLOGY

Semi-PSR	An informal term used to indicate an area that receives sunlight for only part of the year. Volatiles will not be trapped in such areas, making them attractive for practice runs and technology or process demonstrations in advance of going into PSRs.
Shadow	A location where light from a specific source is blocked by an object or feature of local terrain, usually demarcated from its surroundings by stark contrast to where the light does reach
Site	Location on the surface where a specific action takes place (e.g., landing, sampling, instrument deployment)
Site Plan	Similar to a terrestrial site plan, the lunar site plan is a developmental plan showing the growth of the Artemis Base Camp over time, that shows the locations, connections, and orientations of the ABC assets
Slope	Change in elevation across a certain distance (X meters)
Slope Map	A non-directional slope (degrees) at each map pixel location
Spatial Resolution	Spatial resolution is a measure of the smallest object that can be definitively resolved by the sensor, or the ground area imaged for the instantaneous field of view (FOV) of the sensor, or the linear dimension on the ground represented by each pixel
Spherical Distance	Measure of the line that connects two points along the surface of a sphere. Also known as orthodromic distance
Terrain	Physical features of the lunar surface
Terrain Relative Navigation (TRN)	An autonomous, optical, or laser-based system for landmark recognition, spacecraft position estimation, and spacecraft retargeting
Terrain Surface Roughness	Quantified by the deviations in the direction of the normal vector of a real surface from its ideal form. The roughness is measured on a certain surface area
Traverse	Movement across the surface, either by crew or robotic assets that has a starting point and destination points and a path that connects two points
Uncrewed	Operations performed without local crew involvement
Vector	A data model that uses vertices with geographic locations to create geographic features such as points, lines, and polygons. Vector data asl may have associated spatial and non-spatial attribute data
Vehicle Footprint	The surface area bounded by the perimeter of the vehicle, with landing legs extended, on the lunar surface
Vehicle Plume Ejecta	Material that has been moved across the surface because of engine firing during descent/ascent
Zone	An area where regulations or requirements are uniform

A2.1 GLOSSARY OF TERMS: LUNAR SURFACE FEATURE NAMES

The following terminology follows that used in Mazarico et al. (2011). Coordinates have been generated from the DEM files on the PGDA website (South Pole LOLA DEM), so the center points of the original polygons are accurate to 5 to 10 meters.

TABLE A2.1-1 LUNAR SOUTH POLE FEATURES

Shorthand	Name	Latitude	Longitude
DM1	Amundsen Rim	-84.2287	69.44396
DM2	Nobile Rim 2	-83.954	58.82206
Haworth	(Haworth is its name)	-86.7639	-22.777
LM1	Shackleton Rim B	-89.5244	56.30993
LM2	Shoemaker Rim A	-88.0792	11.88866
LM3	Shoemaker Rim B	-88.3828	16.58734
LM4	Shoemaker Rim C	-88.9645	37.23483
LM5	Shoemaker Rim D	-88.632	74.62375
LM6	Shoemaker Rim E	-87.9458	71.27421
LM7	Faustini Rim A	-87.8897	90
LM8	Shoemaker Rim F	-87.3417	60.25512
NPA	Cabeus Exterior Wall 1	-86.9243	-71.5651
NPB	Amundsen 1	-83.9046	89.53545
NPC	Idel'son L Crater 1	-84.5397	126.9045
NPD	Malapert Crater 1	-84.8034	8.387032
R01 or Site01	Connecting Ridge	-89.4632	-137.49
R04 or Site04	Shackleton Rim	-89.7668	-171.87
R06 or Site06	Nobile Rim 1	-85.4381	37.36667
R07 or Site07	Peak Near Shackleton	-88.811	123.6901
R11 or Site11	de Gerlache Rim 1	-88.6834	-67.9321
R20 or Site20	Leibnitz Beta Plateau	-85.4266	31.74276
R23 or Site23	Malapert Massif	-85.9948	-0.23578
R42 or Site42	de Gerlache-Kocher Massif	-85.8296	-116.322
Shoemaker	(Shoemaker is its name)	-87.1835	62.83502
SL2	de Gerlache Rim 2	-88.23	-64.6284
SL3	Connecting Ridge Extension	-89.0324	-101.999

APPENDIX B OPEN WORK

B1.0 TO BE DETERMINED

The table To Be Determined Items lists the specific items in the document that are not yet known. The TBD is inserted as a placeholder wherever the required data is needed and is formatted in bold type within carets. The TBD item is numbered based on the document number (i.e., **<TBD-xxxxx-001>** is the first undetermined item assigned in the document). As each TBD item is resolved, the updated text is inserted in each place that the TBD appears in the document and the item is removed from this table. As new TBD items are assigned, they will be added to this list in accordance with the above-described numbering scheme. Original TBD items will not be renumbered.

TABLE B1.0-1 TO BE DETERMINED ITEMS

TBD	Section	Description
TBD-30044-001	4.11 & 7.3	Discuss the accuracy, resolution, and any smoothing of elevation & slope data. Include error bars if possible.
TBD-30044-002	7.1	Discuss desired and expected characteristics of the candidate south pole infrastructure locations
TBD-30044-003	6.2.2	Discuss whether or not, or in what condition it is or is not, advantageous to travel the same path or land at the same location repeatedly

B2.0 TO BE RESOLVED

The table To Be Resolved Items lists the specific items in the document that are not yet officially baselined. The TBR is inserted as a placeholder wherever the listed data is unofficial and is formatted in bold type within carets. The TBR item is numbered based on the document number (i.e., **<TBR-xxxxx-001>** is the first unresolved item assigned in the document). As each TBR item is resolved, the updated text is inserted in each place that the TBR appears in the document and the item is removed from this table. As new TBR items are assigned, they will be added to this list in accordance with the above-described numbering scheme. Original TBR items will not be renumbered.

TABLE B2.0-1 TO BE RESOLVED ITEMS

TBR	Section	Description
TBR-30044-001	7.3-1	Clarify “illuminated portions of the calendar year” and other timing limitations addressed or specifically ignored for each traverse

B3.0 FORWARD WORK

The table Forward Work (FWD) Issues, lists the specific FWD issues in the document that are not yet completed. The FWD is inserted as a placeholder wherever the required data is needed and is formatted in bold type within carets. The FWD issue is numbered based on the document number, including the annex, volume, and book number, as applicable (i.e., **<FWD-xxxxx-001>** is the first forward work issue assigned in the document). As each FWD is resolved, the updated text is inserted in each place that the FWD appears in the document and the issue is removed from this table. As new FWD issues are assigned, they are added to this list in accordance with the above-described numbering scheme. Original FWD are not renumbered.

TABLE B3.0-1 FORWARD WORK ISSUES

FWD	Section	Description
FWD-30044-001	4.3.5	Provide general illumination maps (by inclusion or link)
FWD-30044-002	4.3.6	Provide general earth visibility maps (by inclusion or link)
FWD-30044-003	4.3.7	Provide general hazard maps (by inclusion or link)
FWD-30044-004	4.11	Provide general geological maps (by inclusion or link)
FWD-30044-005	4.12	Provide general mineralogical maps (by inclusion or link)
FWD-30044-006	6.4	Discussion of general hazard characteristics created by the terrain, including dust, solar wind, plasma, and potential voltage differences in PSRs
FWD-30044-007	7.3.2	Add details to the Short Flat Traverse data presentation – not all the subsections associated with this FWD may be used, after the general maps are added by earlier-occurring FWDs
FWD-30044-008	7.3.3	Add details to the Illuminated Science Traverse data presentation – not all the subsections associated with this FWD may be used, after the general maps are added by earlier-occurring FWDs
FWD-30044-009	7.3.4	Add details to the Steep Traverse data presentation – not all the subsections associated with this FWD may be used, after the general maps are added by earlier-occurring FWDs
FWD-30044-010	7.3.5	Add details to the Long Gentle Traverse data presentation – not all the subsections associated with this FWD may be used, after the general maps are added by earlier-occurring FWDs

FWD-30044-011	7.3.6	Add details to the Lone Challenging Traverse data presentation – not all the subsections associated with this FWD may be used, after the general maps are added by earlier-occurring FWDs
FWD-30044-012	4.9	Provide detailed radiation discussion and context for use of DSNE 3.4.7
FWD-30044-013	4.10	Provide detailed ejecta and micrometeoroid discussion and context for use of DSNE 3.4.8
FWD-30044-014	7.3-1 & 7.3.6	Describe how each example traverse path was chosen (why the start/finish points, why the route, how is it unique, etc.)
FWD-30044-015	F2.0	USGS Lunar Grid Reference System is in work; will add a discussion in the appendix when it is put in service.
FWD-30044-016	7.3-1	Add forward work to include 2 more 20km traverses with 20deg or less slope.
FWD-30044-017	6.3.1	Add data representative of variation of solar elevation angles over 18.6 yr precessional period that is an animation and database
FWD-30044-018	7.2	Forward work to summarize the Terrain 101; also consider “Where Is That Crater? Best Practices for Obtaining Accurate Coordinates from LROC NAC Data” from IOPscience.
FWD-30044-019	4.2.3.2	Forward work to add set of comparison images for uncontrolled vs semi-controlled vs controlled mosaics, at a scale where such images will be notably different in a pdf

APPENDIX C REFERENCE MATERIAL

TABLE C1-1 REFERENCE SOURCES

Alexandrov, O., & Beyer, R. A. (2018). Multiview Shape-From-Shading for Planetary Images. Earth and Space Science, 5(10), 652–666. https://doi.org/10.1029/2018EA000390

Anderson, J. A., Sides, S. C., Soltesz, D. L., Sucharski, T. L., & Becker, K. J. (2004). Modernization of the Integrated Software for Imagers and Spectrometers. Abstract no. 2039. https://ui.adsabs.harvard.edu/abs/2004LPI....35.2039A

Barker, M. K., Mazarico, E., Neumann, G. A., Smith, D. E., Zuber, M. T., & Head, J. W. (2021). Improved LOLA elevation maps for south pole landing sites: Error estimates and their impact on illumination conditions. Planetary and Space Science, 203, 105119. https://doi.org/10.1016/j.pss.2020.105119

Basilevsky, A.T., Florensky, C.P. & Ronca, L.B. A possible lunar outcrop: a study of Lunokhod-2 data. The Moon 17, 19–28 (1977). https://doi.org/10.1007/BF00566850

Connolly, J. and Carrier, W. (2023). "An Engineering Guide to Lunar Geotechnical Properties," 2023 IEEE Aerospace Conference, Big Sky, MT, USA, 2023, pp. 1-9. https://ntrs.nasa.gov/api/citations/20220014634/downloads/Final%20IEEE%20paper%20formatted%20footnote%20added.pdf

Fassett, C. I., Beyer, R. A., Deutsch, A. N., Hirabayashi, M., Leight, C. J., Mahanti, P., Nypaver, C. A., Thomson, B. J., Minton, D. A. (2022). Topographic Diffusion Revisited: Small Crater Lifetime on the Moon and Implications for Volatile Exploration. Journal of Geophysical Research: Planets, 127(12), published electronically. https://doi.org/10.1029/2022JE007510

Gaier, J. R. (2005). The Effects of Lunar Dust on EVA Systems During the Apollo Missions, NASA/TM—2005-213610. https://ntrs.nasa.gov/api/citations/20050160460/downloads/20050160460.pdf

Gladstone, G. R., Stern, S. A., Retherford, K. D., Black, R. K., Slater, D. C., Davis, M. W., Versteeg, M. H., Persson, K. B., Parker, J. W., Kaufmann, D. E., Egan, A. F., Greathouse, T. K., Feldman, P. D., Hurley, D., Pryor, W. R., & Hendrix, A. R. (2010). LAMP: The Lyman Alpha Mapping Project on NASA's Lunar Reconnaissance Orbiter Mission. Space Science Reviews, 150(1), 161–181. https://doi.org/10.1007/s11214-009-9578-6

Gläser, P., Scholten, F., De Rosa, D., Marco Figuera, R., Oberst, J., Mazarico, E., Neumann, G.A., Robinson, M.S. (2014). Illumination conditions at the lunar south pole using high resolution Digital Terrain Models from LOLA, Icarus, 243. 78–90. https://doi.org/10.1016/j.icarus.2014.08.013.

Glenar, D. A., Stubbs, T. J., Schwieterman, E. W., Robinson, T. D., Livengood, T. A. (2019) Earthshine as an illumination source at the Moon, Icarus,321, 841-856, https://doi.org/10.1016/j.icarus.2018.12.025.

Graf, J. C. (1993). Lunar Soils Grain Size Catalog. NASA Reference Publication, NASA-RP-1265. https://ntrs.nasa.gov/citations/19930012474.

Heiken, G. H., Vaniman, D. T., & French, B. M. (1991). Lunar Sourcebook, A User's Guide to the Moon. Cambridge University Press, ISBN 0-521-33444-6. https://www.lpi.usra.edu/publications/books/lunar_sourcebook/

Henriksen, M. R., Manheim, M. R., Burns, K. N., Seymour, P., Speyerer, E. J., Deran, A., Boyd, A. K., Howington-Kraus, E., Rosiek, M. R., Archinal, B. A., Robinson, M. S. (2017). Extracting accurate and precise topography from LROC narrow angle camera stereo observations, Icarus, 283, 122-137. https://doi.org/10.1016/j.icarus.2016.05.012

Jawin, E. R., Kiefer, W. S., Fassett, C. I., Bussey, B. J., Cahill, J. T. S., Dyar, M. D., Lawrence, S. J., Spudis, P. D. (2014). The relationship between radar scattering and surface roughness of lunar volcanic features. Journal of Geophysical Research: Planets, 119 (11), 2331-2348. https://doi.org/10.1002/2014JE004668

Kassel, Simon (1971), Lunokhod-1 Soviet Lunar Surface Vehicle. Santa Monica, CA: RAND Corporation for ARPA, September 1971. https://www.rand.org/pubs/reports/R0802.html.

Kaydash, V., Pieters, C., Shkuratov, Y., & Korokhin, V. (2012). Lunar opposition effect as inferred from Chandrayaan-1 M^3 data. Journal of Geophysical Research: Planets, 118 (6), 1221-1232. https://doi.org/10.1002/jgre.20098

Keller, J. W., Petro, N. E., & Vondrak, R. R. (2016). The Lunar Reconnaissance Orbiter Mission – Six years of science and exploration at the Moon. Icarus, 273, 2–24. https://doi.org/10.1016/j.icarus.2015.11.024

Keszthelyi, L., Becker, T. L., Sides, S., Barrett, J., Cook, D., Lambright, S., Lee, E., Milazzo, M., Oyama, K., Richie, J., Saleh, R., Shinaman, J., Sucharscki, T., Titus, T., Walldren, J., & Weller, L. (2013). Support and Future Vision for the Integrated Software for Imagers and Spectrometers (ISIS). Abstract no. 2546. https://ui.adsabs.harvard.edu/abs/2013LPI....44.2546K/abstract

Kloos, J. L., & Moores, J. E. (2019). Mapping the Limited Extent of Earthshine within Lunar PSRs. Research Notes of the AAS, 3(9), 127. https://doi.org/10.3847/2515-5172/ab4195

Lane, J. E., & Metzger, P. T. (2015). Estimation of Apollo Lunar Dust Transport using Optical Extinction Measurements. Acta Geophysica, 63(2), 568–599. https://doi.org/10.1515/acgeo-2015-0005

Laura, J. R., & Beyer, R. A. (2021). Knowledge Inventory of Foundational Data Products in Planetary Science. The Planetary Science Journal, 2(1), 18. https://doi.org/10.3847/PSJ/abcb94

LEAG-MAPSIT, (2021). Final Report of the Lunar Critical Data Products Specific Action Team. https://doi.org/10.5281/zenodo.7236426

Mandt, K. E., Greathouse, T. K., Retherford, K. D., Gladstone, G. R., Jordan, A. P., Lemelin, M., Koeber, S. D., Bowman-Cisneros, E., Patterson, G. W., Robinson, M., Lucey, P. G., Hendrix, A. R., Hurley, D., Stickle, A. M., Pryor, W. (2016). LRO-LAMP detection of geologically young craters within lunar permanently shaded regions. Icarus 273, 114-120. https://doi.org/10.1016/j.icarus.2015.07.031

Martin, A. C., Grey, P. E., Henriksen, M. R., & Robinson, M. S. (2019). LROC NAC Feature Mosaics: An Effective Tool for Lunar Investigations. 2151, 7077. https://ui.adsabs.harvard.edu/abs/2019LPICo2151.7077M

Mazarico, E., Neumann, G. A., Smith, D. E., Zuber, M. T., Torrence, M. H. (2011). Illumination conditions of the lunar polar regions using LOLA topography. Icarus 211, 1066-1081. https://doi.org/10.1016/j.icarus.2010.10.030

Mazarico, E., Barker, M. K., Jagge, A. M., Britton, A. W., Lawrence, S. J. , Bleacher, J. E., Petro, N. E. (2023). Sunlit pathways between south pole sites of interest for lunar exploration. Acta Astronautica 204, 49-57. https://doi.org/10.1016/j.actaastro.2022.12.023

Melosh, H. J. (2011) Planetary Surface Processes. Cambridge University Press, ISBN 9780511977848. https://doi.org/10.1017/CBO9780511977848.

Metzger, P. T., Immer, C. D., Donahue, C. M., Vu, B. T., Latta, R. C., & Deyo-Svendsen, M. (2009). Jet-Induced Cratering of a Granular Surface with Application to Lunar Spaceports. Journal of Aerospace Engineering, 22(1), 24–32. https://doi.org/10.1061/(ASCE)0893-1321(2009)22:1(24)

Metzger, P. T. (2020a). Dust Transport and its Effects due to Landing Spacecraft. Lunar Dust 2020, LPI Contrib. No. 2141, 5040. https://www.hou.usra.edu/meetings/lunardust2020/pdf/5040.pdf

Metzger, P. T. (2020b). Operating on the Moon: The Economic Geology of Lunar and Asteroid Resources. College of Sciences, University of Central Florida Moon 101 Course. https://sciences.ucf.edu/class/wp-content/uploads/sites/23/2020/02/2020-Lunar-Geology_Metzger.pdf.

Metzger, P. T. (2024). Erosion rate of lunar soil under a landing rocket, part 2: Benchmarking and predictions. Icarus Volume 417, 15JUL2024, 116135, ISSN 0019-1035. https://doi.org/10.1016/j.icarus.2024.116135.

Mitrofanov, I.G., Bartels, A., Bobrovnitsky, Y.I. et al. (2010) Lunar Exploration Neutron Detector for the NASA Lunar Reconnaissance Orbiter. Space Sci Rev 150, 183–207. https://doi.org/10.1007/s11214-009-9608-4

Morris, R. V. (1983) Handbook of Lunar Soils. NASA Planetary Materials Branch, JSC19069. https://www.lpi.usra.edu/lunar/samples/LunarSoils.pdf.

National Aeronautics and Space Administration, (2008) "A Standardized Lunar Coordinate System for the Lunar Reconnaissance Orbiter and Lunar Datasets". https://science.nasa.gov/wp-content/uploads/2024/01/luncoordwhitepaper-10-08.pdf

Plescia, J., "'The Lunar Surface" (Moon 101 Lecture Series, The Lunar and Planetary Institute, July 16, 2008). https://www.lpi.usra.edu/lunar/moon101/#surface.

Plescia, J., "Lunar Regolith – Understanding for Science and Exploration" (LEAG Annual Meeting, November 2, 2016). https://www.hou.usra.edu/meetings/leag2016/presentations/Wednesday/plescia.pdf.

Prabu, T., Muthukkumaran, K., Venugopal, I. (2022) Study on low gravity effect on bearing capacity and slope stability of a new lunar highland soil simulant (LSS-ISAC-1) for futuristic moon habitation. Advances in Space Research, 70(7), 1869-1879. https://doi.org/10.1016/j.asr.2022.06.026.

Raney, R. K., Spudis, P. D., Bussey, B., Crusan, J., Jensen, J. R., Marinelli, W., McKerracher, P., Neish, C., Palsetia, M., Schulze, R., Sequeira, H. B., & Winters, H. (2011). The Lunar Mini-RF Radars: Hybrid Polarimetric Architecture and Initial Results. Proceedings of the IEEE, 99(5), 808–823. https://doi.org/10.1109/JPROC.2010.2084970

Robinson, M. S., Brylow, S. M., Tschimmel, M., Humm, D., Lawrence, S. J., Thomas, P. C., Denevi, B. W., Bowman-Cisneros, E., Zerr, J., Ravine, M. A., Caplinger, M. A., Ghaemi, F. T., Schaffner, J. A., Malin, M. C., Mahanti, P., Bartels, A., Anderson, J., Tran, T. N., Eliason, E. M., … Hiesinger, H. (2010). Lunar Reconnaissance Orbiter Camera (LROC) Instrument Overview. Space Science Reviews, 150(1), 81–124. https://doi.org/10.1007/s11214-010-9634-2

Sanin, A. B., Mitrofanov, I. G.,Litvak, M. L., Bakhtin, B.N., Bodnarik, J. G., Boynton, W. V., Chin, G., Evans, L. G., Harshman, K., Fedosov, F., Golovin, D. V., Kozyrev, A. S., Livengood, T. A., Malakhov, A. V., McClanahan, T. P., Mokrousov, M. I., Starr, R. D., Sagdeev, R. Z., Tret'yakov, V. I., Vostrukhin, A. A. (2017). Hydrogen distribution in the lunar polar regions. Icarus, 283, 20-30. https://doi.org/10.1016/j.icarus.2016.06.002

Smith, D. E., Zuber, M. T., Neumann, G. A., Lemoine, F. G., Mazarico, E., Torrence, M. H., McGarry, J. F., Rowlands, D. D., Head III, J. W., Duxbury, T. H., Aharonson, O., Lucey, P. G., Robinson, M. S., Barnouin, O. S., Cavanaugh, J. F., Sun, X., Liiva, P., Mao, D., Smith, J. C., & Bartels, A. E. (2010). Initial observations from the Lunar Orbiter Laser Altimeter (LOLA). Geophysical Research Letters, 37(18). https://doi.org/10.1029/2010GL043751

Spence, H. E., Case, A. W., Golightly, M. J., Heine, T., Larsen, B. A., Blake, J. B., Caranza, P., Crain, W. R., George, J., Lalic, M., Lin, A., Looper, M. D., Mazur, J. E., Salvaggio, D., Kasper, J. C., Stubbs, T. J., Doucette, M., Ford, P., Foster, R., … Charara, Y. (2010). CRaTER: The Cosmic Ray Telescope for the Effects of Radiation Experiment on the Lunar Reconnaissance Orbiter Mission. Space Science Reviews, 150(1), 243–284. https://doi.org/10.1007/s11214-009-9584-8

Speyerer, E. J., Lawrence, S. J., Stopar, J. D., Gläser, P., Robinson, M. S., & Jolliff, B. L. (2016). Optimized traverse planning for future polar prospectors based on lunar topography. Icarus, 273, 337–345. https://doi.org/10.1016/j.icarus.2016.03.011

Stickle, A., & Stoper, J. (2021). Final Report of the Lunar Critical Data Products Specific Action Team. Lunar Exploration Analysis Group (LEAG). https://doi.org/10.5281/zenodo.7236426

Vondrak, R., Keller, J., Chin, G., & Garvin, J. (2010). Lunar Reconnaissance Orbiter (LRO): Observations for Lunar Exploration and Science. Space Science Reviews, 150(1), 7–22. https://doi.org/10.1007/s11214-010-9631-5

Watkins, R. N., Jolliff, B. L., Mistick, K., Fogerty, C., Lawrence, S. J., Singer, K. N., Ghent, R. R. (2019). Boulder Distributions Around Young, Small Lunar Impact Craters and Implications for Regolith Production Rates and Landing Site Safety. Journal of Geophysical Research: Planets, 124(11), 2754-2771. https://doi.org/10.1029/2019JE005963

Williams, J.-P., Greenhagen, B. T., Paige, D. A., Schorghofer, N., Sefton-Nash, E., Hayne, P. O., Lucey, P. G., Siegler, M. A., & Aye, K. M. (2019). Seasonal Polar Temperatures on the Moon. Journal of Geophysical Research: Planets, 124(10), 2505–2521. https://doi.org/10.1029/2019JE006028

TABLE C1-2 ADDITIONAL REFERENCES NOT CITED IN TEXT

Balakrishnan, K., & Bellan, J. (2018). High-Fidelity Modeling and Numerical Simulation of Cratering Induced by the Interaction of a Supersonic Jet with Granular Soil. International Journal of Multiphase Flow, 99(2), 1-29. https://doi.org/10.1016/j.ijmultiphaseflow.2017.08.008

Balakrishnan, K., & Bellan, J. (2019). A Multi-Species Modeling Framework for Describing Supersonic-Jet Induced Cratering in a Granular Bed: Cratering on Titan Case Study. International Journal of Multiphase Flow, 118, 205–241, 2019. https://doi.org/10.1016/j.ijmultiphaseflow.2019.05.011

Balakrishnan, K., & Bellan, J. (2021). Fluid density effects in supersonic jet-induced cratering in a granular bed on a planetary body having an atmosphere in the continuum regime. Journal of Fluid Mechanics, 915, A29. https://doi.org/10.1017/jfm.2021.29

Balakrishnan, K., & Bellan, J. (2021). Ejecta Formed During Supersonic Jet-induced Cratering in a Granular Medium.), AIAA Journal, 59(10), 3799-3814. https://doi.org/10.2514/1.J060563

Balakrishnan, K., & Bellan, J. (2023). Added Mass and Pseudo-Turbulent Kinetic Energy Effects on Ejecta during Jet-Induced Cratering in a Soil. AIAA Journal, 63(3), 973-990. https://doi.org/10.2514/1.J062405

Fontenot, R.L., Talbot, J., Gale, M., Mehta, R.S., and Capecelatro, J. (2022) “Modeling Enhancements for Eulerian-Eulerian Two-Fluid Methods in Compressible Particle-Laden Flows with Plume-Surface Interaction Applications,” Paper 2022-2195, AIAA SciTech 2022 Forum, San Diego, CA, January 2022. https://arc.aiaa.org/doi/abs/10.2514/6.2022-2195

Gale, M. (2022) “Efficient Pseudo-Polydisperse Model for Plume-Surface Interaction in Spacecraft Propulsive Landings,” AIAA Paper 2022-2002, AIAA SciTech 2022 Forum, San Diego, CA, January 2022. https://arc.aiaa.org/doi/pdf/10.2514/6.2022-2002

Gale, M., and Harris, R. (2022) “Continuum-Rarefied Modeling of Plume-Surface Interaction in Low-Pressure Environments,” AIAA Paper 2022-2003, AIAA SciTech 2022 Forum, San Diego, CA, January 2022. https://arc.aiaa.org/doi/abs/10.2514/6.2022-2003

Gale, M., Mehta, R.S., Liever, P., Curtis, J., and Yang, J. (2020) “Realistic Regolith Models for Plume-Surface Interaction in Spacecraft Propulsive Landings,” AIAA Paper 2020-0797, AIAA SciTech 2020 Forum, January 2020. https://arc.aiaa.org/doi/10.2514/6.2020-0797

Howison, J.C., Gale, M., and Mehta, R.S. (2022) “An Automated Process to Generate Constitutive Models for Granular Mixtures Using LIGGGHTS,” Paper 2022-2194, AIAA SciTech 2022 Forum, San Diego, CA, January 2022. https://arc.aiaa.org/doi/10.2514/6.2022-2194

Liever, P.A, Gale, M.P., Mehta, R.S., Weaver, A.B., West, J.S., Westra, D.G. (2021) “Gas-Particle Flow Simulations for Martian and Lunar Lander Plume-Surface Interaction Prediction,” ASCE Earth and Space 2021 Conference, April 2021. https://ascelibrary.org/doi/10.1061/9780784483374.009

Liever, P.A., and West, J.S. (2021) "Advances in Plume-Surface Interaction Simulation Capability Under Lunar Landing Conditions," International Planetary Probe Workshop, August 2021. https://youtu.be/KpSRkOFEszg

Liever, P., and West, J. (2022) "Particle Interaction Physics Model Formulation for Plume-Surface Interaction Erosion and Cratering," Paper 2022-2317, AIAA SciTech 2022 Forum, San Diego, CA, January 2022. http://dx.doi.org/10.2514/6.2022-2317

Liever, P., and West, J. (2022) "Demonstration of Capability to Simulate Particle Irregular Shape and Poly-Disperse Mixtures Within Lunar Lander Plume-Surface Interaction," ASCE Earth and Space 2022 Conference, April 2022. https://ascelibrary.org/doi/10.1061/9780784484470.006

Riley, S., DeGloria, S., Elliot, S. (1999). A Terrain Ruggedness Index that Quantifies Topographic Heterogeneity. Internation Journal of Science. 5. 23-27. https://download.osgeo.org/qgis/doc/reference-docs/Terrain_Ruggedness_Index.pdf

Shurtz, T.P., Krolick, W., Weaver, A.B., and West, J. (2022) "A Hybrid CFD/Engineering Model for Predicting Plume Induced Erosion and Cratering," 19th International Planetary Probe Workshop, Santa Clara, CA, September 2022. https://drive.google.com/file/d/1FBbKn9HovFDO-5cqDYJVZjz6dIm5TVPB/view

Shurtz, T., Liever, P., Weaver, A., and West, J. (2020) "Flow Simulations for Martian and Lunar Lander Plume-Surface Interaction Prediction," NASA In-Space Chemical Propulsion TIM, Huntsville, AL, September 2020. https://ntrs.nasa.gov/citations/20205004634

Weaver, A.B., Krolick, W.C., Liever, P.A., and West, J.S. (2022) "Overview of Predictive Simulation Capability Development for Crater Evolution and Ejecta in Continuum/Rarefied Flows," Paper 2022-2320, AIAA SciTech 2022 Forum, San Diego, CA, January 2022. https://arc.aiaa.org/doi/abs/10.2514/6.2022-2320

West, J. S., and Liever, P.A. (2022) "Gas-Particle Interaction Model Development in Plume Surface Interaction Erosion and Cratering," Paper 2022-2321, AIAA SciTech 2022 Forum, San Diego, CA, January 2022. https://arc.aiaa.org/doi/abs/10.2514/6.2022-2321

West, J.S., Liever, P., Weaver, A., Shurtz, T.P., Gale, M., Krolick, W. C., and Griffin, L.W. (2022) "Overview of the Predictive Simulation Capability Element of the Plume Surface Interaction Project," Paper 2022-2319, AIAA SciTech 2022 Forum, San Diego, CA, January 2022. https://arc.aiaa.org/doi/10.2514/6.2022-2319

TABLE C1-3 REFERENCE LINK SHORTHAND

Short Name	Description	First Use	Link
Analyst's Notebook	Analyst's Notebook Home Page	3.1	https://an.rsl.wustl.edu/
Apollo 11 Data	Apollo 11: NASA - NSSDCA - Spacecraft – Details	3.1.1	https://nssdc.gsfc.nasa.gov/nmc/spacecraft/display.action?id=1969-059C
Artemis Plan 2020	NASA's Lunar Exploration Program Overview - Artemis Plan - Sept 2020	6.1	https://www.nasa.gov/sites/default/files/atoms/files/artemis_plan-20200921.pdf
Connecting Ridge LROC DTM	Shackleton - de Gerlache Connecting Ridge DTM	4.2.4.2	https://wms.lroc.asu.edu/lroc/view_rdr/NAC_DTM_SHACKRDGE02
Diviner Data Sets	Planetary Data System Geosciences Node Diviner Data Sets	3.2.1.2	https://pds-geosciences.wustl.edu/missions/lro/diviner.htm
Diviner Maps	Index of Diviner Additional Maps	3.2.1.2	https://luna1.diviner.ucla.edu/~jpierre/diviner/level4_polar/additional_maps/
Diviner PDS Archive	Diviner Lunar Radiometer Experiment Planetary Data System Data Archive	3.2.1.2	https://www.diviner.ucla.edu/data
GDA Library	Geospatial Data Abstraction Library	4.3	https://gdal.org/index.html
GDAL Aspect Slope Map	GDAL Aspect Slope Map	4.3.4	https://gdal.org/programs/gdaldem.html?highlight=aspect+slope
GDAL DEM	gdaldem, Tools to analyze and visualize DEMs	4.3	https://gdal.org/programs/gdaldem.html
Haworth DEM SfS	Lunar LRO NAC Haworth Photoclinometry DEM 1m	4.2.4.3	https://astrogeology.usgs.gov/search/map/lunar_lro_nac_haworth_photoclinometry_dem_1m
Lighting Environment	Lighting and the Lunar Surface Environment - June 2020	6.3	https://ntrs.nasa.gov/citations/20220008695
South Pole NAC	Lunar Reconnaissance Orbiter Camera South Pole Narrow Angle Camera Mosaic	4.2.3.1	https://wms.lroc.asu.edu/lroc/view_rdr/NAC_POLE_SOUTH
South Pole WAC	Lunar Reconnaissance Orbiter Camera South Pole Wide Angle Camera Mosaic	4.2.3.3	https://wms.lroc.asu.edu/lroc/view_rdr/WAC_ROI_SOUTH_SUMMER

Short Name	**Description**	**First Use**	**Link**
LROC Next Steps	Lunar Reconnaissance Obiter Camera - Lunar Exploration: Planning the Next Steps	7.3.2	http://lroc.sese.asu.edu/posts/937
Malapert Massif LROC DTM	Lunar Reconnaissance Orbiter Camera Malapert Massif Peak Potential Landing Site for ESA Lunar Lander Digital Terrain Model	4.2.4.2	https://wms.lroc.asu.edu/lroc/view_rdr/NAC_DTM_ESALL_MP1
Moon 101 Lecture Series	Lunar Planetary Institute - Moon 101 Lecture Series	6.2.2	https://www.lpi.usra.edu/lunar/moon101/#surface
Moon Trek	Moon Trek	4.2.3.3	https://trek.nasa.gov/moon
Nobile to Malapert LROC DTM	Lunar Reconnaissance Obiter Camera Terrain Between Nobile and Malapert Craters Digital Terrain Model	4.2.4.2	https://wms.lroc.asu.edu/lroc/view_rdr/NAC_DTM_NOBILE01
NSSDC Home Page	NASA's Space Science Data Coordinated Archive Home Page	3.1	https://nssdc.gsfc.nasa.gov/
NSSDC Master Catalog	NASA's Space Science Data Coordinated Archive Master Catalog	3.2.1.1	https://nssdc.gsfc.nasa.gov/nmc/
PDS Home Page	NASA's Planetary Data System Home Page	3.1	https://pds.nasa.gov/
Polar Illumination	NASA's Planetary Geology, Geophysics and Geochemistry Laboratory Lunar Polar Illumination	5.1	https://pgda.gsfc.nasa.gov/products/69
Polar LOLA DEM	NASA's Planetary Data System Lunar Orbiter Laser Altimeter Digital Elevation Model for Wider Polar Regions	4.2.4.1	https://pds-geosciences.wustl.edu/lro/lro-l-lola-3-rdr-v1/lrolol_1xxx/data/lola_gdr/polar/
South Pole LOLA DEM	NASA's Planetary Geology, Geophysics and Geochemistry Laboratory South Pole Lunar Orbiter Laser Altimeter Digital Elevation Model Mosaic	4.2.4.1	https://pgda.gsfc.nasa.gov/products/81

Short Name	**Description**	**First Use**	**Link**
South Pole LOLA Hi-Res	NASA's Planetary Geology, Geophysics and Geochemistry Laboratory High-Resolution Lunar Orbiter Laser Altimeter Topography for Lunar South Pole Sites	4.2.4.1	https://pgda.gsfc.nasa.gov/products/78

APPENDIX D DATA REQUEST PROCESS

D1.0 OVERVIEW OF THE DATA REQUEST PROCESS

Write a brief statement with the requestor's name, the data needed, the need-by-date, names and email addresses of other parties to be included on additional communication, and the purpose/program for which the requested data will be used.

D1.1 HOW TO INITIATE A FORMAL DATA REQUEST

To request existing data as listed in this data book or to request a new data product from the Artemis Geospatial Data Team, send the statement via electronic mail to JSC-ArtemisGeospatialTeam@mail.nasa.gov.

D1.2 HOW A FORMAL DATA REQUEST WILL BE PROCESSED

The statement will be reviewed and forwarded to the appropriate data representative for further collaboration with the requestor. Please allow ten business days for initial processing; clarification may be sought by reply to the sending address and the listed other parties.

APPENDIX E MAXIMUM CONTINUOUS DARKNESS

E1.0 "SURVIVE THE NIGHT" (EXPLANATION OF 150 HOURS OF DARKNESS)

The typical lunar night duration is approximately 14 days with the lunar poles experiencing extremes in illumination such as permanently shadowed regions within craters or areas with increased lighting duration on crater rims or ridges during the lunar summer season. The duration of light and shadow are influenced by location, elevation, and season. Figure E1.0-1 shows a map of the solar illumination, averaged over hourly timesteps spanning 18.6 years, for the lunar south pole region from 85°S-90°S (E.Mazarico, PGDA - Lunar Polar Illumination)

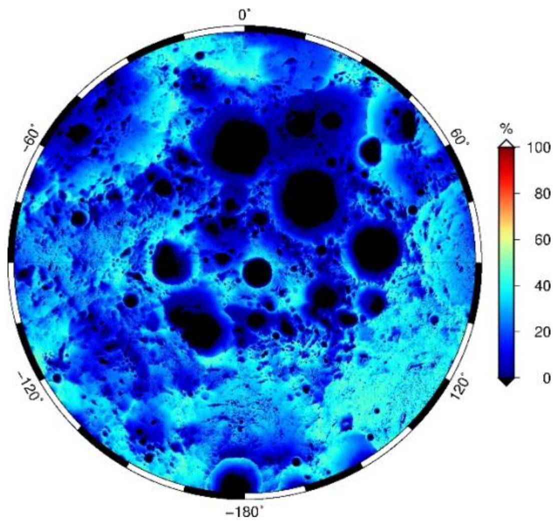

FIGURE E1.0-1 MAP OF AVERAGE SOLAR ILLUMINATION

Figure E1.0-1 is averaged over hourly timesteps spanning 18.6 years, for the south polar region, 85 degrees south to 90 degrees south (Center, 60 meters per pixel).

Using an initial lighting analysis of the Connecting Ridge location as an example, results show there is no site with 100% illumination on the Connecting Ridge. A minimum shadow duration of 85 hours will be needed to complete a shorter traverse, ~10 km in distance, on the Connecting Ridge.

Figure E1.0-2 shows an example, longer traverse path between Connecting Ridge and de Gerlache displayed as an path illumination matrix (distance vs time) and stereographic plots on specific days (E.Mazarico, Sunlit pathways between south pole sites of interest for lunar exploration - ScienceDirect). Planning this ~55km traverse involves finding a path that prioritizes illumination (represented as yellow or white) and minimizes periods of darkness (represented as blue or black) resulting in an approximately 30-day trip.

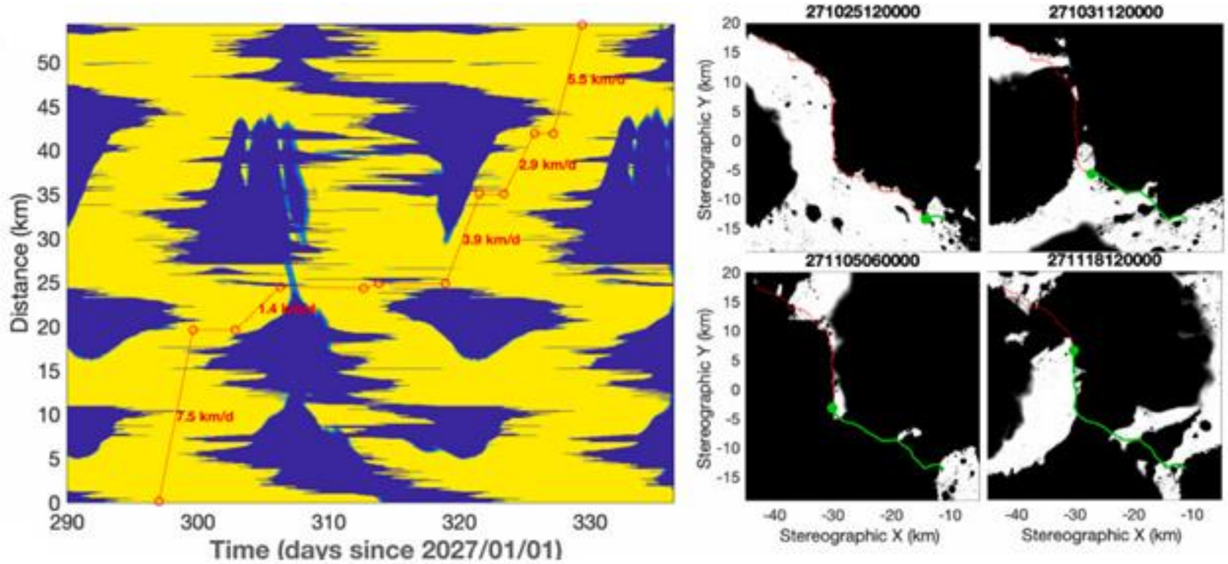

FIGURE E1.0-2 EXAMPLE TRAVERSE ILLUMINATION MATRIX (LEFT) AND ILLUMINATION CONDITIONS (RIGHT)

Figure E1.0-2 illustrates an example traverse between the Connecting Ridge and de Gerlache Rim. The left plot shows the path illumination matrix (distance vs time), and the right images show illumination conditions at four times during the traverse with the date/time for each shown as YYMMDDHHMMSS.

While shorter traverses (less than 10 km) in conjunction with 85-hour shadow survival are possible every month, longer traverses (greater than 10km) with 85-hour shadow survival may only be possible in the lunar summer season to avoid longer shadow periods.

During the winter season, results show illuminated safe havens where the lunar asset could hibernate. A lunar asset could travel away from an illuminated safe haven early in the lunar summer season and return to the safe haven before the winter season.

Increasing survival thresholds from 85 hours to 150 hours expand the illuminated safe havens in the winter season for Connecting Ridge, de Gerlache, Slater. A 150-hour survival threshold decreases hibernation needs during winter season, increases longer traverse potential, and reduces the need for external power to survive. The lunar asset's independent survival threshold will define the exploration range throughout the year.

Although the provided example was specific to Connecting Ridge and de Gerlache, site selection for lunar assets has not been determined. The expectation is assessments address illuminated safe havens or points of light to successfully reach Artemis science points of interest and commercial objectives.

APPENDIX F REFERENCE FRAMES

F1.0 PRINCIPAL AXIS VS. MEAN EARTH

There are pros and cons to any choice of reference frame in navigation and planning. A reference frame must be selected and used consistently for both cartography and navigation.

Cartography, or for our purposes the process of mapping, knowing where something is on the lunar surface, needs a common framework for assigning surface coordinates to features. Doing so enables sharing of scientific observations: Where is a mountain? Where is ice? Where is a crater edge? It needs a fixed frame with a defined coordinate system based on observational parameters and it can be used to correct knowledge of an orbiter or tie swaths of observations together to produce a larger picture than what can be directly observed in one image (for example, the approach used for high accuracy LOLA DEMS). Cartography enables navigation.

Navigation, or for our purposes knowing where you are relative to objects on the surface and within inertial space, requires knowledge to anchor an observation. Navigation information is needed in real-time to provide input to direct observations on the surface and is driven by understanding of planetary dynamics and geophysics.

Both are needed to reach any desired landing site. A spacecraft or EVA crew needs to know where they are, where the target is, and how to get from the latter to the former. Lunar reference frames have evolved significantly over time; current efforts are underway that will influence future capabilities.

For clarity on the Principal Axis and Mean Earth reference frames, please refer to the White Paper, “A Standardized Lunar Coordinate System for the Lunar Reconnaissance Orbiter and Lunar Datasets”, LRO Project and LGCWG White Paper Version 5, 2008 October 1, available at https://science.nasa.gov/wp-content/uploads/2024/01/luncoordwhitepaper-10-08.pdf.

F2.0 LUNAR GRID REFERENCE SYSTEM

<FWD-30044-015>